Universidade do Minho
Escola de Engenharia

Sónia da Glória Linhares Barbosa

Bioelectrochemically-assisted recovery of valuable resources from urine: investigation of anode performance and microbial community dynamics

março de 2017

Bioelectrochemically-assisted recovery of valuable resources from urine: investigation of anode performance and microbial community dynamics
Sónia da Glória Linhares Barbosa
UMinho | 2017

Universidade do Minho
Escola de Engenharia

Sónia da Glória Linhares Barbosa

Bioelectrochemically-assisted recovery of valuable resources from urine: investigation of anode performance and microbial community dynamics

Tese de Doutoramento em Engenharia Química e Biológica

Trabalho realizado sob a orientação da
Prof. Doutora Maria Alcina Alpoim de Sousa Pereira
e da
Doutora Luciana de Jesus dos Santos Peixoto
e da
Prof. Doutora Annemiek ter Heijne

março de 2017

DECLARAÇÃO DE INTEGRIDADE

Declaro ter atuado com integridade na elaboração da presente tese. Confirmo que em todo o trabalho conducente à sua elaboração não recorri à prática de plágio ou a qualquer forma de falsificação de resultados. Mais declaro que tomei conhecimento integral do Código de Conduta Ética da Universidade do Minho.

Universidade do Minho, 29 / 03 / 2017

Nome completo: Sónia da Glória Linhares Barbosa

Assinatura: Sónia da Glória Linhares Barbosa

ACKNOWLEDGMENTS

Obrigada!

To my supervisors Alcina Pereira, Luciana Peixoto and Annemiek ter Heijne I would like to thank for sharing the knowledge, the constant guidance and availability as well as the confidence and incentive. I also thank for the friendship shown during these 4 last years.

À Madalena Alves, um muito obrigada pela possibilidade de ingressar neste projeto tão ambicioso, e também pelos ensinamentos e sugestões fundamentais.

I also thank to Philipp for the first knowledge on bioelectrochemical systems assembly and operation as well as for the interesting suggestions and discussions. To the participants of the research theme "Resource Recovery" for the fruitful discussions mainly, Mariana Rodríguez, Patricia Zamora, Michel Saakes and Adriaan Jeremiasse. To Steve Tennison, thank you for providing the carbon electrode materials.

Gostaria de agradecer também ao Professor Fernando Pereira e à Doutora Salomé Soares pela disponibilidade e ajuda na caracterização dos materiais de carbono utilizados neste trabalho. Ao Sr. Azevedo, obrigada pela ajuda na caracterização dos cristais de estruvite e à Drª Elisa Pinto obrigada pela ajuda nas análises de NMR.

Gostaria igualmente de agradecer a todo o staff técnico do CEB pela constante disponibilidade.

A todas as meninas e meninos do LBA que sempre estiveram disponíveis, nomeadamente à Andreia e à Joana pela ajuda no trabalho molecular, agradeço a partilha de conhecimentos, de problemas e soluções bem como o companheirismo e o excelente ambiente proporcionado.

Ao Pedro e à Cris, obrigada pela hospitalidade e pelos passeios por terras Holandesas.

Obrigada ao Sérgio, à Salomé, ao João, à Daniela, à Carla e à Ana Luísa pela amizade, os bons momentos dentro e fora do LBA, pelos nossos momentos de convívio e de partilha. A todos os meus amigos de vida, obrigada pelo apoio e motivação constantes.

Obrigada à D. Marta, ao Sr. Júlio, ao Carlos, à Helena e à pequena Maria.

Obrigada aos meus pais e ao meu irmão, que sempre me apoiaram e encorajaram em todas as etapas da minha vida.

Ao meu Pequeno Grande Jorginho, a quem dedico esta tese, obrigada por Tudo.

A todos que de alguma forma contribuíram para este trabalho, muito Obrigada.

The work presented in this thesis was financially supported by the European Union's Seventh Programme for research, technological development and demonstration [Value from Urine FP-ENV-2012-Two stage., grant number 308535], by the Portuguese Foundation for Science and Technology (FCT) under the scope of the strategic funding of UID/BIO/04469/2013 unit and COMPETE 2020 (POCI-01-0145-FEDER-006684) and BioTecNorte operation (NORTE-01-0145-FEDER-000004) funded by the European Regional Development Fund under the scope of Norte2020 - Programa Operacional Regional do Norte and by the Portuguese Foundation for Science and Technology (FCT) under the scope of the Project RECI/BBB-EBI/0179/2012 (FCOMP-01-0124-FEDER-027462).











ABSTRACT

BIOELECTROCHEMICALLY-ASSISTED RECOVERY OF VALUABLE RESOURCES FROM URINE: INVESTIGATION OF ANODE PERFORMANCE AND MICROBIAL COMMUNITY DYNAMICS

Source separated urine is highly concentrated in nutrients and biodegradable compounds. This thesis explores the potential of combining nutrient recovery from urine with simultaneous energy production in bioelectrochemical systems (BESs).

Non-spontaneous phosphorus (P) recovery by struvite precipitation was analysed by adding three different magnesium (Mg) sources (magnesium chloride ($MgCl_2$), magnesium hydroxide ($Mg(OH)_2$) and magnesium oxide (MgO)). A statistical design of experiments was used to evaluate the effect of Mg:P molar ratio (1:1, 1.5:1 and 2:1) combined with stirring speed (30, 45 and 60 rpm) for each Mg source tested. MgO at 2:1 molar ratio and a stirring speed of 30 rpm allowed to achieve the highest P recovery efficiency (99 %) with struvite crystals size of 50 to 100 µm.

Urine obtained after P recovery, showed high concentration of biodegradable compounds being subsequently fed as substrate in a microbial fuel cell (MFC). Microbial acclimation to urine was performed in a MFC resulting in an anaerobic community successfully enriched in "urine-degrading" electroactive microorganisms. When compared to the control assay operated without preliminary microbial enrichment (81±9 mA m^{-2}), the acclimation method achieved significantly higher current density (455 mA m^{-2}) (p<0.05). *Tissierella* and *Paenibacillus* were the dominant genus identified in the adapted microbial community. *Tissierella* can convert creatinine to acetate, whereas bacterial species belonging to the *Paenibacillus* genus are known to function as exoelectrogens. *Corynebacterium* that comprise urea-hydrolysing bacteria was also detected in the developed biofilms.

The potential of urine obtained after P recovery for energy production in a microbial electrolysis cell (MEC) was evaluated using three different carbon anode materials, phenol-based (Keynol), cellulose-based (C-TEX) and polyacrilonitrile-based (PAN). The MECs were inoculated using the previously acclimated microbial community. Analyses of textural, chemical and electrochemical properties of the tested anodes made possible to conclude that the difference between the anode materials morphology, namely surface area available for microbial attachment which significantly affect current production. MEC using C-Tex generated the highest current density (904 mA m^{-2}), which was almost 3-fold higher than the MEC with Keynol (338 mA m^{-2}) and almost 8-fold higher than the MEC with PAN (118 mA m^{-2}) at an anode potential of -0.300 V vs. Ag/AgCl. The higher percentage of bacteria belonging to Lactobacillales and Enterobacteriales identified on C-Tex, suggest that microbes assigned to these orders were the responsible for the higher current generation.

Finally, raw and anaerobically digested urine were investigated in MEC. Anaerobic digestion was performed as pre-treatment to promote the acidification of urine. The main compounds initially identified in the acidified urine were methylamine, acetate and propionic acid. The combined anaerobic digestion-MEC system achieved higher average current density (218±6 mA m^{-2}), higher Coulombic efficiency (17±1 %), and higher COD removal rate (0.14±0.02 g L^{-1} d^{-1}) than MEC with raw urine. Furthermore, MEC with acidified urine displayed the lower effluent ammonium nitrogen (NH_4^+-N) concentration (678±127 mg L^{-1}) which corresponds to a removal efficiency of 87±3 %. Bioaugmentation with *Geobacter sulfurreducens* to the native microbial population slightly improved the current generation suggesting that the abundance of electrochemically active bacteria (EAB) was one of the limiting factors.

In conclusion, this thesis contributed with new insights on the degradation of organics in urine, changes in anodic bacterial community, the effect of anode materials and pre-acidification of urine, aiming at improving anode performance on BESs operating with urine.

RESUMO

RECUPERAÇÃO BIOELECTRICAMENTE-ASSISTIDA DE RECURSOS COM VALOR A PARTIR DE URINA: INVESTIGAÇÃO DA PERFORMANCE DO ÂNODO E DA DINÂMICA DA COMUNIDADE MICROBIANA

A urina separada de outras correntes de resíduos apresenta elevada concentração em nutrientes e compostos biodegradáveis. Esta tese explora o potencial da recuperação de nutrientes a partir de urina combinado com a produção simultânea de energia em sistemas bioelectroquímicos.

A recuperação não espontânea de P através da precipitação de estruvite foi analisada adicionando três diferentes fontes de magnésio (Mg) (cloreto de magnésio ($MgCl_2$), hidróxido de magnésio ($Mg(OH)_2$) e óxido de magnésio (MgO)). Foi utilizado um desenho experimental baseado em modelos estatísticos para avaliar o efeito da razão molar Mg:P (1:1, 1.5:1 e 2:1), combinada com a velocidade de agitação (30, 45 e 60 rpm) para cada fonte de Mg testada. O MgO com uma razão molar de 2:1 e uma velocidade de agitação de 30 rpm, permitiu obter a maior eficiência de recuperação de P (99 %) e cristais de estruvite de tamanho entre 50 e 100 μm.

A urina obtida após a recuperação de P apresentou elevada concentração de compostos biodegradáveis sendo posteriormente usada como substrato numa célula de combustível microbiana (CCM). A adaptação microbiana à urina foi realizada numa CCM resultando numa comunidade anaeróbia enriquecida em microrganismos electroactivos capazes de degradar urina. Em comparação com o ensaio de controlo operado sem o enriquecimento microbiano prévio (81±9 mA m^{-2}), o processo de adaptação microbiana permitiu obter uma densidade de corrente significativamente superior (455 mA m^{-2}) (p<0.05). Na comunidade microbiana adaptada identificaram-se predominantemente os géneros *Tissierella* e *Paenibacillus*. *Tissierella* tem a capacidade de converter creatinina a acetato, enquanto algumas espécies pertencentes ao género *Paenibacillus* são conhecidas pela sua atividade electroactiva. *Corynebacterium*, que incluí bactérias capazes de hidrolisar ureia, foi também detetado no biofilme desenvolvido.

O potencial da urina obtida após a remoção de P, para a produção de energia em células de eletrólise microbiana (CEM) foi avaliado usando três materiais de carbono diferentes como ânodo, com base em fenol (Keynol), celulose (C-Tex) e poliacrilonitrilo (PAN). As CEMs foram inoculadas utilizando a comunidade microbiana previamente adaptada. As análises às propriedades texturais, químicas e eletroquímicas dos materiais possibilitaram concluir que a diferença na morfologia dos materiais, nomeadamente a área de superfície disponível para a adesão microbiana, afetou significativamente a produção de corrente elétrica. A CEM com C-Tex gerou a maior densidade de corrente (904 mA m^{-2}), que corresponde a aproximadamente 3x a corrente elétrica gerada na CEM com Keynol (338 mA m^{-2}) e 8x a corrente elétrica gerada na CEM com PAN (118 mA m^{-2}) a um potencial do ânodo controlado a -0.300 V vs. Ag/AgCl. A elevada percentagem de bactérias pertencentes a Lactobacillales e Enterobacteriales identificadas na CEM com C-Tex, sugerem que os microrganismos pertencentes a estas ordens são os responsáveis pela elevada produção de corrente.

Finalmente, urina digerida anaerobiamente e não digerida foram estudadas na CEM. A digestão anaeróbia foi o processo utilizado para promover a acidificação da urina. Os principais compostos identificados na urina acidificada foram metilamina, acetato e propionato. A combinação dos processos de digestão anaeróbia e a CEM permitiram obter maior densidade de corrente (218±6 mA m^{-2}), maior eficiência Coulômbica (17±1 %) e maior taxa de remoção de CQO (0.14±0.02 g L^{-1} d^{-1}). Além disso, a CEM com urina acidificada demonstrou a menor concentração de NH_4^+-N (678±127 mg L^{-1}) no efluente, que corresponde a uma taxa de remoção de 87±3 %. A bioaumentação com *Geobacter sulfurreducens* melhorou ligeiramente a corrente produzida o que sugere que a abundância de microrganismos eletroactivos foi um fator limitante.

Em conclusão, esta tese contribuiu com novos conhecimentos sobre a degradação de compostos orgânicos na urina, sobre as dinâmicas na comunidade bacteriana anódica, o efeito de diferentes materiais anódicos e a pré-acidificação da urina com o objetivo de melhorar o desempenho do ânodo em sistemas bioelectroquímicos operados com urina.

TABLE OF CONTENTS

1. THESIS SCOPE
1.1 Perspective and motivation 3
1.2 Research aim 4
1.3 Thesis outline 4

2. LITERATURE REVIEW
2.1. Bioelectrochemical systems 9
2.1.1. Microbial Fuel Cell 10
2.1.2. Microbial Electrolysis Cell 11
2.2. Anode chamber 12
2.3. Anode materials 13
2.3.1. Carbon anode materials 14
2.3.2. Metal anode materials 19
2.4. Surface anode modifications 20
2.4.1. Chemical anode modification 20
2.4.2. Anode modification with carbon nanotubes/carbon nanofibres 20
2.4.3. Anode modification with metal oxides 21
2.4.4. Anode modification with conductive polymers 22
2.4.5. Anode modification with external mediators 22
2.5. Electrochemically active bacteria 23
2.6. Extracellular electron transfer mechanisms 23
2.6.1. Direct electron transfer 24
2.6.2. Mediated electron transfer 27
2.6.3. Direct interspecies electron transfer 28
2.7. Applications of BES 29
2.8. Urine as a resource 35
2.8.1. Phosphorus recovery from urine 36
2.8.2. Urine as substrate for BES 38

3. A design of experiments to assess phosphorous removal and crystal properties in struvite precipitation of source separated urine using different Mg sources
Abstract 47
3.1. Introduction 48
3.2. Materials and methods 50
3.2.1. Design of experiments and statistical analysis 50
3.2.2. Phosphorus removal by struvite precipitation 51
3.2.3. Precipitate analysis – crystal size, XRD and SEM-EDS 52
3.3. Results and Discussion 53
3.3.1. Phosphorus removal by struvite precipitation 53

3.3.2. Precipitate analysis 57
3.3.3. Economic overview 61
3.4. Conclusions 63

4. Investigating bacterial community changes and organic substrate degradation in Microbial Fuel Cell operating on real human urine
Abstract 67
4.1. Introduction 68
4.2. Materials and Methods 69
4.2.1. Urine and inoculum source 69
4.2.2. MFC experimental setup and operation 70
4.2.3. Electrochemical characterization 71
4.2.4. Chemical analysis 71
4.2.5. Calculation 72
4.2.6. Microbial community investigation 72
4.3. Results and Discussion 73
4.3.1. Current generation as a function of urine concentration 73
4.3.2. ^{1}H-NMR analysis 77
4.3.3. Microbial communities 79
4.4. Conclusions 82

5. Effect of different carbon materials on the performance of Microbial Electrolysis Cells operated on urine and their microbial composition
Abstract 85
5.1. Introduction 86
5.2. Materials and methods 87
5.2.1. Urine and inoculum source 87
5.2.2. Electrodes characterization 87
5.2.3. Reactor set up 89
5.2.4. Chemical analysis and measurements 90
5.2.5. Microbial community investigation 90
5.3. Results and discussion 91
5.3.1. Electrodes characterization 91
5.3.2.Effect of different anodes on the performance of a MEC under cell potential control versus anode potential control 96
5.3.3. Microbial community analysis 100
5.4. Conclusions 104

6. Pre-acidification of urine as a strategy to enhance the performance of a Microbial Electrolysis Cell

Abstract **109**

6.1. Introduction **110**

6.2. Material and methods **111**

6.2.1. Urine source 111

6.2.2. Anaerobic biodegradability of urine 111

6.2.3. Anaerobic acidification of urine 113

6.2.4. MEC experimental setup and operation 113

6.2.5. Chemical analysis and measurments 114

6.3. Results and discussion **116**

6.3.1. Anaerobic biodegradability of urine 116

6.3.2. MECs performance using raw versus acidified urine 118

6.3.3. MECs performance after bioaugmentation with *G. sulfurreducens* 124

6.4. Conclusions **126**

7. General conclusions and future perspectives **129**

References **133**

ABBREVIATIONS

AC - activated carbon
AP - adequate precision
BES - bioelectrochemical system
BET - Brunauer-Emmett-Teller
BMFC - benthic/sediment microbial fuel cell
BMP - biochemical methane production
BNR - biological nutrient removal
CCF - central composite face
CE - Coulombic efficiency
CNF - carbon nanofibre
CNT - carbon nanotube
COD - chemical oxygen demand
tCOD - total chemical oxygen demand
sCOD - soluble chemical oxygen demand
CV - coefficient of variation
DET - direct electron transfer
DIET - direct interspecies electron transfer
DTG - derivative thermogravimetric
EAB - electrochemically active bacteria
EDS - energy dispersive spectrometer
EET - extracellular electron transfer
EU - European Union
FTIR - Fourier transform infrared spectroscopy
^{1}H NMR - proton nuclear magnetic resonance
HRT - hydraulic retention time
IFDC - International fertilizer development centre
MDC- microbial desalination cell
MEC - microbial electrolysis cell
MES - microbial electrosynthesis cell
MET - mediated electron transfer
MFC - microbial fuel cell
MRC - microbial remediation cell)
MREC - microbial reverse-electrodialysis cell
Mtr - metal reducing respiratory
NHE - normal hydrogen electrode
Omc - outer membrane cytochrome
PAN - polyacrylonitrile
PANI - polyaniline

PMFC - photosynthetic microbial fuel cell
PPY - polypyrrole
PVC - polyvinyl chloride
RSM - response surface methodology
SAA - specific acetoclastic activity
SEM - scanning electron microscope
SHE - standard hydrogen electrode
SHMA - specific hydrogenotrophic methanogenic activity
STP - standard temperature and pressure
TAN - total ammonia nitrogen
TG - thermogravimetric
TMCS - transmembrane chemisorption
TPD - temperature programmed desorption
TSBP - two-stage bioconversion process
VFA - volatile fatty acid
VS - volatile solids
WWTP - wastewater treatment plant
XRD - X-ray diffraction

LIST OF FIGURES

FIGURE 2.1 Schematic representation of a typical configuration of the two most common bio-electrochemical systems (BES): **A)** microbial fuel cell (MFC) and **B)** microbial electrolysis cell (MEC)..... 9
FIGURE 2.2 Number of scientific journal articles published from 2000 to 2016 containing the phrases "microbial fuel cell" (grey) or "microbial electrolysis cell" (black) (Scopus, February 2017). 10
FIGURE 2.3 Scanning electron microscope (SEM) photograph of cellulose-based carbon fibres. 16
FIGURE 2.4 Chemical steps for synthesis of carbon fibres from polyacrylonitrile (PAN). **A)** Polymerization step; **B)** stabilization (cyclization and oxidation) step; **C)** and **D)** carbonization step. Adapted from [79]. 17
FIGURE 2.5 Proteins involved in direct electron transfer (DET) mechanism, particularly in **A)** Geobacter sulfurreducens and **B)** Shewanella oneidensis. FL- flavins; CP- cytoplasm; PP – periplasm; OM – outer membrane. Solid line represents the main route and dotted line represents the minor path. Adapted from [127]. 26
FIGURE 2.6 Models for extracellular electron transfer (EET) mechanisms occurring in bio-anodes: **A)** direct electron transfer (DET) mechanism by outer membrane cytochromes (Omcs) or by electrically conductive pili (nanowire); **B)** mediated electron transfer (MET) mechanism by using endogenous or exogenous electron mediators and **C)** direct interspecies electron transfer (DIET) from cell to cell through conductive pili. 28
FIGURE 2.7 Research trends on **A)** different type of BESs (PMFC: photosynthetic microbial fuel cell; BMFC: benthic/sediment microbial fuel cell; MES: microbial electrosynthesis cell; MDC: microbial desalination cell; MREC: microbial reverse-electrodialysis cell and MRC: microbial remediation cell) and **B)** different BESs applications. 30

FIGURE 3.1 Response graphs showing the effect of Mg:P ratio (1:1; 2:1 and 3:1) and stirring speed (60, 90 and 120 rpm) on phosphorus (P) recovery efficiencies with different Mg sources **A)** MgO; **B)** $MgCl_2$ and **C)** $Mg(OH)_2$. 54
FIGURE 3.2 Response graphs showing the effect of Mg:P ratio and stirring speed on phosphorus (P) recovery efficiencies with different Mg sources **A)** MgO; **B)** $MgCl_2$ and **C)** $Mg(OH)_2$. 57
FIGURE 3.3 Graphs showing the effect of Mg:P ratio and stirring speed on crystal size (left) and particle size distribution (right) with **A)** MgO; **B)** $MgCl_2$ and **C)** $Mg(OH)_2$ as Mg sources. 59
FIGURE 3.4 Scanning electron microscopy (SEM) picture, respective elemental analysis and X-ray diffraction (XRD) spectra of the precipitates (left to right) from batch experiments at 1.5:1 of Mg:P and 45 rpm with **A)** MgO; **B)** $MgCl_2$ and **C)** $Mg(OH)_2$ as Mg sources. Vertical lines (pink) at XRD analysis corresponds to standard struvite (Powder diffraction file (PDF) No. 15-0762). 61

FIGURE 4.1 Schematic representation of the microbial fuel cells (MFCs) configuration: **A)** Flat graphite plates; **B)** carbon paper; **C)** plexiglass plates; **D)** silicone gaskets; **E)** graphite insert; **F)** carbon felt and **G)** cation exchange membrane (CEM). 71

FIGURE 4.2 Measured current density over time with undiluted urine as substrate without any acclimation strategy. 73
FIGURE 4.3 Measured current density during the start-up period with anaerobic sludge and 50x diluted urine **A)** MFC A and **B)** MFC B. 74
FIGURE 4.4 Measured current density during the experimental period with urine concentration increase: **A)** MFC A and **B)** MFC B. I: dilution 1/50 (0.06 g L^{-1} (COD)); II: dilution 1/25 (0.14 g L^{-1} (COD)); III: dilution 1/10 (0.64 g L^{-1} (COD)); IV: dilution 1/3 (2.37 g L^{-1} (COD)) and V: dilution 1/1 (7.71 g L^{-1} (COD)). 75
FIGURE 4.5 Correlation between maximum current density and coulombic efficiency (CE) with urine concentration for **A)** MFC A and **B)** MFC B. 76
FIGURE 4.6 Polarization (○) and power curves (□) obtained by varying the external resistance between the electrodes for: **A)** MFC A and **B)** MFC B. 77
FIGURE 4.7 ^{1}H-NMR spectral data of anolyte from **A)** MFC A and **B)** MFC B. 78
FIGURE 4.8 Bacterial community distribution at genus level for biofilms developed in **A)** anode of the MFC A; **B)** anode of MFC B as well as for the bacterial community present in **C**) initial sludge inoculum and **D)** urine used as substrate. 81
FIGURE 4.9 Archaea community distribution at genus level for biofilms developed in the anode of the **A)** MFC A and **B)** MFC B. 82

FIGURE 5.1 Scanning electron microscopy (SEM) images of different carbon anode materials (160 x): **A)** Keynol **B)** C-Tex and **C)** PAN. The insets show a higher magnification image of the electrodes (1000 x). 91
FIGURE 5.2 Temperature programmed desorption curves profile of different anodes, corresponding to the evolution of **A)** CO and **B)** CO_2 upon decomposition of the various types of oxygen functional groups. 92
FIGURE 5.3 N_2 adsorption/desorption isotherms measured at 77 K for different anodes. 93
FIGURE 5.4 **A)** Thermogravimetric (TG) and **B)** derivative thermogravimetric (DTG) curves under N_2 atmosphere from room temperature to 800 °C for different electrode materials. 95
FIGURE 5.5 Electrochemical properties of different electrodes in 1M KOH aqueous electrolyte: **A)** and **B)** cyclic voltammetry and charge-discharge curves of Keynol, **C)** and **D)** cyclic voltammetry and charge-discharge curves of C-Tex and **E)** and **F)** cyclic voltammetry and charge-discharge curves of PAN. 96
FIGURE 5.6 Measured current density for different anodes under **A)** cell potential control (**- - -** represents the cell potential for C-Tex and **- - -** represents the cell potential for PAN and Keynol) and **B)** anode potential control (**- - -** represents the anode potential). 98
FIGURE 5.7 Cyclic voltammograms of biofilms developed in the different anodes. The scanning rate was 0.15 mV s^{-1} and Ag/AgCl was used as the reference electrode. 100
FIGURE 5.8 Scanning electron microscopy images (500 X) of biofilms grown under anode potential control on MECs using **A)** Keynol, **B)** C-Tex and **C)** PAN anodes. The insets show a higher magnification image of the biofilm (left: 10 000x, and right: 50 000x). 101
FIGURE 5.9 Bacterial community distribution of biofilm grown on different anodes tested (C-Tex, Pan and Keynol) under cell and anode potential control at **A)** phylum level, **B)** order lever assigned to Firmicutes phyla and **C)** order level assigned to Proteobacteria phyla. 104

FIGURE 6.1 Cumulative methane production during anaerobic biodegradability assays of urine at COD concentrations of: (◊) 0 g L^{-1} (Blank); (+) 0.5 g L^{-1}; (O) 1 g L^{-1}; (Δ) 2 g L^{-1}; (□) 5 g L^{-1}; (x) 8 g L^{-1}. The symbols represent the experimental data with respective standard deviation (n = 3 points). The lines represent the predicted data by the modified Gompertz equation. 117
FIGURE 6.2 Current density during experiment on microbial electrolysis cells fed with **A)** raw and **B)** acidified urine for three sequential batches (I, II and III). 120
FIGURE 6.3 Average COD removal (○), NH_4^+-N removal (Δ) and pH (□) for three different batches during experiment on microbial electrolysis cells fed with **A)** raw and **B)** acidified urine. 121
FIGURE 6.4 Proton nuclear magnetic resonance (^{1}H-NMR) spectral data of **A)** raw urine; **Ai)** raw urine after suppression of acetate peak; **B)** acidified urine and **Bi)** acidified urine after suppression of acetate peak. 123
FIGURE 6.5 Current density during experiment after bioaugmentation with *Geobacter sulfurreducens* on microbial electrolysis cells fed with **A)** raw and **B)** acidified urine. 124
FIGURE 6.6 Average COD removal (○), NH_4^+-N removal (Δ) and pH (□) during experiment on microbial electrolysis cells fed with **A)** raw and **B)** acidified urine..... 125

LIST OF TABLES

Table 1.1 Structure of the thesis. 5

Table 2.1 A brief account of different carbon-based anode materials used in microbial fuel cell research, and their performance. 15
Table 2.2 Isolated electrochemically active bacteria (EAB) divided by their class, substrate preference and performance. 24
Table 2.3 Various wastewaters used as anodic fuel in MFCs and their performances. 31
Table 2.5 Various wastewaters used as anodic fuel in MECs and their performances. 34

Table 3.1 Experimental design matrix with operating conditions for P recovery efficiency assays. 51
Table 3.2 Composition of fresh and stored human urine (n=3). 53
Table 3.3 ANOVA analysis for the effect of Mg:P ratio and stirring speed on P recovery efficiency. 56
Table 3.4 ANOVA analysis for the effect of Mg:P ratio and stirring speed on crystal size. 58
Table 3.5 Estimated struvite production costs using industrial grade magnesium salts. 62

Table 4.1 Composition of urine after phosphorus precipitation. 70
Table 5.1 Composition of urine after phosphorus precipitation. 87

Table 5.2 Textural characterisation of the different anode materials. 94

Table 6.1 Methane production parameters predicted by the modified Gompertz equation and experimental results obtained at the end of anaerobic biodegradability batch assays. 118
Table 6.2 Characterization of raw and acidified human urine used as feedings in the MECs (n=3). 119

Chapter 1

Thesis scope

1. THESIS SCOPE

1.1 PERSPECTIVE AND MOTIVATION

The European Union (EU) is currently relying on phosphorous (P) mineral importation as well as the energy intensive recovery of nitrogen (N) to produce fertilizers. Around 90 % of the P rock extracted is actually for food production, however, it is estimated that P reserves will be depleted within 50 to 100 years [1]. On the other hand, N can be obtained as ammonia (NH_3) from nitrogen gas (N_2) by the Haber-Bosh process, however, this NH_3 production process is highly energy demanding [2]. The recovery of these nutrients from waste streams will help to prevent future shortage and reduce the need of P imports and energy demand for NH_3 production (Haber-Bosh process). Furthermore, the separation of P from the wastewater will prevent pipe blockages in municipal wastewater treatment plants due to struvite accumulation [3] whereas removal of N from wastewater will avoid the risk of eutrophication of water bodies [4].

Urine is a liquid waste that represents only approximately 1 % of municipal wastewater. However, it is highly concentrated in nutrients contributing to more than 80 % of the total N load and around 45 % of the total P load [5]. Separation of urine from other wastewater streams is therefore an interesting strategy to develop a suitable nutrient recovery concept, with simultaneous improvement of effluent quality and energy saving in biological nutrient removal (BNR) process. An extensive range of options are available for the treatment and reuse of collected urine [6, 7, 8].

Bioelectrochemical systems (BESs), that include microbial fuel cells (MFCs) and microbial electrolysis cells (MECs), appear as an effective energy efficient system for the recovery of nutrients with simultaneous energy production from wastewaters. The principle of BESs is to convert chemical energy into electrical energy by electrochemically active bacteria (EAB). EAB have the ability to oxidise organic compounds transferring the electrons to an electrode surface [9].

BESs display a high potential to improve wastewater treatment, however this technology still presents a poor efficiency, thus important challenges remain, especially for large scale applications [10]. Several parameters can influence current density in BES including, microbial community [11], anode catalysts [12], cathodic catalysts [13] electrolyte pH [14] and biodegradability of substrate [15], among others. Furthermore, the substrate's characteristics namely the conductivity, the strength and the biodegradability influences not only the bacterial community in the anode biofilm but also the BES performance, including the current density and Coulombic efficiency (CE) [16].

For these reasons, there is an urgent need to address solutions to the low current densities in BESs, for example, by optimizing the design to minimize the losses, increasing the population density of the EAB, improving electrode transfer mechanisms between the biocatalyst and the electrode and increasing the biodegradability of the substrate.

1.2 RESEARCH AIM

This thesis envisaged the development and optimization of an innovative and integrated system for the recovery of nutrients from urine with a simultaneous production of energy. The possibility of combining energy production in a BES with the P and N recovery is a crucial alternative to the conventional wastewater treatment processes while producing added value compounds. Removal of P from urine is an essential prerequisite for the successful operation of the BES. P removal above 95 % is necessary to reduce the scaling risk (deposit of crystals) inside the system. For this purpose, a statistical design of experiments was applied to optimize the P recovery in a useful form, specifically as struvite, which can be used as fertilizer in the agricultural sector. Furthermore, a suitable strategy to develop an anaerobic community enriched in EAB acclimated to undiluted urine was promoted in a BES, namely in a MFC, to treat the urine obtained after P removal. Further, the relation between the degradation of organics in urine and dynamics in anodic bacterial community was also established.

Several strategies were adopted in order to improve the BES performance. Different carbon anodes such as Keynol (phenol-based), C-Tex (cellulose-based) and PAN (polyacrilonitrile-based) were texturally, chemically and electrochemically characterized and tested as anode material in a MEC. Additionally, anaerobic digestion was used to increase the biodegradability of urine to evaluate the possible improvement in the MEC performance.

1.3 THESIS OUTLINE

This thesis was organized according to the follow structure (Table 1.1).

TABLE 1.1 Structure of the thesis.

CHAPTER 1	**Context, aim and thesis outline** Perspective and motivation the research aim and outline.
CHAPTER 2	**Literature review** Comprises an overview of the state of the art on bioelectrochemical systems with a particular focus on anode compartment. Urine as a resource was also studied.
CHAPTER 3	**A design of experiments to assess phosphorous removal and crystal properties in struvite precipitation of source separated urine using different Mg sources** The optimum parameters (stirring speeds, reaction and sedimentation times and Mg:P ratio) for P recovery by struvite precipitation were investigated.
CHAPTER 4	**Investigating bacterial community changes and organic substrate degradation in microbial fuel cell (MFC) operating on real human urine** A strategy for microbial acclimation to undiluted urine in a MFC by decreasing human urine dilution was studied.
CHAPTER 5	**Effect of different carbon materials on the performance of microbial electrolysis cells (MECs) operated on urine and their microbial composition** The relationship between microbial community composition and current generation was analysed for three different carbon anodes, namely Keynol (phenolic-based), C-Tex (cellulose-based) and PAN (polyacrylonitrile-based).
CHAPTER 6	**Pre-hydrolysis of urine as a strategy to enhance the performance of a microbial electrolysis cell (MEC)** The biodegradability of urine was promoted using anaerobic digestion to evaluate MEC performance using a previously acidified urine versus raw urine.
CHAPTER 7	**General conclusions and future perspectives** The general conclusions as well as some future perspectives of the current work.

Chapter 2

LITERATURE REVIEW

2. LITERATURE REVIEW

2.1. BIOELECTROCHEMICAL SYSTEMS

The increase of energy demand in combination with several environmental concerns gave a big impulse towards the development of renewable energy sources. A technology that allows the conversion of available substrates from sustainable sources (*e.g.* wastes) into energy is an attractive proposition. In this context, bioelectrochemical systems (BESs) represents a new generation of technology that allows to transform energy-intensive and treatment-focused processes into integrated systems which not only produce energy but also recover nutrients as useful products [17].

In a BES, a fuel is continuously fed to the anode and an oxidant is continuously fed to the cathode, similarly to a chemical fuel cell. The chemical energy of biodegradable substrates (*e.g.* acetate) is converted into electrical energy by electrochemically active bacteria (EAB) in BES. The microbial oxidation of substrate at the anode chamber is a common principle for the main types of BESs, however the released electrons to the cathode chamber can be captured for direct electricity production or used to produce chemicals [17]. The two principal BESs are:

i) Microbial fuel cell (MFC) (Figure 2.1A) if electrical energy is directly harvested [18] and

ii) Microbial electrolysis cell (MEC) (Figure 2.1B) if the electrons are used to produce hydrogen (H_2) [19] and other value added chemicals such as methane (CH_4) [20] and hydrogen peroxide (H_2O_2) [21] with additional energy input.

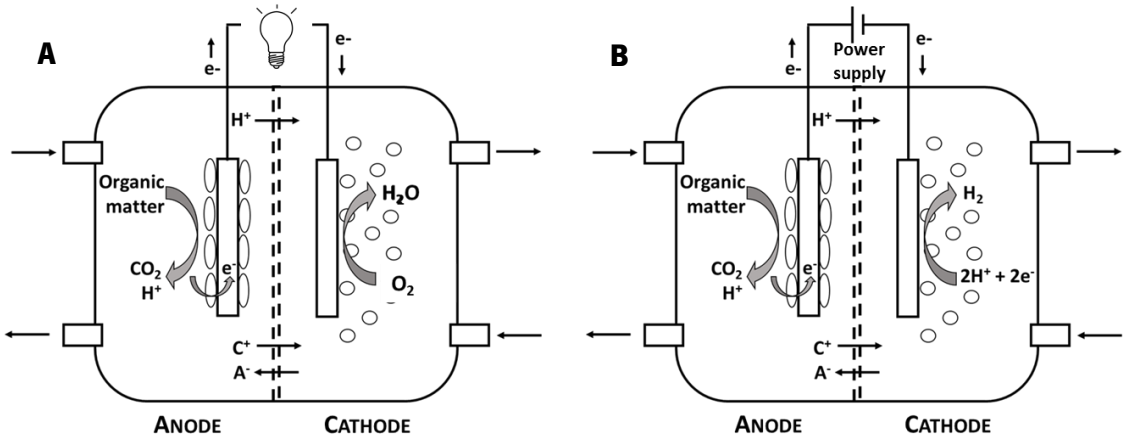


FIGURE 2.1 Schematic representation of a typical configuration of the two most common bioelectrochemical systems (BES): **A)** microbial fuel cell (MFC) and **B)** microbial electrolysis cell (MEC).

The exponential growth in the number of journal publications since year 2000 demonstrates the increase of interest in this research concept (Figure 2.2).

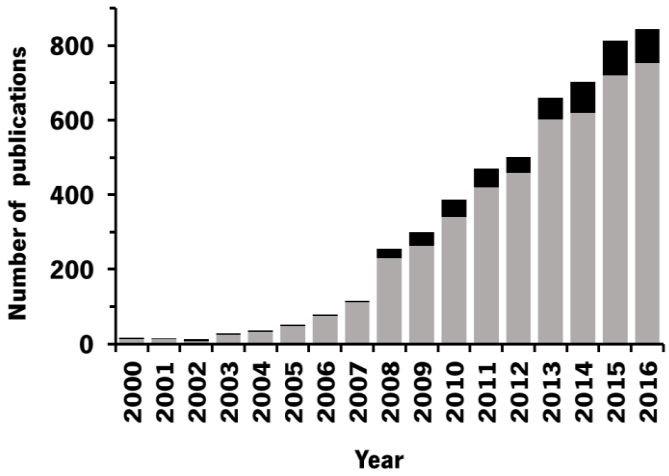


FIGURE 2.2 Number of scientific journal articles published from 2000 to 2016 containing the phrases "microbial fuel cell" (grey) or "microbial electrolysis cell" (black) (Scopus, February 2017).

2.1.1. Microbial Fuel Cell

MFC represents an approach for electricity generation from a biodegradable substrate by microorganisms. In comparison to conventional fuel cells MFCs present some operational advantages: mild operating conditions (ambient temperature and pressure), use of inexpensive catalysts (microorganisms) and unlimited range of potential applications using different electron donors [22].

In 1911, Potter reported for the first time the generation of current by bacteria [23]. However, MFC became of more interest when it was recognized that current generation was also possible in the absence of electron mediators. Kim and co-workers named this MFC type as a "mediator– less microbial fuel cell" [24]. In 2003, Bond and Lovley revealed the capability of metal-reducing bacteria such as *Geobacter sulfurreducens* to perform extracellular electron transfer directly to an electrode surface [25].

A MFC consists of two chambers, an anode and a cathode, which can be separated by a membrane or, in case of membrane-less MFC, without membrane. At the anode chamber, the biodegradable substrate (electron donor) (*e.g.* acetate) is oxidized by microorganisms producing electrons and protons (Equation 2.1) [26]. EAB, which grow at the anode chamber forming a biofilm in the electrode surface, are responsible for the oxidation reaction of organic matter [27]. The electrons

are then transferred from organic matter to the anode by different mechanisms (Section 2.6) and posteriorly flow to the cathode chamber through an external circuit. The protons and other cations flow to the cathode chamber through the membrane [9]. Electrons and protons are consumed in the cathode chamber generating electricity, simultaneously with the reduction of oxygen (O_2) to water (H_2O) (Equation 2.2) [26].

$$C_2H_4O_2 + 2H_2O \rightarrow 2CO_2 + 8H^+ + 8e^- \quad \text{E = - 0.289 V vs. NHE (pH=7)} \quad \textbf{EQUATION 2.1}$$

$$2O_2 + 8H^+ + 8e^- \rightarrow 4H_2O \quad \text{E = 0.805 V vs. NHE (pH=7)} \quad \textbf{EQUATION 2.2}$$

2.1.2. Microbial Electrolysis Cell

Electrolysis of water (decomposition of water into O_2 and H_2) may be the cleanest technology for H_2 production. However, electricity costs account for 80 % of the operating total budget [28]. Biological H_2 production is a viable alternative in accordance with sustainable development. Dark fermentation (conversion of carbohydrates to H_2 by fermentative bacteria) and photo-fermentation (conversion of organic acids to H_2 by photosynthetic bacteria) are two bioprocesses for H_2 production [28]. The greatest challenge of H_2 production by dark fermentation is the low H_2 yield. In practice, 25 % is the maximum yield conversion of substrate into H_2 [29]. Organic acids (*e.g.* butyrate, propionate) and alcohols (*e.g.* ethanol) are also generated lowering the H_2 yield [30]. Therefore, several research and development projects are dedicated to photo-fermentation process in order to improve its H_2 production yield. However, photo-fermentation requires light, which increases exponentially the complexity of the reactor design, making the scale-up unfeasible mainly due to the enormous reactor surface area required [31]. H_2 production based on MEC was presented by two research groups and provides an absolutely novel approach [31, 32].

In a MEC, EAB oxidise organic compounds (*e.g.* acetate) at the anode and release electrons and protons into a solution (Equation 2.3) [19]. Electrons are transferred to an electrode surface and subsequently transferred from the anode through an external circuit to the cathode [19]. At the cathode, electrons are combined with protons (H^+) to form H_2 (Equation 2.4) [33]. However, since potential difference is negative (-0.140 V vs. normal hydrogen electrode (NHE)), acetate cannot be oxidized to H_2 spontaneously. Therefore, additional energy has to be applied. Energy can be added by using an external power source or setting an electrode potential using a potentiostat [34]. The

small voltage requirement (0.140 V) in comparison to the voltage needed for H_2 production by electrolysis of water (1.220 V) makes the MEC an attractive system for H_2 production [35]. However, due to several potential losses, a minimum applied voltage of 0.250 V is needed in practice [36].

$$CH_3COO^- + 4H_2O \rightarrow 2HCO_3^- + 9H^+ + 8e^- \qquad E = -0.279 \text{ V vs. NHE (pH=7)} \qquad \textbf{EQUATION 2.3}$$

$$8H^+ + 8e^- \rightarrow 4H_2 \qquad E = -0.414 \text{ V vs. NHE (pH=7)} \qquad \textbf{EQUATION 2.4}$$

Despite the promising potential of BESs with the current density being improved in MFCs by 1000-fold during the previous year, power density rarely exceed 1 W m^{-2} for reactor volumes larger than 1 L [37]. Several limitations related to the anode, membrane and cathode components contribute to the diminishment of BES performance [10]. Nevertheless, the anode biofilm is the key factor in the most common BESs performance since it directly affects the electron transfer from bacteria to anode and consequently the performance of system [38]. Thus, research efforts to improve the anode performance are essential to increase the feasibility of practical applications of BESs [39, 40].

2.2. ANODE CHAMBER

Anaerobic anode compartment is one of the main components of BESs. Anode chamber requires a biodegradable substrate, a microbial community and an electrode (anode). Substrate oxidation by the microbial community that use the anode as an external electron acceptor is a shared principle by the most common type of BES [26].

The performance of the anode can be evaluated by two main efficiency parameters: the voltage efficiency and the coulombic efficiency (CE) [41]. Voltage efficiency is related to the internal losses, so-called overpotential, which lower the potential of the system. Overpotential is a measure of the energy lost in electron transfer reaction, *i.e.*, the difference between the theoretical potential at which the reaction occurs, and the observed potential of the electrode [27]. In a MFC, higher overpotential means that less energy will be recovered than the thermodynamically predicted, whereas in a MEC higher overpotential implies that the system will require more energy than thermodynamically expected to perform a reaction. These internal losses include: activation overpotential, ohmic losses and concentration overpotential [42].

Activation overpotential occurs during the transfer of electrons from the cell electron carrier to the anode surface [10]. The electrochemical and textural characteristics of the anode (*e.g.* area and roughness), as well as the anode potential, and the mechanism of electron transfer affect the extent of these losses [9]. At low current densities, activation overpotential is the dominant loss [40].

Ohmic losses, also called internal resistance occur on anode due to limitations in charge transport. These limitations are prompted by the electrodes and electrolyte´s resistance, presence of diffusion barriers (membrane) or high distance between anode and cathode [40]. Concentration overpotential is related to mass transfer resistance due to the concentration gradient of the reagents and products on the anode surface [10]. Enhance mass transport of substrate by stirring contribute to minimise the concentration overpotential [33].

CE is another important parameter for anode performance evaluation. CE represents the part of electrons present in the electron donor (substrate) that end up as electric current [43]. Low CE occurs if electrons produced during substrate oxidation are diverted to another electron acceptor (*e.g.* sulphur or nitrogen compounds) or to generate another product (*e.g.* CH_4) [44]. Since the anode chamber in BESs is anaerobic, methanogenic archaea can grow at the anode oxidising organic compounds and produce methane. The competition between EAB and methanogens can be analysed by CE assuming that no other electron acceptor than the electrode is present [41]. Thus, in order to improve the CE, the growth of other microorganisms that can compete for the substrate, should be minimized (*e.g.* lower the retention time of the anolyte) [45]. Further, the flow of electrons to other electron acceptors should be avoided with an effective oxygen barrier (*e.g.* a membrane between anode and cathode) [43]. Membranes separate the anode chamber from the cathode reactions, and also facilitate the transport of ions from anode to the cathode in order to maintain system neutrality [46]. However, membranes can increase the internal resistance of the system [47].

Despite the several losses identified at the anode of BES the characteristics of anode electrode material also play a significant role in the performance of the BESs [48].

2.3. ANODE MATERIALS

In order to increase BESs performance, novel anode materials have been investigated envisaging a reduction in manufacturing cost and operation expenses. The ideal anode materials require high electrical conductivity, high specific surface area accessible to microorganisms, high chemical

stability in the reactor solution, high biocompatibility and low cost [49]. In addition, it should also possess anti-corrosion properties and suitable mechanical strength and toughness [50]. The materials used for anodes in MFCs can also be applied in MEC [19].

Several anode materials have been tested, such as carbon, metal or composite materials as well as different surface modifications. Change the surface properties of the electrode can improve the performance by increasing the interactions of the anodic microorganisms with the electrode surface. Different pre-treatment strategies involving surface chemical modification (*e.g.* nitric acid) have been employed to improve the anode performance [51]. Further, different materials (*e.g.* conductive polymers) have been applied to the surface area [52].

2.3.1. Carbon anode materials

Carbon-based materials are the most commonly used materials in BESs, since they meet many of the requirements previously mentioned [30]. Graphite and carbon are the most widely used materials because of their high biocompatibility, their low overpotentials and their low costs [53]. Carbon-based materials commonly used at lab and pilot scale include: carbon cloth [54], carbon paper [55], graphite felt [56], graphite granules [57] and carbon mesh [58].

In 2007, Logan and co-workers reported that switching from planar structure to three dimensional anodes shown better system performance [59]. In this work, graphite brush anodes were tested for electricity production compared with a traditional carbon cloth. Three dimensional structures allow an increase of the electron transfer rate due to the higher electrode surface area accessible for microbial attachment [60]. Three dimensional anodes include: reticulated vitreous carbon [61], carbon sponge [62], graphite foam [63], granular carbon [64], graphite rod [65], among others.

Enlargement of the surface area for bacteria attachment and biofilm formation to increase the electron transfer rate is one of the most straight forward approaches to enhance the BES performance [66]. Furthermore, an porous three-dimensional structure is required to promote internal bacterial colonization and an efficient transport of substrates [67]. Three dimensional arrangement combined with a structured porosity prospects the development of high-performance anodes. However, large surface area does not necessarily mean that the area is accessible to exoelectrogens. Due to the typical bacteria size (1 μm to 3 μm) [68], only the external surface area and the surface area related with pores with a large diameter (macropores) and pores introduced by material assembly are useful for bacterial attachment [69]. The information provided in Table

2.1 demonstrates that, in general, a higher performance is obtained when using three-dimensional porous anodes.

TABLE 2.1 A brief account of different carbon-based anode materials used in microbial fuel cell research, and their performance.

Substrate	Anode	Current/ power density	Reference
Acetate	Carbon cloth	1.1 W m^{-2}	[59]
Acetate	Graphite brush	2.4 W m^{-2}	[59]
Acetate	Roughened graphite	4.6 A m^{-2}	[70]
Acetate	Glassy carbon rods	2.5 A m^{-2}	[71]
Acetate	Polycrystalline carbon rods	5.0 A m^{-2}	[71]
Acetate	Carbon fibre veil	7.1 A m^{-2}	[71]
Acetate	Graphite rod	11.2 A m^{-2}	[72]
Acetate	Carbon felt	12.1 A m^{-2}	[73]
Acetate	Macroporous carbon nanofibre	32.5 A m^{-2}	[72]
Acetate	Layered PAN-based fibres	20.0 A m^{-2}	[73]
Glucose	Carbon paper	0.6 W m^{-2}	[59]
Glucose	Carbon nanotube-sponge	21.3 A m^{-2}	[67]
Glucose	Carbon cloth	2.8 A m^{-2}	[74]
Glucose	Graphite brush	1.2 W m^{-2}	[59]
Glucose	Carbon nanotube-textile	7.2 A m^{-2}	[74]
Lactate	Graphite	0.1 A m^{-2}	[75]
Lactate	PAN-based carbon nanofibre	1.2 A m^{-2}	[75]

Among these, carbon-based fibres are promising electrodes for BESs due to their highly porous architecture [76]. Carbon-based fibres are a novel high-performance electrode composed by at least 92 % of carbon [77]. Figure 2.3, shows a scanning electron microscope (SEM) picture of a cellulose-based carbon fibre (manufactured by Mast Carbon International), displaying its typically cylindrical structure with a not completely smooth surface, since striations along the fibre axis are observable.

Carbon fibres produced by different precursors display different properties. Polyacrylonitrile (PAN), pitch and cellulose are the main precursors for carbon fibre production, since they demonstrate an

easy conversion to carbon, high carbon yield, and cost-effective processing [78]. Carbon fibres can be characterized in terms of final mechanical properties into ultra-high modulus (>500 GPa), high modulus (>300 GPa), intermediate modulus (>200 GPa), low modulus (100 GPa), and high strength (>4 GPa) carbon fibres [77].

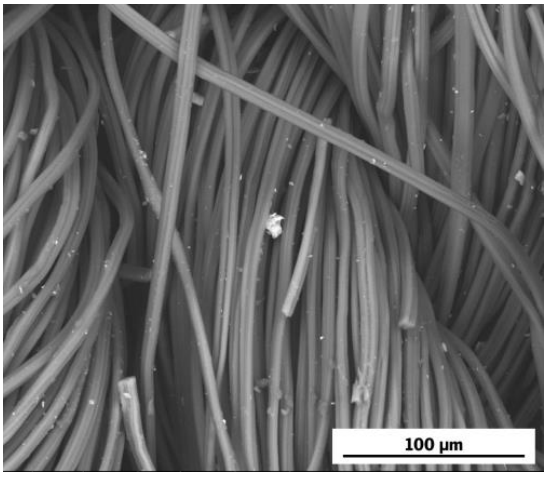


FIGURE 2.3 Scanning electron microscope (SEM) photograph of cellulose-based carbon fibres.

PAN-based carbon fibre

PAN ($(C_3H_3N)_n$) is formed from acrylonitrile by a polymerization reaction. PAN is the most common polymeric carbon fibre precursor material representing 90 % of the carbon fibre production [79]. PAN is converted to carbon fibres through a number of chemical steps [79, 78, 80]:

1) Production of PAN fibres step (Figure 2.4A): PAN is produced by polymerization of acrylonitrile. In wet spinning, PAN is first dissolved into a highly polar solvent (*e.g.* dimethyl formamide) to form a solution that is then filtered and extruded. The extruded PAN goes through a coagulation bath where the fibres in a gel state are formed. The coagulated fibres are then recovered, washed and drawn at temperature between 130 °C to 150 °C using glycerol.
2) Stabilization (cyclization and oxidation) step (Figure 2.4B): the linear chains of PAN-based polymer precursor are converted to a heteroaromatic structure through the change from C≡N to C=N. The PAN-based polymer precursor is converted in the presence of O_2 at temperature heating range of 200 °C to 300 °C. Acidic additives (*e.g.* itaconic acid) can be used to initiate the cyclization but also to lower the temperature of cyclization.

3) Carbonization (Figure 2.4C and Figure 2.4D) and graphitization step: the stabilized fibres are then heated in an inert environment (N_2) to 1500 °C (carbonization). Crosslinking reactions (dehydration and denitrogenation) take place in the oxidized PAN in which cyclized structures start to link up in the lateral direction forming a planar structure ("high strength" fibres). Maximum strength is observed at around 1500 °C. An additional heat treatment at temperature from 1600 °C to 1800 °C (graphitization) leads to higher modulus but lower the structural strength of carbon fibres.

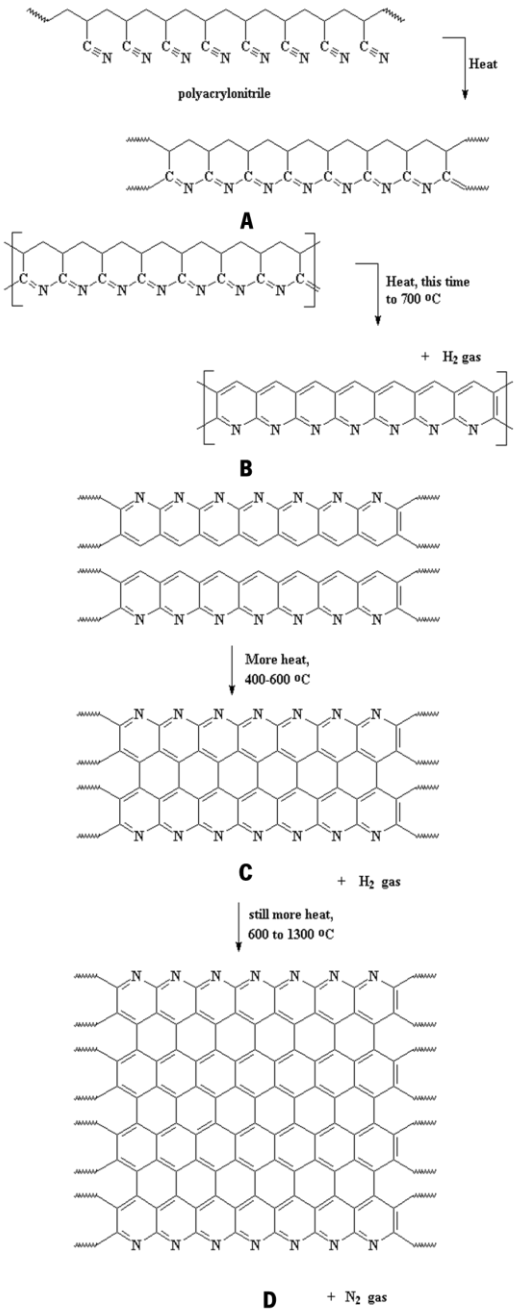


FIGURE 2.4 Chemical steps for synthesis of carbon fibres from polyacrylonitrile (PAN). **A)** Polymerization step; **B)** stabilization (cyclization and oxidation) step; **C)** and **D)** carbonization step. Adapted from Chung *et al.* [79].

Pitch-based carbon fibre

Pitch is composed of aromatic hydrocarbons and heterocyclic compounds. Pitch can contain more than 80 % carbon, and the composition of a pitch varies with its source: petroleum pitch (obtained by the distillation of crude oil), coal pitch (derived as a by-product from coal) and synthetic pitch (produced from synthetic polymers) [80].

Pitch-precursor is converted to carbon fibres through a number of chemical steps [79, 78, 80]:

1) Production of pitch-precursor fibres step: mesophase pitch is produced by the pitch polymerization. Mesophase is a crystalline liquid composed of aromatic hydrocarbons. Mesophase pitch is then melt spun into precursor fibres at around 300 °C. Melt spinning involves three steps: melting the precursor, extruding the melted into a gaseous atmosphere (*e.g.* N_2) and drawing the fibres as they cool.
2) Stabilization (infusiblization or oxidization) step: similarly to PAN-based fibres, the pitch-based fibres are stabilized before being exposed to the final high temperature carbonization treatment. The infusibilization or oxidation process comprises the fibres oxidation in the presence of O_2 at a temperature range of 200 °C to 400 °C.
3) Carbonization/graphitization step: carbon fibres are then produced by carbonizing the stabilized fibres at temperature between 1500 °C to 1800 °C in an inert atmosphere. An additionally graphitization step up to 3000 °C can be applied in order to obtain high moduli carbon fibres.

Cellulose-based carbon fibre

Cellulosic fibres including viscose, cotton, rayon, sisal, and linen have been studied as carbon fibre precursors. Among them, rayon has been the most extensively used [77]. Cellulose-precursor is converted to carbon fibres through a number of chemical steps [77, 78]:

1) Production of cellulose-precursor fibres step: rayon is produced from cellulose pulp by spinning. Insoluble cellulose is treated with sodium hydroxide (NaOH) to convert the cellulose to alkali cellulose and carbon disulphide (CS_2) to form cellulose xanthate. The xanthated cellulose is dissolved in NaOH and extruded into a coagulation bath containing sulphuric acid (H_2SO_4). The xanthated cellulose precipitates is then recovered from the coagulation bath.
2) Stabilization step: unlike PAN and pitch precursors, cellulose-based fibre need to be oxidised to increase the carbon yield, which is usually preformed in presence of O_2 at

temperature of 400 °C. During this treatment carbon monoxide (CO), CO_2 and other carbon containing gases are released and begins the aromatization of the structure.

3) Carbonization/graphitization step: stabilized fibres are then carbonized in an inert atmosphere at temperature up to 900 °C to form carbon fibres. The carbonized fibres can be posteriorly submitted at temperatures between 900 °C to 3000 °C (graphitization) to obtain higher modulus fibres.

Carbon fibre derived from other precursors

Several other carbon fibre precursors comprising low cost, high carbon content and bio-renewability have also been investigated. Bio-renewable lignin has been investigated as a potential precursor material for carbon fibre as it is the major by-product from chemical pulping processes [81]. Other natural bio-polymer such as silk [82], chitosan [83], and eucalyptus tar pitch [84] have also been investigated as precursors for carbon fibres. Furthermore, other synthetic polymers have been investigated as an alternative precursors such as, polyethylene [85], polystyrene [86] and phenolic resins [87], among others. Phenolic resins present several advantages such as versatility, low cost, anti-corrosion properties and low toxicity [88]. Phenolic-precursor is converted to carbon fibres by the reaction of phenol with formaldehyde in the presence of an acid catalyst. A melt spun novalac resin is obtained and then heat treated in an inert atmosphere at 700 °C to achieve a carbon content of 95 %. The carbonized fibres can be treated at temperatures up to 1700 °C (graphitization) to increase the carbon content to 100 %, but decreasing its structural strength [89].

2.3.2. Metal anode materials

Metal materials have been tested as anode due to conductivity properties, which are higher than the achieved by carbon materials. Several noble metal materials such as, gold [90], titanium [70] and copper [91] have been used as anode material. Noble metal materials decrease the internal resistance of the BES, although their high cost and corrosive nature are considered unsuitable as anode material application [48, 92]. In contrast, stainless steel has been employed as anode material due to its low cost and resistance to corrosion [50]. However, stainless steel also presents some limitations due to their smooth surface, which leads to a fragile surface adhesion by the EAB [92].

2.4. SURFACE ANODE MODIFICATIONS

As previously discussed, an efficient anode should meet some key requirements, such as high biocompatibility, high electrical conductivity and high surface area for bacterial attachment in order to improve the overall performance of the BESs [49]. Changing the surface of the carbon electrodes may improve the performance of the system by increasing the interactions of the EAB with the electrode surface [93] or by increasing the electron transfer rate [69].

2.4.1. Chemical anode modification

Electrochemical oxidation is an effective and cost-efficient method for anode modification by introducing specific functional groups on electrode surface improving the bacterial attachment and consequently facilitating the electron transfer process [50]. Three different electrolytes, nitric acid (HNO_3), ammonium nitrate (NH_4NO_3) and ammonium persulfate ($(NH4)_2S_2O_8$) were studied for surface modification of carbon mesh electrode [94]. Among these electrolytes, the MFC using carbon mesh modified with nitric acid achieved almost 1.5-fold higher power density compared to the MFC using unmodified carbon mesh. In general, all the modified electrodes outperformed the unmodified carbon mesh, due to the decrease in their internal resistance improving the electron transfer rate [94].

In another study, nitric acid, ethylenediamine and diethanolamine were tested for chemical modification of polyaniline (PANI) anode [51]. Based on power density curves, MFC using PANI modified with ethylenediamine demonstrated the highest power density, corresponding to an increase of 1.5-fold in comparison to a MFC using unmodified PANI. MFC using PANI modified with ethylenediamine displayed the lowest internal resistance, when compared to the unmodified PANI. Similarly to the previous study the improvement on MFC performance was achieved by decreasing the internal resistance [51].

2.4.2. Anode modification with carbon nanotubes/carbon nanofibres

Carbon nanotubes (CNT) demonstrate a high potential to be used as electrode material [95]. Furthermore, CNT has been employed to modify the anode electrode surface due to this high electrical conductivity and large surface area [96, 48]. In order to improve the performance of the traditional graphite felt, researchers have developed a modified graphite felt coated with CNTs [97]. The CNTs were electrophoretically immobilized onto graphite felt by applying an anode current.

The maximum power density obtained with the CNT graphite felt coated was almost 4.5-fold higher when compared to the unmodified graphite felt anode maximum power density. CNT coating exhibited a considerable improvement of the attached bacteria attributed to high effective surface area, and to the one-dimensional nanoscale morphology of the CNTs [97]. In other study, a CNT-sponge composite was prepared by immersing the polyurethane sponges into a CNT solution [67]. Compared with a CNT-coated textile electrode, CNT-sponge electrodes shown a 2-fold higher current density due to the lower internal resistance and macroporous structure (pores up to 1mm in diameter) [67]. Wang and co-workers investigated the growth of carbon nanofibres (CNFs) onto stainless steel mesh via a chemical vapour deposition [76]. The results shown that the current density obtained with CNFs onto stainless steel was almost 200-fold higher compared with the current density obtained with the unmodified stainless steel. The great increase in current density comparing to the unmodified stainless steel was reached by the porous CNFs layers, which provided higher surface area for bacterial attachment [76].

2.4.3. Anode modification with metal oxides

Anode surface modification by metal oxides have been described to enhance the performance of BESs by reducing the ohmic loss, followed by the improvement of bacterial cell adhesion [50]. Titanium (Ti) [98], tin (Sn) [99], manganese (Mn) [100] and iron (Fe) [55] oxides, among others, have been used for anode surface modification. Phansroy and co-workers tested the potential effect of iron oxide (FeO_2) immobilization on the surface of non-woven carbon fibres to improve the performance of the system [101]. The performance was assessed by the amount of biofilm and the number of living cells of *Shewanella oneidensis* on the electrode. Experimental FeO_2 was immobilized on carbon fibres by electroplating technique. *S. oneidensis* was found to be able to form a biofilm on this modified FeO_2 carbon fibre anode, thus displaying biocompatibility, and good surface properties for bacteria cell adhesion [101].

In another study, the surfaces of commercial activated carbon, carbon paper, and carbon cloth were modified using FeO_2 [102]. Iron was fixed to the electrodes surface by an electrodeposition technique. Compared with the unmodified anode materials, the proposed treatment process led to an increase of the maximum produced power by 19 %, 48 % and 66 % for the treated activated carbon, carbon cloth, and carbon paper anodes, respectively. The increase of the modified electrode hydrophilicity was also described due to the chemical composition modification of the anodes surface, as well as the increase of the surface roughness [102]. Hydrophilic electrode

surface promotes the contact of the microorganisms with the electrode surface [103]. Furthermore, the electrodepositing of iron led to an higher electrical conductivity due to the decrease of the internal resistance, which resulted in an higher electron transfer [102]. Guo and co-workers reported a heat treatment as an effective method to increase the bioelectrocatalytic performance of stainless steel [104]. Heat treatment of stainless steel felt (600 °C for 5 min) generated an iron oxide rich layer on electrode surface. The results showed that the iron oxide layer considerably enhanced the biocompatibility promoting the biofilm development on electrode surface. Thereby, a considerably improving of the current production was observed with heat-treated electrodes [104].

2.4.4. Anode modification with conductive polymers

Coating of the anode surface using conductive polymers is an alternative method for anode surface modification. Conductive polymers for anode surface modification have been studied to improve the system performance by enhancing bacterial attachment [50]. Several polymers such as PANI [97], polypyrrole (PPY) [105], hydrogels [106], poly(aniline-co-o-aminophenol) [69], among others, have been tested to modify the anode surface in order to improve the BESs performance. PANI and PPY have been the mostly studied polymers due to their high electrical conductivity, good redox properties and straight forward synthesis [92]. Various PANI modified anodes have been developed, including CNT/PANI carbon paper [107], PANI modified glassy carbon [108] and tartaric acid doped PANI modified carbon cloth anode [109]. Similarly, various PPY modified anodes have been produced such as PPY hydrogels/CNTs [110], PPY coated CNTs [105] and polyurethane/graphite/PPY [111]. Li and co-workers tested the effect of two conductive polymer materials, PANI and poly(aniline-co-o-aminophenol) to improve the carbon felt anode performance [52]. The results showed that the maximum power density obtained with MFCs using PANI and poly(aniline-co-o-aminophenol) were 0.027 W m^{-2} and 0.024 W m^{-2}. Comparing with unmodified MFC (0.020 W m^{-2}), the power density increased by 35 % and 18 % for PANI and poly(aniline-co-o-aminophenol) MFCs, respectively [52].

2.4.5. Anode modification with external mediators

External mediators can be immobilized onto the anode surface to improve the electron transfer rate, since the electron transfer is usually the rate-limiting step during the BESs operation [50]. Incorporation on the anode of Mn^{4+}, Fe^{3+}, Mn^{2+}, Ni^{2+} and neutral red, among others, as electron

mediators has been evaluated [112, 113]. Liu and co-workers tested six different electron mediators, 2-hydroxy-1, 4-naphthoquinone, methyl viologen, neutral red, methylene blue, 1, 5-dichloroanthraquinone and anthraquinone immobilized onto the activated carbon (AC) pressed on nickel foam [114]. The results shown that the MFC using 2-hydroxy-1, 4-naphthoquinone doped AC anode exhibited the best performance, which is comparable with MFC using methyl viologen doped AC anode. The 2-hydroxy-1, 4-naphthoquinone coated AC anode enhanced charge transfer and provided more reactive sites on the anode surface, being an attractive alternative to methyl viologen due to its lower toxicity [114].

2.5. ELECTROCHEMICALLY ACTIVE BACTERIA

In MFCs which convert chemical energy into electrical energy, the anode is the electrode that receives the electrons released during the oxidation of the biodegradable substrate. In MECs, which convert electrical energy into chemical energy, H_2 production at the cathode occurs through the oxidation of organic compounds at the anode. Similar to the MFCs, anode is the electrode used as electron acceptor from degradation of substrate. In both applications, the use of an insoluble electron acceptor requires that the microorganisms have the ability to transfer the electrons to an electrode. Most microorganisms are only able to use soluble electron acceptors, however some microorganisms that have the ability of use insoluble electron acceptors, are usually present in environments deprived of soluble electron acceptors. EAB (also known as electrogens, electricigens, exoelectrogens or anode respiring bacteria) have the ability to transfer electrons from the substrate to a insoluble anode surface [115]. EAB can be found in a wide range of environments, including ocean and marine sediments [116, 117, 118]. Some examples of isolated EAB are presented in Table 2.2. The most extensively studied EAB are *S. oneidensis* and *G. sulfurreducens* [119].

2.6. EXTRACELLULAR ELECTRON TRANSFER MECHANISMS

Currently, three extracellular electron transfer (EET) mechanisms have been described, direct electron transfer (DET), mediated electron transfer (MET) and direct interspecies electron transfer (DIET) [127].

TABLE 2.2 Isolated electrochemically active bacteria (EAB) divided by their class, substrate preference and performance.

Class	EAB	Substrate	Current/ power density	Reference
δ Proteobacteria	*Geobacter metallireducens*	Acetate	40 mW m^{-2}	[120]
	Geobacter sulfurreducens	Acetate	64 mA m^{-2}	[25]
	Desulfobulbus propionicus	Lactate Propionate	28 mA m^{-2} 27 mA m^{-2}	[121]
γ Proteobacteria	*Shewanella putrefaciens*	Lactate	8 mA m^{-2}	[24]
	Klebsiella pneumoniae	Glucose Starch	410 mW m^{-2} 216 mW m^{-2}	[122]
	Pseudomonas aeruginosa	Acetate	125 mA m^{-2}	[123]
α Proteobacteria	*Gluconobacter roseus*	Glucose	213 mW m^{-3}	[124]
	Acetobacter aceti	Glucose	396 mW m^{-3}	[124]
β Proteobacteria	*Rhodoferax ferrireducens*	Glucose	31 mA m^{-2}	[63]
	Comamonas denitrificans	Acetate	35 mW m^{-2}	[125]
Holophagae	*Geothrix fermentans*	Acetate Propionate Lactate	13 mA m^{-2} 50 mA m^{-2} 42 mA m^{-2}	[126]
Clostridia	*Clostridium acetobutylicum*	Acetate	14 mA m^{-2}	[123]

2.6.1. Direct electron transfer

DET implies a physical contact between the cell membrane or an organelle with the anode surface [128]. During this process there are no intermediate species involved in the electron transfer from the microorganism to the electrode. DET may occur by the c-type cytochromes associated with bacterial outer membrane of the cell or by electrically conductive pili or nanowires [129] (Figure 2.6A). *G. sulfurreducens* and *S. oneidensis* are considered as EAB models, and their EET mechanisms have been intensively studied to better understand the mechanism of DET. The complete genome sequence of these two microorganism allowed the thoroughly analysis of their EET mechanism [103].

Several studies have described the c-type outer membrane cytochromes (Omcs) associated to the *G. sulfurreducens* and *S. oneidensis* cell membrane as the responsible organelle for the DET between the cell and the anode surface [130]. In *G. sulfurreducens*, it has been proposed that the electron flows from the inner membrane protein MacA to the periplasmic protein PpcA, which

subsequently transfers the electrons to the Omcs at the cell surface [130] (Figure 2.5A). Different Omcs were identified in the membrane of *G. sulfurreducens* such as, OmcB, OmcS, OmcE, or OmcZ that play a different role on EET [131]. For example, several studies have demonstrated the prominent role of OmcZ in the electrochemical communication between *G. sulfurreducens* and the anode. It was reported that the current production was severely inhibited when the OmcZ was deleted, compared to the other Omcs [131]. Relatively to OmcS of *G. sulfurreducens*, this protein has been associated to the pili and contributes to the electron transfer through them to anode surface [132].

On the other hand, in *S. oneidensis*, metal-reducing (Mtr) respiratory pathway is directly involved in the EET between the cell and the anode surface [133]. Mtr consists of an inner membrane-associated quinol oxidase (CymA) and an outer-membrane MtrCAB-OmcA complex [127]. The electrons flow to the inner membrane CymA, then to protein MtrA, which subsequently transfers the electrons to the MtrC and OmcA (Figure 2.5B) [133]. Several studies have been demonstrating the involvement of MtrC and OmcA in EET between the cell and the anode surface, being the MtrC known for playing a major role [134].

In monolayer biofilms, the cells remain attached to the anode surface transferring the electrons by direct contact of the c-type Omcs with the anode surface, however, in multiple-layer biofilms, only a few cells have direct access to the anode surface. In this cases, some EAB such as S*. oneidensis* and *G. sulfurreducens* develop pili nanofilaments, known as microbial nanowires, which enable long-range EET by forming a physical connection between the EAB and the anode surface [135]. Nanowires are conductive filaments of proteins that grow on the outer surface of the cell [136]. The role of nanowires in EET to the anode surface has been mainly studied for *G. sulfurreducens* [137]. Conductivity measurements performed to the nanowire of *G. sulfurreducens* demonstrated that it was highly conductive [103, 135].

Two different theories have been presented to elucidate the role of nanowires in EET. Some authors have described that electron transport in nanowire occurs through electron tunnelling from cytochrome to cytochrome present in the surface of the nanowire [138], while other authors propose that nanowire possess a metallic-like conductivity similar to the conductivity found in synthetic conducting polymers [136]. Malvankar and co-workers, suggest that the conductivity of the nanowires is not due to the cytochromes present at the bacterium surface, since the cytochromes are spaced too far from each other to enable electron hopping [137]. Furthermore, these authors demonstrated that adding a c-type cytochrome denaturant did not diminish the

conductivity of the nanowire [139] Thus, additional investigations are required to elucidate the features that confer conductivity to the nanowires of *G. sulfurreducens*.

As found for *G. sulfurreducens,* it was observed that *S. oneidensis* also produces extracellular appendages when it is cultured in electron acceptor limiting conditions [140]. However, Pirbadian and co-workers clarified that *S. oneidensis* does not produce conductive nanowires, which only consist in extensions of outer membrane and periplasm that include its associated cytochromes [141]. Furthermore, the authors identified MtrC and OmcA along the nanowire surface extension. Interestingly, Gorby and co-workers demonstrated that the deletion of MtrC and OmcA produced nonconductive nanowires [140]. Thus, in contrast to the *G. sulfurreducens* nanowires that possess a theoretical intrinsic metal-like conductivity, *S. oneidensis* nanowire conductivity is Omcs dependent [103].

DET to the electrodes has also been reported for various other microorganisms, such as *Desulfobulbus propionicus* [121], *Klebsiella pneumoniae* [142], *Geobacter metallireducens* [120] and *Enterobacter aerogenes* [143].

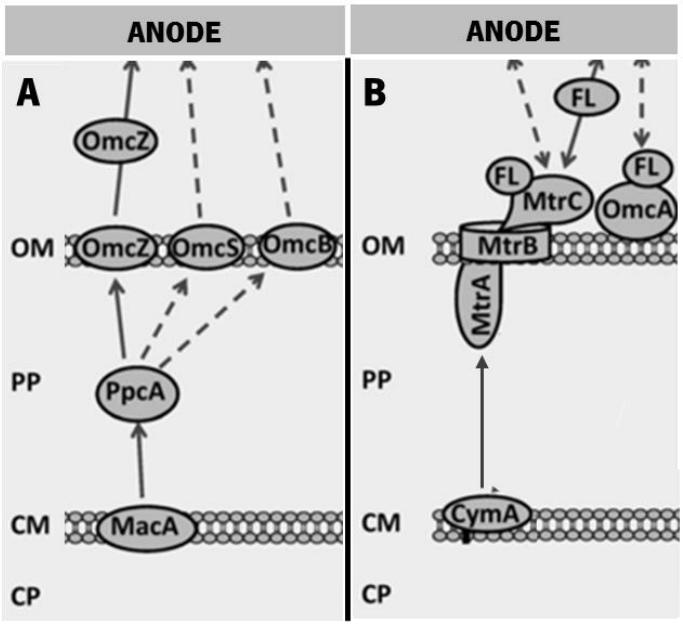


FIGURE 2.5 Proteins involved in direct electron transfer (DET) mechanism, particularly in **A)** *Geobacter sulfurreducens* and **B)** *Shewanella oneidensis*. FL- flavins; CP- cytoplasm; PP – periplasm; OM – outer membrane. Solid line represents the main route and dotted line represents the minor path. Adapted from Sydow *et al.* [127].

2.6.2. Mediated electron transfer

EAB that are not capable of using a DET route or are not in physical contact with the anode surface (planktonic cells) utilize an EET mechanism mediated by electron mediators (Figure 2.6B). Ideally electron mediators should a) form a reversible redox couple at the electrode, b) not interfere with the cellular metabolism, c) be stable in both the oxidized and the reduced state and d) be stable during long-term redox reaction [133,144]. Electron mediators can be self-secreted by the microorganism (endogenous mediators) or can be artificial (exogenous mediators).

Endogenous redox mediators

Several species of EAB such as*, S. oneidensis, Pseudomonas aeruginosa, Geothrix fermentans*, self-secret soluble electron mediators. The model EAB, *S. oneidensis*, is known to use self-secreted flavins (riboflavin and flavin mononucleotide) to mediate EET [145]. Although, *S. oneidensis* is able to develop a biofilm on anode surface and use DET via MtrC, experiments have demonstrated that up to 75 % of EET occurs via flavin-based [145]. *P. aeruginosa* showed the ability to transfer the electrons to anode surface by producing pyocyanin and phenazine-1-carboxamide [146]. Rabaey and co-workers demonstrated that strains unable to synthesis of pyocyanin and phenazine-1-carboxamide, only achieved a 5 % power output in comparison to the wild type strain. Furthermore, this study demonstrated the power output was re-established to 50 % after pyocyanin addition [146]. *G. fermentans* has been also reported to self-secret electron mediators [126]. To date, riboflavin and a unknown mediator were detected in *G. fermentans* cultures [147].

In addition, primary metabolites such H_2 and H_2S can be used as electron mediator [42]. Electrons are transferred to the electrode via the oxidation of reduced metabolites produced during fermentation. Schröder and co-workers used *Escherichia coli* K12 for generation of H_2 gas, which was oxidized at anode surface [148]. Energy production using H_2 as an electron mediator is only possible when a catalytic anode is employed. In this study, a polyaniline coated platinum electrode was used [148].

Exogenous electron mediators

Nevertheless, some microorganisms cannot transfer electrons directly to the electrode and it is possible to promote electron transport with the addition of electron mediators (*e.g.* methyl viologen, humic acid, sulphide, cysteine and neutral red) [36]. However, such artificial electron mediators have a poor long-term stability and are typically toxic to humans, thus greatly limiting their

application [136]. Further, artificial electron mediators are only viable in processes with relatively long residence times (batch mode operation), otherwise (continuous mode operation) mediator will be washed out. Their use is currently declining, although some exogenous mediators are still being used to improve MFC performance, specifically methylene blue [149,150] and neutral red [151].

2.6.3. Direct interspecies electron transfer

Microorganisms can also exchange electrons directly through the direct interspecies electron transfer (DIET) mechanism (Figure 2.6C). DIET was firstly reported by Summer and co-workers in a co-culture of *G. sulfurreducens* and *G. metallireducens,* where ethanol metabolism favoured the formation of electrically conductive aggregates, which further evinced the exchange of electrons through pili in the aggregates [132]. DIET was also reported by Rotaru and co-workers in a co-culture of *G. metallireducens* and *Methanosarcina barkeri* [152]. *M. barkeri* was co-cultured with *G. metallireducens* using ethanol as the electron donor. The results showed that *G. metallireducens and M. barkeri* formed aggregates that shared electrons during the conversion of ethanol to methane. DIET through electron transfer along pili was confirmed by using co-cultures with a pilA-deficient *G. metallireducens.* This co-culture failed to metabolize ethanol or produce methane [152].

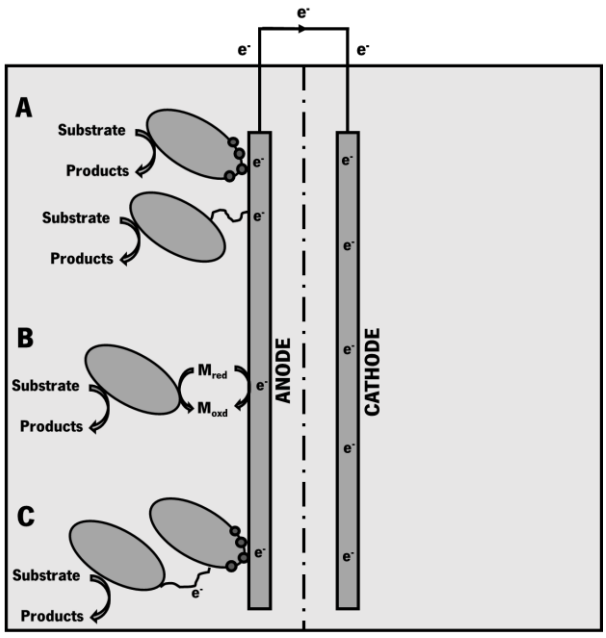


FIGURE 2.6 Models for extracellular electron transfer (EET) mechanisms occurring in bio-anodes: **A)** direct electron transfer (DET) mechanism by outer membrane cytochromes (Omcs) or by electrically conductive pili (nanowire); **B)** mediated electron transfer (MET) mechanism by using endogenous or exogenous electron mediators and **C)** direct interspecies electron transfer (DIET) from cell to cell through conductive pili.

2.7. APPLICATIONS OF BES

As previously mentioned, the popularity of research and development of BESs is increasing rapidly, as clearly seen in Figure 2.2, which shows the two-fold increase of MFCs and MECs scientific papers during a six-year period (2010 to 2016).

Power output produced by BESs, namely by MFCs, is gradually being enhanced over the last decade [153]. Several developments in BESs technology concerning various parameters are contributing for the increase in power generation, specifically, different MFCs designs and configurations [154], improved electrodes and electrode surface modifications [93], better knowledge of the microbial communities [44] and optimized operational conditions [155], among others.

According to the reduction reaction at the cathode, a BES can be used for a wide range of applications. Figure 2.7A displays the research trends on the different types of BESs. If the main function of the cathode is to produce biofuels and synthetize valuable products such as hydrogen peroxide (H_2O_2) [21], acetate [156] or ethanol [157] the BESs can be named as microbial electrosynthesis cell (MES). However, if the main function of the cathode is to reduce pollutants such as uranium [158] or petroleum hydrocarbons [159], the BES can be named as microbial remediation cell (MRC). Another type of BES, named microbial desalination cell (MDC) allows to remove salt from water without continuous energy input [160]. Benthic/sediment microbial fuel cell (BMFC) consists in a BES based on MFC concept that generate electrical current from the natural redox gradients that commonly occur across the sediment/water interface [161]. Integrating the reverse electrodialysis with a MEC concept was possible to develop a BES able to perform reverse-electrodialysis to produce H_2 without any external power supply, a microbial reverse electrodialysis cell (MREC) [162]. Photosynthetic microbial fuel cell (PMFC) is a BES which comprises the use of synergistic relationships between photosynthetic organisms and EAB for the production of electricity or valued-added chemicals [163].

Depending of the type of BES, these systems can be used for various applications. Figure 2.7B shows the number of articles per year on different applications. Unexpectedly, the data indicates electricity generation as the main application of BES, since the fundamental purpose of BES is to recover electricity from organic matter. Wastewater treatment is the second main application of BES. The global market for water and wastewater technology is set to expand at an annually at rate of 5 %, representing an increase from $72 billion in 2016 to an estimated $92 billion in 2021

[164]. The estimated growth on water and wastewater treatment market highlights the excellent prospects for BESs application to wastewater treatment.

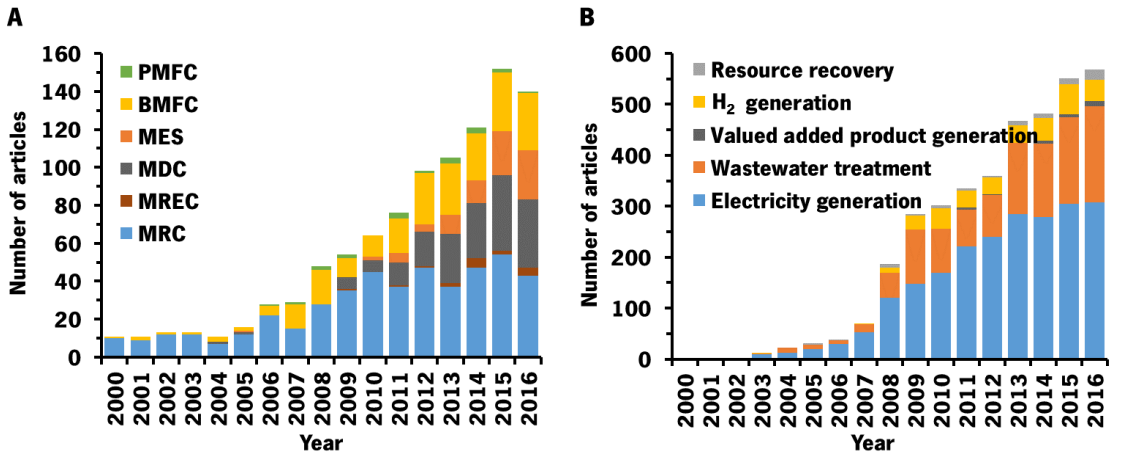


FIGURE 2.7 Research trends on **A)** different type of BESs (PMFC: photosynthetic microbial fuel cell; BMFC: benthic/sediment microbial fuel cell; MES: microbial electrosynthesis cell; MDC: microbial desalination cell; MREC: microbial reverse-electrodialysis cell and MRC: microbial remediation cell) and **B)** different BESs applications.

Pham and co-workers compared MFC performance to conventional anaerobic wastewater treatment [165]. The authors reported that MFCs presented some advantages when compared to anaerobic wastewater treatment such as production of electricity directly from organic waste, and no gas treatment requirement. Furthermore, MFCs can operate at low temperatures and low COD concentration [166]. Also, wastewater treatment in MFCs allows nutrient recovery, such as N [167]. This opportunity to combine simultaneous electricity generation and wastewater treatment in BESs have been contributing for the development of MFCs. Using MFC to recover energy from wastewater was first presented by Habermann in 1991 [168]. Different types of wastewaters, *i.e.* domestic, agricultural and industrial wastewaters, containing organic compounds that needed to be removed prior to their discharge into environment have been tested. An overview of various wastewaters used as feed sources for MFCs is presented in Table 2.3.

TABLE 2.3 Various wastewaters used as anodic fuel in MFCs and their performances.

Wastewater	Inoculum	Anode	COD removal	Current/power density	CE	Reference
Cereal-processing wastewater	Anaerobic sludge	Toray carbon paper	95 %	81 mW m^{-2}	40 %	[169]
Swine wastewater	Swine wastewater	Carbon paper	90 %	101 mW m^{-2}	7 %	[170]
Hospital wastewater	Anaerobic and aerobic mix sludge	Graphite rod packed with graphite granules	N.A.	14 mW m^{-3}	13 %	[171]
Brewery wastewater	Brewery wastewater	Carbon cloth	85 %	155 mW m^{-2}	9 %	[172]
Paper recycling wastewater	Paper recycling wastewater	Graphite-fibre brush	76 %	506 mW m^{-2}	16 %	[166]
Chocolate industry wastewater	Activated sludge	Graphite rods	75 %	2487 mA m^{-2}	N.A.	[173]
Fermented apple juice	garden compost	Graphite felt	N.A.	44 mW m^{-2}	N.A.	[174]
Cattle dung	Anaerobic sludge	Carbon brushes with graphite granules	74 %	200 mW m^{-3}	3 %	[175]
Potato wastewater	Anaerobic sludge	Graphite granules	80 %	0.03 mA m^{-2}	2 %	[176]
Slaughterhouse wastewater	Granular anaerobic sludge	Carbon cloth	93 %	1290 mA m^{-2}	64 %	[177]
Animal carcass wastewater	Anaerobic granular sludge	Graphite felt packed with granular activated carbon	51 %	2190 mW m^{-3}	0.3 %	[178]

N.A. not available

TABLE 2.3 Various wastewaters used as anodic fuel in MFCs and their performances (continued).

Wastewater	Inoculum	Anode	COD removal	Current/power density	CE	Reference
Mustard tuber wastewater	Mustard tuber wastewater	Non-wet proof carbon cloth	85 %	246 mW m^{-2}	12 %	[179]
Cheese whey wastewater	Digested sludge	Carbon fibre brush	54 %	1300 mW m^{-3}	4 %	[180]
Winery waste	MFC effluent	Graphite fibres	90 %	262 mW m^{-2}	15 %	[181]
Dairy industry wastewater	Activated sludge	Graphite plate	91 %	621 mW m^{-2}	37 %	[182]
Domestic wastewater	Primary sludge	Non-wet proof carbon	89 %	251 mW m^{-2}	7 %	[183]
Food industry wastewater	Food industry wastewater	Carbon cloths	63 %	112 mA m^{-2}	N.A.	[184]

N.A. not available

Wastewater treatment can also be achieved in other BESs, such as MECs, comprising the H_2 production by biocatalysed electrolysis [32]. An overview of various wastewaters used to feed MECs is presented in Table 2.4.

The data displayed in Table 2.3 and Table 2.4, shows that, in general, low CE is an issue in BESs treating real wastewater. Low CE in BESs suggest that a significant portion of the electrons released during oxidation of the organic compounds were not recovered in the form of energy [178]. It could be mainly attributed to: a) diversion of electrons into non-EAB biomass growth [55] or b) substrate consumption via other metabolic pathways, such as, methanogenesis [185], nitrate and/or sulphate reduction [186].

Furthermore, substrate's electrical conductivity may also influence BESs performance. Liu and co-workers examined the effect of substrate ionic strength, electrode spacing, and temperature on electricity generation [187]. The authors demonstrated that the maximum power density was increased about 85 % when the substrate's ionic strength was increased by adding sodium chloride (NaCl). CE may have also increased slightly with the addition NaCl as a consequence of the decrease in the internal resistance [187]. However, adding salts and buffers to increase the ionic strength of wastewater, can be highly expensive and therefore unfeasible.

Domestic and several industrial wastewaters exhibit low conductivities, typically in the order of only 1 mS cm^{-1} [53]. However, urine properly separated from faecal matter, at its source, presents an electrical conductivity ranging from 7 to 20 mS cm^{-1}, thus it is a good candidate to be use as substrate in BESs [188]. Furthermore, the electrical conductivity of urine increases approximately 3-fold after 4 days of its collection. This increase is due to the breakdown of urea and consequent release of ions (*e.g.* ammonium ions). Finally, this source separated urine not only fuels the energy production at BESs, but also implies significant cost reduction in wastewater treatment plant process, by diminishing the nutrient load of the effluent [5]. Furthermore, the nutrients present in urine, namely P and N, become available for recovery and may be used in agricultural applications [2].

TABLE 2.4 Various wastewaters used as anodic fuel in MECs and their performances.

Wastewater	Inoculum	Anode	Applied voltage	COD removal	Current density	H_2 production rate	H_2 content	CE	Reference
Fermentation effluent	Domestic wastewater	Carbon fibre brushes	0.9 V	82 %	3.8 A m^{-2}	0.35 L g^{-1} (COD)	60 %	76 %	[189]
Industrial wastewater	Industrial wastewater	Graphite fibre brushes	0.7 V	89 %	2.1 A m^{-2}	1.80 m^3 m^{-3} d^{-1}	32 %	10 %	[190]
Food processing wastewater	Food processing wastewater	Graphite fibre brushes	0.7 V	67 %	2.4 mA m^{-2}	0.41 m^3 m^{-3} d^{-1}	86 %	35 %	[190]
Potato wastewater	Potato wastewater	Graphite fibre brushes	0.9 V	79 %	20 mA m^{-2}	0.74 m^3 m^{-3} d^{-1}	73 %	80 %	[191]
Molasses wastewater	Domestic wastewater	Graphite-fibre brush	0.8 V	N.A.	179 A m^{-3}	1.82 m^3 m^{-3} d^{-1}	35 %	95 %	[192]
Domestic wastewater	Domestic wastewater	Nonwet-proofed carbon paper with graphite granules	0.5 V	95 %	471 mA m^{-2}	0.15 L g^{-1} (COD)	16 %	23 %	[193]
Swine wastewater	Swine wastewater	Graphite-fibre brush	0.5 V	19 %	106 A m^{-3}	0.90 m^3 m^{-3} d^{-1}	58 %	29 %	[194]
Winery wastewater	Raw wastewater	Graphite fibre brushes	0.9 V	62 %	7.4 A m^{-3}	0.28 m^3 m^{-3} d^{-1}	33 %	N.A.	[195]
Fermented landfill leachate	Anaerobic digester sludge	Graphite fibres mounted on a stainless steel rod	-0.3 V	26 %	16 mA m^{-2}	N.A.	N.A.	68 %	[196]

N.A. not available

2.8. URINE AS A RESOURCE

Urine is a liquid waste stream that contributes to around 1 % of the total volume of municipal wastewater. Despite its small volume, urine contains most of the nutrients excreted by humans, representing about 75 % of the N load and around 50 % of the P load in domestic wastewater [197]. Furthermore, it has a high BOD_5, 67 % of the measured COD (9.0±4.1 g L^{-1}), which demonstrate the high biodegradability of the organic compounds found in urine [198]. Analysis of the relative contribution of the organic compounds to the urine COD showed that it is composed by aliphatic compounds (73 %), creatinine/creatine (21 %), aromatic and hetero aromatic compounds (3 %) and proteins (3 %) [198]. Due to these characteristics, urine can be considered as a valuable resource for N and P recovery and for energy production.

P is known to readily precipitate at certain process conditions, forming a compound with a particular interest for agricultural application, named struvite (magnesium ammonium phosphate hexahydrate (MAP) ($NH_4MgPO_4 \cdot 6H_2O$)) [3]. Accumulation of struvite is known to cause operational problems due to clogging on effluent piping walls, in deposits, in pumps, aerators, valves, and other equipment, thus damaging the piping system capacity of WWTPs and increasing the maintenance costs [199, 200]. Therefore, separation of urine from other wastewater streams is a highly interesting procedure to simultaneous recovery of valuable nutrients, and considerably reduce operational costs.

Urine separation in specific No-Mix toilets is a promising technology aiming to divert urine from faeces without flushing water. According to Lienert and Larsen, around 80 % of NoMix toilets users liked the technology and 75 % to 85 % were satisfied with design, hygiene, smell, and seating comfort [201]. Fertilizers recovered from urine are also well accepted by the general public, since 85 % like the idea and nearly 70 % are willing to purchase such food [201]. However, NoMix-toilets users encountered problems mainly related with phosphate precipitation causing blockages, or the necessity to sit to urinate. The disposal of toilet paper in a separate bin is also reported as a challenge to NoMix technology acceptance [201]. Thus, No-Mix technology requires further developments not only technical ones, but also in the sociological area to convince people that the concept makes sense for ecological reasons.

Source separated urine can be treated and/or reused by an extensive range of applications [7]. A few studies have investigated the recovery of nutrients (*e.g.* ammonia [6, 167] and phosphorous

[202, 203], allied to the treatment of urine with simultaneous energy production in BESs [167, 204].

2.8.1. Phosphorus recovery from urine

P, similarly to N, is an essential nutrient for life [205]. However N and P discharged in excess into the environment lead to eutrophication which dramatically reduces the biodiversity in the receiving waters [206]. The main source of P is rock phosphate, which is still currently being exponentially prospected. P maximum exploration peak was estimated to occur by 2035 [207]. However, it is expected that P reserves will be depleted within 50 to 100 years [1]. P crystallization processes from effluents allows P recovery as useful products (*e.g.* struvite, hydroxyapatite and calcium phosphates) [208]. Therefore, P recovery by struvite precipitation from wastewaters, such as swine wastewater [209] and industrial wastewater [210] is increasingly gaining importance. In addition, as previously mentioned, P removal from municipal wastewater treatment facilities is an economically favourable strategy, since it considerably reduces the operational issues and maintenance costs [211].

Fortunately, there is growing awareness of the added value nutrients that are being discharged in the human excreta, urine and faeces. According to Mihelcic and co-workers, P recovery from urine presents a huge potential mainly in under developing regions in Africa and Asia [212]. These regions have a high population density, most of which currently do not have access to proper sanitation facilities. This allows the installation of innovative technologies that collect urine at its source (separated form faeces) in newly constructed sanitation systems [212].

P recovery from urine may occur through spontaneous and non-spontaneous precipitation. The spontaneous precipitation comprises several physiochemical steps that occur during the storage or urine. Firstly, urea is completely hydrolysed by urease to ammonia and carbamate. A variety of microorganisms possess the ability to produce urease such as, *Staphylococcus aureus* and *Proteus mirabilis* [213]. Then, carbamate decomposes to carbonic acid and ammonia/ammonium (NH_3/NH_4^+) [167, 214]. These reactions can be summarized in the following overall reaction (Equation 2.5):

$$(NH_2)_2 + 2H_2O \rightarrow NH_3 + NH_4^+ + HCO_3^- \qquad \textbf{EQUATION 2.5}$$

Urea hydrolysis increase the pH of stored urine, thus promoting P recovery by struvite precipitation [167]. Struvite chemical stoichiometry formation is shown in Equation 2.6 [3].

$$Mg^{2+} + NH_4^+ + HPO_4^{2-} + 6H_2O \rightarrow MgNH_4PO_4 \cdot 6H_2O + H^+ \qquad \textbf{EQUATION 2.6}$$

In urine, struvite precipitation is limited by the availability of Mg, therefore in order to achieve a complete removal of P the addition of an exogenous Mg source is required. This procedure corresponds to the non-spontaneous precipitation [215].

Morales and co-workers tested the co-treatment of pre-treated urine with sludge liquid from an anaerobic digester in a stripping system [216]. The urine pre-treatment consisted of a precipitation step by Mg addition at pilot-scale. The Mg source consisted of MgO added in two different ways: a) pre-dissolved in acid solution and b) added directly as powder. The results demonstrated that after 30 minutesof reaction, more than 95 % of P was removed from the stored urine. Furthermore, no significant differences were observed for the different MgO forms of addition [216].

More recently, Zamora and co-workers reported a pilot-scale reactor for P recovery as struvite from source-separated urine [217]. A fluidized bed reactor operated for one year, allowed the recovery of 85 % of P from urine. The harvested product was acceptably pure struvite (>90 %) showing crystals from 0.3 to 6 mm in size. The 10 % of impurities consisted mainly of calcium and potassium precipitates. Finally, the struvite pellets were characterized and found to be in accordance to the legal requirements to be used as slow-release fertilizer in The Netherlands [217].

Struvite containing P, N and Mg in equal molar concentrations is an odourless compact white powder, that can be stored and transported easily [218]. Struvite crystals have an orthorhombic structure (*i.e.* straight prisms with a rectangular base) and can be identified via X-ray diffraction (XRD) by corresponding the intensity and position of the peaks with a database information for the crystal [219]. Struvite precipitation reaction can be separated into nucleation (crystal birth) and crystal growth (development of crystals until equilibrium) and these two stages influence directly the particle size of struvite crystals [211]. Nucleation process includes the induction period and the secondary nucleation period. Induction period comprised the time required for the appearance of the first crystal nuclei (primary nucleation), and the secondary nucleation consists of the time period required for the formation of nuclei when other struvite crystals are present [211]. The next stage includes the crystal growth, defined by the incorporation of solutes into the crystal structure through the transport of ions from the bulk to the crystal and their adsorption on the crystal surface

[220]. Struvite recovered from urine can be used as fertilizers in agriculture [216]. The slower nutrient release and its fertilizer purity make struvite an eco-friendly fertilizer [221]. Furthermore, struvite possesses three essential elements (P, N and Mg), and its impurities are two or three orders of magnitude lower than that of commercial phosphate fertilizers [208].

Gell and co-workers, evaluated the safety and effectiveness of struvite fertilizer recovered from urine in a maize field experiment under Dutch regulations [222]. Struvite composition was 12 % P, 12 % Mg, 6 % N, and 0.5 % to1.5 % of several micronutrients, demonstrating their suitability for use as fertilizer. Further, the concentration of heavy metals only represented 15 % of the regulatory defined threshold level. In addition, struvite did not exceed Dutch regulations for pathogens. In the maize field experiment, P uptake using the struvite recovered from urine was comparable to that of soluble fertilizer. So, based on these findings the struvite recovered from urine was considered safe and effective fertilizer [222].

González-Ponce and co-workers investigated the potential of struvite recovered from municipal wastewater for the cultivation of lettuce under greenhouse conditions was examined [223]. The performance of the recovered struvite was compared to the effectiveness of a commercial P fertilizer derived from phosphate rock (superphosphate). The results showed that struvite was significantly more effective in increasing lettuce yield and P uptake. In conclusion, this study showed that the use of struvite in lettuce cultivation was more effective than a commercial P fertilizer [224].

According to the previously mentioned works, struvite recovered from urine can be an attractive and effective P source for the fertilizer market. In addition, its use may significantly attenuate the consumption of phosphate rock and reduce P concentration load on the effluents that require wastewater treatment, and also prevents further contamination of surface and groundwater systems.

2.8.2. Urine as substrate for BES

The remaining organic matter present in the pre-treated urine after P recovery can be used as feed for BESs [225]. The wide number of different treatment options implies that various treatment concepts can be developed for urine. This section presents a summary of several studies on real urine used as substrate for BESs conducted by two research groups from two different research centres.

Bristol BioEnergy Centre, University of the West of England, UK

Ieropoulos and co-workers reported in 2012, the direct utilisation of urine in MFCs for electricity production [204]. This work stated that the efficiency of urine conversion was inversely correlated with the amount of urine added. For a volume of urine up to 25 mL the CE ranged from 60 % to 70 %, whereas for higher volumes (<700 mL), the CE ranged from 22 to 30 % [204].

In 2013, the same research group described the use of urine as fuel in 3 types of MFCs a) single MFC (50 mL total volume, 25 mL anode volume); b) small prototyped MFC (1.4 mL total volume) and c) stack of small-scale MFCs (48 units with 6.25 mL total volume each) [226]. The results showed that their smallest MFC (1.4 mL) presented a power output 25 % higher than a single unit (6.25 mL). However, the data indicated that the stack of small-scale MFCs allowed higher levels of power output to be obtained, as well as accelerate the biodegradation rate. The authors stated that for the same amount of urine (*i.e.* 100 mL), a single MFC of 25 mL would need 20 days to completely degrade urine, while the MFC stack (48 units with 6.25 mL each) would need only 3 days [226]. In this study, efficiencies of 67 % and 22 % were reported for low volumes and high volumes of urine, respectively.

In both studies previously mentioned, fresh urine without any pre-treatment was directly submitted as fuel in MFCs. In this context, a new study was conducted in order to explore the feasibility of struvite harvesting during MFC operation [227]. Also the performance of platinum (Pt) based and Pt free cathodes was compared to evaluate the potential of low-cost electrode materials. The main results reported by this study state that a single chamber microbial fuel cell can be successfully applied to degrade the COD of urine. The monitored COD removal efficiency achieved was 60 % to 75 % after cycles of 4 days. Further, concentration of P decreased up to 50 % due to the precipitation on anode chamber and cathode surface. However, the high pH caused by urea hydrolysis at the anode, as well as the precipitation of salts on cathode surface severely limited the anodic and cathodic performance decreasing the performance of the system over time [227]. Finally, this study reported that the power generation using Pt- based cathode was higher than those with Pt-free cathodes at the beginning of the assays, however this difference decreased over time.

The same research and development group also studied the dynamics of the pH and urine conductivity at the same conditions of the previous work [188]. The obtained results were similar to the previous work. It was reported that pH increase from 5.4 to 6.4 to 9.0 over time limited the overall MFC performance due to urea hydrolysis in the anode chamber. This study also reported

that conductivity of the urine increased up to 3-fold of the initial value due to urea hydrolysis. Although a reduction of ohmic resistance was expected due to the increase of urine conductivity, it was found that performance of the system was not affected by the increase of urine conductivity [188].

Also in 2013, the authors reported for the first time a practical application using the energy produced by the MFC stacks fed with urine. Two different stacks were used to demonstrate the charging and powering of a commercially available mobile phone [228]. First stack was composed by 12 cylindrical ceramic MFCs (49 mL each) arranged in cascades of three units, with the four cascades forming the stack. The second stack was composed by 24 MFCs (prepared as described in by Ieropoulus and co-workers [229], connected in groups of 2 units in parallel and the 12 groups formed, connected in series (2x12 stack). Both configurations showed to be a viable approach for practical applications, successfully charging the mobile phone battery [228].

The use of fresh urine had previously shown to lead to decrease of the system performance due to urea hydrolysis in the anode chamber. In this context, a 3-stage MFC/struvite extraction process system that generates electricity while collecting P in the form of struvite was proposed [230]. In the first stage, untreated urine was supplied to a first group of MFCs (four units). The effluent from the first stage was then mixed with magnesium chloride hexahydrate ($MgCl_2 \cdot 6H_2O$) in the second stage to recover P by struvite precipitation. Subsequently, the supernatant from the second stage was supplied to a second group of MFCs (four units) in the third stage and the final effluent was collected for analysis. The results showed that placing the first group of MFCs before precipitation process helps struvite collection by accelerating urea hydrolysis. In addition removing struvite from urine before the second group of MFCs avoid the diminishment of the MFC performance since the precipitation on electrode surface did not occur [230].

To further improve the performance of the system, several studies have focussed on the improvement of electrode materials or the reactor's architecture, since, little is known about the selection of manufacturing materials used to build MFC reactors. Papaharalabos and co-workers used three different thermoplastics, PC-ISO (medical-grade biocompatible polycarbonate), ABS (acrylonitrile butadiene styrene) and RC25 Nanocure (ceramic-filled photo curable resin) to manufacture a new MFC [231]. Also a novel MFC design (“Twist n' Play”) was designed (6.25 mL reactor volume). A fully tested model (EcoBot-III MFC) (6.25 mL reactor volume) was used as control. The results showed that the new MFCs design outperformed the control unit in all three different materials tested. The MFCs manufactured with PC-ISO was the unit that displayed the

highest power and current generation amongst the different materials. In the second part of the experiment, triplets made from the same material were connected electrically in parallel. Only the parallel-connected MFCs made of RC25 Nanocure showed a performance improvement when compared to individual units. Furthermore, in individual test, the highest COD removal efficiency of 44 % was achieved for the MFC made of PC-ISO compared to COD removal efficiency of 29 % achieved for the control MFC. When MFCs were connected in parallel again the MFC made by PC-ISO showed the highest COD removal efficiency (53 %) compared to the control unit (38 %) [231].

In 2016, Walter and co-workers investigated the effect of both electrodes, anode and cathode, being submerged in urine [232]. Two different module sizes were investigated. The small boxed MFC (M0.25-6) consisted of six self-stratifying urine column connected in parallel. Each self-stratifying urine column composed by two anodes and two cathodes surrounding a single ceramic support into a PVC tube and a perforated acrylic sheet to prevent any physical contact between anode and cathode. A larger unit (M5–21) consisted of 20 MFCs being that each MFC had the same height and thickness as in M0.25-6 but twice the length. The results demonstrated that compared to a preliminary experiment using a small scale MFC (two self-stratifying urine column MFCs), the scale-up increased power density and showed higher stability over time [232].

A previous research conducted in 2013 by this research group demonstrated the possibility of charging a basic mobile phone with urine as the fuel for MFCs (battery partially charged up to 3.7 V in 24 h) [228]. A new experimental outline was established with the following goal: fully charge the battery of both a basic and a smart phone, up to 4.2 V (full charge) [233]. To achieve usable levels of power, six MFCs modules identical to the described by Walter and co-workers [232] were assembled into the single cascade stack. The developed system demonstrated for the first time the full charge of mobile phones, including smart phones, with urine as fuel showing its possible application to power telecommunication devices in remote areas [233].

In a more recent experiment, the effect of Mg additives to urine on the power output of the MFCs and on the catholyte properties generation was evaluated [219]. $MgCl_2$, artificial seawater and a commercially available sea salts were mixed with fresh urine in order to promote struvite precipitation. Then, the supernatant of each mixture was tested as a feedstock for the MFCs. Six different types of feedstock were tested: a) raw urine; b) urine supernatant after $MgCl_2 \cdot 6H_2O$ addition; c) raw urine stirred; d) urine supernatant after artificial seawater addition; e) urine supernatant after commercial sea salts addition and f) urine diluted with deionised water. The commercial sea salts showed the best performance in terms of struvite precipitation and power

performance of the MFC. Also the properties of the catholyte collected changed according to the Mg source added. Higher pH, higher conductivity and higher concentration of chloride ions were observed when using commercial sea salts [219].

The latest work of the same research group, aimed to evaluate the effect of ceramic membrane thickness on power, as well as on the properties of produced catholyte in urine fed-MFCs [234]. Cylindrical MFCs (200 mL anode volume) were assembled with three different wall thicknesses ceramic membranes, 2.5, 5 and 10 mm. The results showed that the power generated increased when the membrane thickness decreased. Further, the amount of catholyte and its composition was observed to change with the ceramic wall thickness. The amount of catholyte collected also decreased with the wall thickness, whereas the pH and conductivity increased, suggesting that different compositions of catholyte from urine can be achieved only by changing the thickness of the ceramic membrane [234]. However, further understanding on which parameters affect the catholyte generation and its composition are still needed.

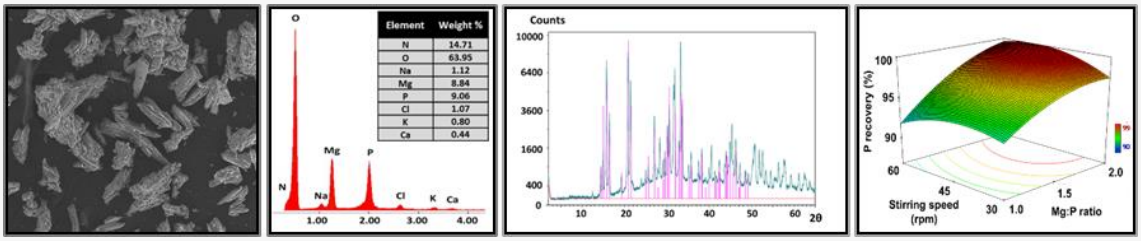
Wetsus, Centre of Excellence for Sustainable Water Technology, NL

Kunkte and co-workers reported, in 2012, an innovative concept that coupled energy production from urine by an MFC with NH_3 stripping [167]. The experimental setup consisted of a dual chamber MFC made from Plexiglas plates (20 mL anode volume). In the first part of the experiment, the effect of an increase in anode NH_4^+ concentration and an increasing current density on the NH_4^+ transport was investigated. The results showed that no adverse effects were found on current production in the tested NH_4^+ concentration range. Furthermore, for all applied anode ammonium concentrations, a linear relation was found between NH_4^+ transport and charge production. In the second part of the experiment, NH_4^+ recovery from real urine was investigated. The high pH in the cathode chamber resulted into a NH_3 gas that was then stripped by the air stream supplied to the-cathode. NH_3 was subsequently recovered as NH_4^+ by adsorption in an acid solution from the gas stream leaving the cathode. This study found a CE of 10 % during the operation on real urine [167]. The use of an MEC for H_2 production and simultaneous NH_4^+ recovery from urine was reported by this research group [235]. The setup consisted of a dual chamber MEC made from titanium with Pt coated flow fields (40 mL anode volume). During stable operation on five times diluted urine, the generated current density and NH_4^+ removal rates exceed the results obtained in the previous work [167], suggesting that a MEC NH_4^+ recovery concept is more promising than the MFC NH_4^+ recovery concept. During the stable operation, a CE of 84 %, a COD removal efficiency of 30 % and

an NH_4^+ removal efficiency of 34 % were reported. However further research is required to maximize NH_4^+ removal efficiency in a MEC [235]. In order to enhance NH_4^+ recovery, COD conversion to electrical energy should be optimized, with a special focus on CE and an effective NH_3 stripping process should be developed.

In this context, the authors reported the recovery of NH_3 by using a transmembrane chemisorption (TMCS) module integrated in the catholyte compartment of an MEC [236]. The experimental setup consisted of a MEC composed of 4 anode and cathode pairs with an integrated TMCS module. According to the TMCS concept, the NH_4^+-N present in the inflow was transported as NH_4^+ through the membrane from the anode to the cathode. Subsequently, the NH_3 crossed over the TMCS and was recovered as NH_4^+ in H_2SO_4. During the stable operation a CE 78 % and a COD removal efficiency of 40 % were obtained. This study also stated an average NH_4^+ removal of 42 %. Thus, the results demonstrated that a TMCS was successfully employed in a MEC for NH_4^+ recovery, however further research will be necessary [236].

In conclusion, over the last years, urine has been tested as a fuel source for energy production, essentially electricity. However, according to most of the previous works, additional research is required to further improve the efficiency of BESs. Furthermore, to date, very little was described about the degradation of the organic compounds present in urine and the associated microbial community. In addition, H_2 production from urine has been poorly investigated. H_2 is considered as an important energy fuel as it has the highest energy content per unit weight [237]. Thus, there are still several challenges to overcome to develop an efficient system for energy production from urine with simultaneous treatment.



Chapter 3

A DESIGN OF EXPERIMENTS TO ASSESS PHOSPHOROUS REMOVAL AND CRYSTAL PROPERTIES IN STRUVITE PRECIPITATION OF SOURCE SEPARATED URINE USING DIFFERENT MG SOURCES

3. A design of experiments to assess phosphorous removal and crystal properties in struvite precipitation of source separated urine using different Mg sources

The work presented in this chapter corresponds to the following scientific article:

Barbosa, S.G., Peixoto, L., Meulman, B., Alves, M.M., Pereira, M.A., 2016. A design of experiments to assess phosphorous removal and crystal properties in struvite precipitation of source separated urine using different Mg sources. Chemical Engineering Journal.298,146–153.

ABSTRACT

Phosphorus recycling and recovery has received special attention due to its non-replaceable and non-renewability. Phosphorus recovery from human urine in the form of struvite crystals is a potential alternative source. In this work, the efficiency of struvite precipitation from source separated human urine and struvite crystals size were analysed using three different magnesium (Mg) sources (magnesium chloride ($MgCl_2$), magnesium hydroxide ($Mg(OH)_2$) and magnesium oxide (MgO)), individually evaluated using a statistical design of experiments to assess the combined effect of Mg:P molar ratio (1:1, 1.5:1 and 2:1) and stirring speed (30, 45 and 60 rpm). Formation of struvite crystals was confirmed by X-ray Diffraction (XRD) and scanning electron microscopy (SEM) with an energy dispersive spectrometer (EDS). Using the optimal conditions determined, MgO as Mg source at 2:1 molar ratio and a stirring speed of 30 rpm, 99 % of P was recovered as struvite crystals with a size of 50 to 100 μm.

3.1. INTRODUCTION

Phosphorus (P) is an essential nutrient for all types of life. Phosphate rock is the major source of P predominantly originating from China, United States, Morocco and Russia [238]. An annual increase in phosphorus consumption has been observed and its overall future demand is anticipated to rise due to the increase in population growth and per capita phosphorus demand. Depending of the different assumptions, a vast range of global phosphate depletion estimates indicating different peak years have been reported [239]. In general, the different scenarios described depend of the assumptions about demand, supply, and the depletion model employed. Cordell and co-workers estimated phosphorus to peak by 2035 based on 2009 USGS reserve data, however the International Fertilizer Development Centre (IFDC) re-estimated global phosphate rock reserves and the peak shifts to 2051 to 2092 [1]. Therefore, its efficient use, recovery and recycling methods are priorities to face the needs of this non-renewable and non-replaceable nutrient.

Crystallization processes have the potential to recover P in the form of useful products such as struvite ($MgNH_4PO_4 \cdot 6H_2O$), hydroxyapatite ($Ca_{10}(PO_4)_6(OH)_2$) and calcium phosphate ($Ca_3(PO_4)_2$) [1, 208]. Struvite presents some advantages compared to the other crystal forms: a) nutrients are released at a slower rate compared to other fertilizers, b) the impurities in the recovered struvite are two or three orders of magnitude lower than the commercial phosphate fertilizers, and c) the essential nutrients (P, nitrogen (N) and Mg) are simultaneously on the same crystal [208]. Research focused on P recovery through struvite precipitation has received attention in the last years and, specifically, P recovery from urine has been reported using several processes such as hybrid anion exchange resins [240], single chamber microbial fuel cells [227] or electrolytic Mg dosage [241].

Human urine contributes with only 1 % to the volume of municipal wastewater, however contributes to about up to 50 % of the P load [225]. On average, urine contains 1 g L^{-1} of P, 9 g L^{-1} of N and 10 g L^{-1} of chemical oxygen demand (COD) [7]. Due to these high concentrations, human urine can be a valuable resource for N, P and energy recovery [167]. P recovery from urine has received a lot of attention with regard to struvite production in simply operated reactors that only requires an Mg source. Struvite precipitation from source-separated urine have been reported mainly in developing and emerging countries, where P levels in soils is frequently below optimal and consequently more fertilizers are required due to the rapidly increase of food production [239] [212]. Reactors manufactured to produce struvite from urine in decentralized treatment systems have been used for P recover on a small scale in developing countries [218, 242, 243]. In

developed countries P recovery from urine have been also reported in decentralized settings after which the treated liquid would be discharged via existing sewers [244]. Several technologies have been proposed for P recovery from urine [8, 203, 215, 241]. P recovery by precipitation from separated human urine is possible if NoMix toilets and waterless urinals are used. NoMix technology is well accepted; around 80 % of users liked the idea, 75 % to 85 % were satisfied with design, hygiene, smell, and seating comfort of NoMix toilets, 85 % regarded urine-fertilizers as good idea and 70 % would purchase such food [201].

P recovery from urine occurs in two successive steps namely spontaneous and non-spontaneous precipitation [203]. During storage of urine, urea is completely hydrolysed into carbon dioxide and ammonia (Equation 3.1) [214]. Ammonium (NH_4^+) in equilibrium reacts with the phosphate (PO_4^{3-}), and Mg ions present in the urine, and struvite crystallization occurs spontaneously (Equation 3.2) [220].

$$(NH_2)_2CO + H_2O \rightarrow CO_2 + 2NH_3 \qquad \textbf{EQUATION 3.1}$$

$$Mg^{2+} + NH_4^+ + PO_4^{3-} \cdot 6H_2O \rightarrow MgNH_4PO_4 \cdot 6H_2O \qquad \textbf{EQUATION 3.2}$$

This precipitation is limited by the availability of Mg and the addition of a Mg source, results in an effective P recovery in a process called non-spontaneous struvite precipitation [215]. The most common precipitants are MgO [8] $MgCl_2$ [211] and $Mg(OH)_2$ [245]. Due to its basic character MgO and $Mg(OH)_2$, can serve a dual purpose of Mg addition and pH increase. On the other hand, $MgCl_2$ has been reported as a more effective for P recovery reducing the reaction time due to its greater solubility [246].

Several physico-chemical parameters influence the P recovery efficiency, such as, pH [247], stirring speed [248], temperature [249], Mg:P molar ratio [250], presence of seeding materials [251] and presence of foreign ions [214]. In this work, a statistical design of experiments is applied to optimize the struvite precipitation from source separated human urine. The combined effect of the stirring speed, the stirring time, the sedimentation time and the Mg:P ratio is evaluated on the P removal efficiency and struvite crystal properties. The power of the design of experiments that decreases the number of experiments intercorrelated, maintaining the security of the results, is herein demonstrated on the assessment of fundamental parameters affecting the complex struvite precipitation process from human urine.

3.2. MATERIALS AND METHODS

3.2.1. Design of experiments and statistical analysis

In order to understand which factors affect P removal and to optimize P recovery efficiency ($P_{recovery}$), several preliminary batch assays were performed. Three different stirring times (10, 35 and 60 min), three stirring speeds (60, 90 and 120 rpm), three Mg:P molar ratios (1:1, 2:1 and 3:1) and three sedimentation times (30, 45 and 60 min) were investigated for each Mg source (MgO, $Mg(OH)_2$ and $MgCl_2$) tested. The Design-Expert® software package (Stat-Ease Inc., Minneapolis, USA) was used for planning the assays and a set of 52 experiments were performed. A central composite face-centred design (CCF), using response surface methodology, was carried out according to a three-level factorial design, containing a central point.

The results obtained in the preliminary assays were used to refine the test and plan a new set of experiments, with the same software, correlating only two variables at high (+1) and low (-1) levels. According to the results obtained by previous factorial design experiment, (A) Mg:P molar ratio (1:1, 1.5:1 and 2:1) and (B) stirring speed (30 , 45 and 60 rpm) were the parameters studied at three levels with two repetitions (duplicates) with a central point tested in triplicate (3 central points) (Table 3.1). Fixed parameters were stirring time (10 min) and sedimentation time (30 min). A set of 19 experiments were carried out for each Mg source.

The performance of all the models suggested was assessed based in different parameters. The correlation coefficient (R^2) measures the fraction of the total variability in the response. R^2 value closer to unity indicated that the standard deviation was reduced and the predicted results were in good agreement with experimental data. Coefficient of variation (CV) is a measure of the amount of variation as a percentage of the total mean. A CV less than 10 % represents means that the model is reproducible [252]. Adequate precision (AP) is a measure of the difference in predicted response relative to its associated error (a signal to noise ratio). AP can be certified with a signal greater than 4 [252].

TABLE 3.1 Experimental design matrix with operating conditions for P recovery efficiency assays.

Run	Mg:P ratio	Stirring speed rpm
1	1.0	30
2	1.5	60
3	1.5	30
4	1.5	60
5	1.0	60
6	1.5	45
7	1.0	30
8	1.0	45
9	1.0	60
10	2.0	60
11	2.0	30
12	1.5	45
13	2.0	45
14	1.5	45
15	2.0	60
16	2.0	30
17	2.0	45
18	1.5	30
19	1.0	45

3.2.2. Phosphorus removal by struvite precipitation

Urine from different individuals, males and females with a broad age range between 20 and 50 years old, was collected at different times in different days, mixed and analysed. The P and COD concentrations were determined using Hach-Lange cuvette tests (LCK 350 and LCK 338, respectively) and total Kjeldahl nitrogen (TKN) and ammonium nitrogen (NH_4^+-N) by using the Kjeldahl method according to Standard Methods [253]. Electrical conductivity and pH were measured with portable conductivity meter (Multi 340i, WTW, Germany) and a portable pH meter (HI 83141, Hanna, Italy), respectively.

To determine the time course of spontaneous precipitation of struvite from real undiluted human urine, a first experiment was performed. Fresh collected urine was stored at room temperature in a plastic container during several days. Samples were taken daily to monitor changes in pH and to measure TKN, NH_4^+-N, COD and P concentrations. The collected samples were preserved with 5 % sulphuric acid (H_2SO_4) (1M) and stored at 4 °C until analysis. Following the spontaneous struvite

precipitation, the supernatant was decanted and several Mg sources were then added to induce additional struvite precipitation. The use of different Mg sources was investigated in 600 mL beakers (work volume of 300 mL) in a jar-test apparatus (AMF/60, Vittadini, Italy) at room temperature, adding MgO, $Mg(OH)_2$ and $MgCl_2$ at different Mg:P molar ratios. Mg dose added was calculated based on initial P concentration and the initial pH of the urine was kept at the designed level (8.5) [6]. After Mg addition, the solution was stirred for 10 minutesand was rested to sediment for 30 minutes. P removal efficiency was calculated after determination of initial and final P concentration.

3.2.3. Precipitate analysis - crystal size, XRD and SEM-EDS

The different conditions applied on struvite precipitation influenced the size of the crystals obtained. Therefore, the same CCF experimental design mentioned in section 3.2.1. was used to assess the effect of Mg:P ratio and stirring speed on particle size. Thereby, 1 mL of struvite precipitated after non-spontaneous precipitation from each experiment were collected for a Petri dish to microscopic analysis and particle size assessment. Samples were stored at 4 °C until observation. Precipitated crystals were observed in a Nikon inverted microscope Diaphot 300, at 100x total magnification, coupled with a Sony CCD video camera and the software IMAGE-PRO. Images were acquired in the upper, middle and bottom of the sample with controlled distances, in order to ensure the representativeness of the sample. The longitudinal size of the precipitated crystals was measured by Image J, image edition program. Around 20 images were obtained per sample and an average of 876 crystals were analysed per assay.

Samples from the precipitates were also collected and dried at 45 °C in order to characterize the crystals by XRD and SEM-EDS. XRD allowed matching the intensity and position of the peaks in the diffractogram of each sample and a standard model diffractogram for struvite crystals. The XRD measurements were performed on a Phillips X-Ray model PW 1710 BASED powder diffractometer equipped with CuKα monochromatic radiation. SEM-EDS allowed to identify the crystals precipitated by comparing the chemical composition obtained in an energy dispersive spectrograph with a standard spectra of pure struvite. Surface morphological and compositional analyses were carried out using a SEM FEI Nova 200 with integrated EDS analysis (EDAX, Pegasus X4M).

3.3. RESULTS AND DISCUSSION

3.3.1. Phosphorus removal by struvite precipitation

Fresh urine was stored and P concentration and pH were followed over time, in order to obtain the time course of struvite spontaneous precipitation. The pH increased from 5.9 to 8.6 as a result of urea hydrolysis, leading to a P concentration decrease as a result of the reaction with NH_4^+ and Mg^{2+} ions (Table 3.2). Liu *et al.* reported that during urea hydrolysis, the pH increased and stabilized at around 9.0 [6]. As a consequence of pH increase, it was observed that after 6 days of urine storage, 30 % of P was recovered through spontaneous struvite precipitation. Similar results were reported by Etter *et al.* with about 30 % of the P removed due to spontaneous precipitation as calcium phosphate and struvite in undiluted urine [13]. Liu and co-workers demonstrated that after 5 days of urine storage almost 38 % of P was recovered, after which only a minimum variation was observed [254]. Since struvite precipitation is limited by availability of Mg, addition of a Mg source will induce additional precipitation. In fact Mg was depleted by 90 % in the spontaneous precipitation process.

TABLE 3.2 Composition of fresh and stored human urine (n=3).

		Fresh urine	Stored urine
pH		5.92±0.02	8.59±0.01
COD	g L^{-1}	12.50±2.23	9.29±0.57
TKN	g L^{-1}	8.40±0.68	9.18±0.36
NH_4^+-N	g L^{-1}	0.54±0.08	1.92±0.07
P	g L^{-1}	0.79±0.01	0.55±0.00
Conductivity	mS cm^{-1}	23.10±1.20	-

Preliminary batch assays were performed in order to understand which factors affect P removal in non-spontaneous precipitation (Figure 3.1). From these preliminary assays, it could be concluded that the Mg:P ratio and the stirring speed were the most relevant parameters. Thus, a process analysis CCF was performed with the purpose of correlate these two variables: (A) stirring speed (30, 45 and 60 rpm) and (B) Mg:P molar ratios (1:1; 1.5:1 and 2:1) in order to optimize the P

recovery efficiency. The effect of each variable was described by modulation according to a two-factor, three-level central composite design with response surface methodology (RSM). Based on preliminary experiments, the reaction and the sedimentation times, of 10 and 30 minutes, were respectively established. In each run, Mg dose added was calculated based on the initial phosphorus concentration. The initial pH was kept at the designed level (8.5) [6] by H_2SO_4 (1M) addition.

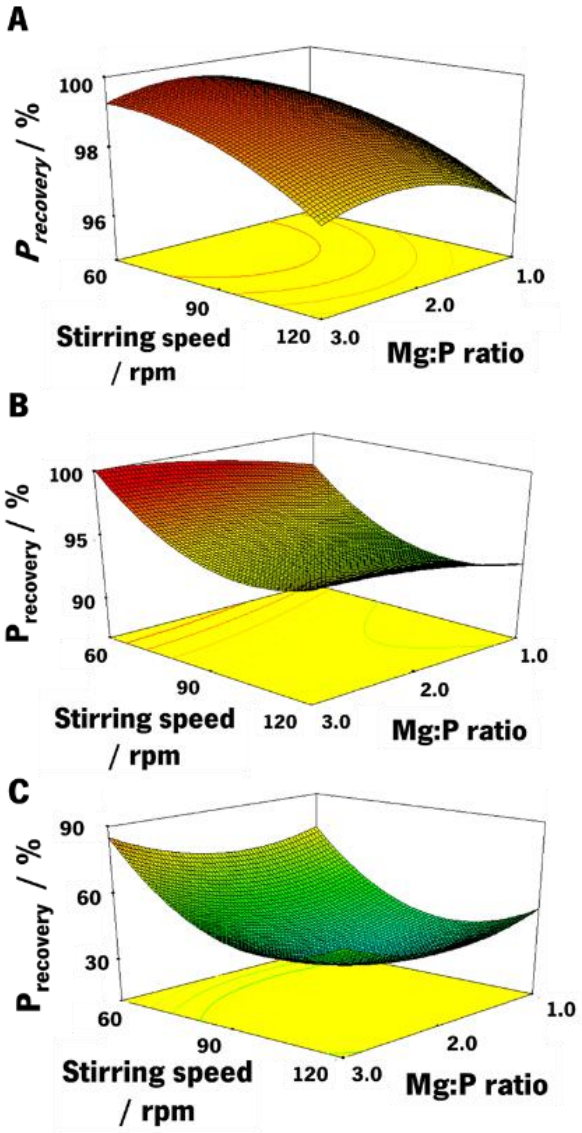


FIGURE 3.1 Response graphs showing the effect of Mg:P ratio (1:1; 2:1 and 3:1) and stirring speed (60, 90 and 120 rpm) on phosphorus (P) recovery efficiencies with different Mg sources **A)** MgO; **B)** $MgCl_2$ and **C)** $Mg(OH)_2$.

Figure 3.2 shows the effect of the stirring speed and Mg:P molar ratio on P recovery efficiency using three different Mg sources. In order to access the significance of each variable in the selected

model, an analysis of variance (ANOVA) was applied. The value of statistical significance was set at $p<0.05$, which means that the model terms are significant for values of p lower than 0.05. The highest P recovery efficiencies, ranging from 90 % to 99 %, depending on the operating conditions applied, were obtained using MgO as Mg source. After the addition of MgO in the beakers, the pH increased from 8.5 - 8.7 to 9 in the first 3 minutes and remained at 8.9 - 9.2 during stirring time (10 minutes). The role of each variable can be described by the Equation 3.3 (F-value = 7.12) where $P_{recovery}$ (%) is the phosphorus recovery efficiency. Only the variable *A*, Mg:P ratio, had a significant influence on P recovery efficiency (Table 3.3). A maximum P recovery of 99 % was obtained in the experiment with Mg:P ratio = 2:1 for the three stirring speeds studied, which was also predicted by the model (100 % P recovery for Mg:P ratio = 2:1), evidencing a clear match between model prediction and the experimental response (Figure 3.2A). Capdevielle *et al.* demonstrated that the optimal conditions for the removal of P from synthetic swine wastewater were Mg:P molar ratio of 2.25:1, moderate stirring rate (between 45 and 90 rpm) and low temperature (below 20 °C) [255].

$$P_{recovery} = 73.07 + 16.40A + 0.36B + 0.12AB - 5.22A^2 - 5.80E\text{-}3B^2 \quad \textbf{EQUATION 3.3}$$

With $MgCl_2$ as Mg source, P recovery efficiency ranged from 82 % to 89 %, depending of the conditions applied. The pH value decreased from 8.5 to 7 to 8 in the first 3 minutes after the addition of $MgCl_2$. The pH remained at 7 to 7.5 during the reaction time (10 minutes). The model was described by the Equation 3.4 (F-value = 4.05). ANOVA analysis showed that A^2 was the only significant variable for the model (Table 3.3). According to the quadratic model, the maximum P recovery that can be achieved for experimental parameters applied was 89 % at Mg:P ratio of 2:1 and a 60 rpm (Figure 3.2B). The experimental value obtained (89 %) was consistent with the predicted response and validates the model. Despite the stoichiometric Mg:P ratio of 1:1, studies reported a low P removal for Mg:P ratio around this value. Munch and Barr [34] reported a P recovery of 94 % using a Mg:P ratio of 1:1.3 whereas Adnan and co-workers reported a P recovery of 62 % for a Mg:P ratio of 1.2:1 [256] . Song *et al.* showed that increasing Mg:P molar ratio up to 2.2:1 promotes the removal efficiency at different pH studied, furthermore at a low pH value of 8.0 the P removal efficiency increased significantly [250]. Wilsenach and co-workers demonstrated that with addition of $MgCl_2$, the P removal was linear with increasing Mg:P ratio and with initial pH of 8.2, a P removal efficiency of 75 % was achieved with an overdose of Mg (Mg:P ratio = 2:1) [8].

$$P_{recovery} = 79.41 - 23.31A + 0.88B + 0.02AB + 8.13A^2 - 8.74E\text{-}3B^2$$ **EQUATION 3.4**

Using $Mg(OH)_2$, the experimental values of P recovery efficiency ranged from 79 % to 93 %. After $Mg(OH)_2$ addition, the pH at 8.5 - 8.7 during 3 minutes and stabilized at these values during all the reaction (10 minutes). The effect of each variable on P recovery was described by a quadratic model as shown in the Equation 3.5 (F-value = 5.52). The variables that demonstrated a significant effect on P recovery efficiency were B and B^2 (Table 3.3). The optimized solution suggested by the software, consisted of Mg:P ratio of 1.5:1 and a stirring speed of 60 rpm which correspond to 89 % of P recovery (Figure 3.2C). The maximum experimental P recovery of 93 % was achieved at the same conditions (Mg:P ratio of 1.5:1 and 60 rpm). Quadratic model showed clearly that mixing intensity had a significant effect on P recovery by struvite precipitation for the range of speeds tested. A stirring speed increase leads to CO_2 liberation increasing the pH and therefore an increase in P recovery through struvite precipitation was achieved [257].

$$P_{recovery} = 85.65 + 34.49A - 1.53B - 0.05AB - 10.91A^2 + 0.02B^2$$ **EQUATION 3.5**

TABLE 3.3 ANOVA analysis for the effect of Mg:P ratio and stirring speed on P recovery efficiency.

	Prob > F		
	MgO[a]	**$MgCl_2$[b]**	**$Mg(OH)_2$[c]**
Model	0.0021	0.0195	0.0061
A: Mg:P ratio	0.0193 (+)	0.5621 (-)	0.6669 (+)
B: Stirring speed	0.1889 (+)	0.1007 (+)	0.0028 (-)
AB	0.2193 (+)	0.8607 (+)	0.7149 (-)
A^2	0.1781 (-)	0.0506 (+)	0.0656 (-)
B^2	0.1781 (-)	0.0574 (-)	0.0054 (+)

[a]SD = 1.92, R^2 = 0.73, R^2adj. = 0.63, AP = 7.44, CV = 1.99 %.
[b]SD = 1.98, R^2 = 0.61, R^2adj. = 0.46, AP =6.01, CV = 2.30 %.
[c]SD = 1.46, R^2 = 0.67, R^2adj. = 0.51, AP = 5.77, CV = 1.80 %.

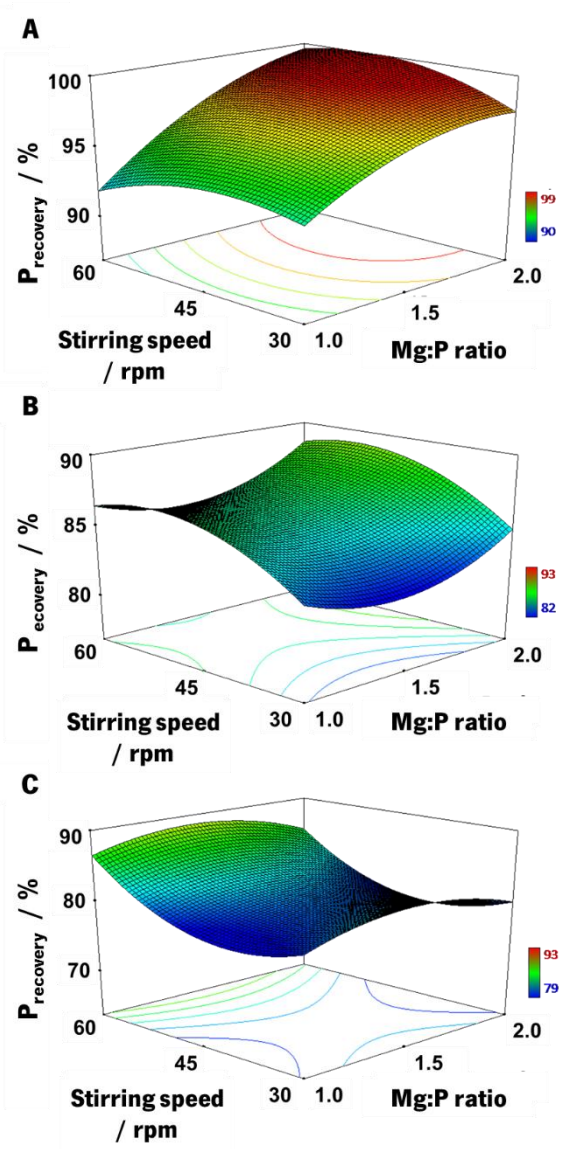


FIGURE 3.2 Response graphs showing the effect of Mg:P ratio and stirring speed on phosphorus (P) recovery efficiencies with different Mg sources **A)** MgO; **B)** $MgCl_2$ and **C)** $Mg(OH)_2$.

3.3.2. Precipitate analysis

i. Crystal size measurement - Image J

Precipitation of struvite occurs in two stages: nucleation and crystal growth. These stages influence directly the particle size of crystals [3, 250]. Nucleation is strongly dependent on the super saturation and crystals growth rate depends on the stirring speed because it is a mass transport limited process [254]. The effect of Mg:P ratio and stirring speed on crystal size (Figure 3.3) was assessed for the same set of 19 experiments, determined by CCF experimental design (Table 3.1).

Using MgO as Mg source, the variable that had a significant effect on crystal size was B^2 (Figure 3.4). At 30 rpm, the particle size distribution showed a slightly bimodal behaviour with the presence of fine particles around 50 μm and larger crystals around 100 μm size. Crystals around the 50 μm were more frequent in the experiments with 45 and 60 rpm (Figure 3.3Aa).

TABLE 3.4 ANOVA analysis for the effect of Mg:P ratio and stirring speed on crystal size.

	Prob > F		
	MgO[a]	**$MgCl_2$**[b]	**$Mg(OH)_2$**[c]
Model	<0.0001	0.0260	0.0111
A: Mg:P ratio	0.5051 (-)	0.3505 (+)	0.0043 (-)
B: Stirring speed	0.1265 (-)	0.0014 (+)	0.0229 (-)
AB	0.5255 (+)	0.4227 (-)	0.0111 (+)
A^2	0.9311 (+)	0.4326 (-)	0.9379 (-)
B^2	0.0242 (+)	0.0012 (-)	0.0268 (+)

[a]SD=0.011, R^2=0.872, R^2adj. = 0.823, AP = 10.097, CV = 17.95 %.
[b]SD = 0.013, R^2 = 0.645, R^2adj. = 0.483, AP = 5.107, CV = 31.81 %.
[c]SD = 8.76E-3, R^2 = 0.701, R^2adj. = 0.565, AP = 8.027, CV = 27.43 %.

Using $MgCl_2$, the variables B and B^2 were the leading process parameters on crystal size (Figure 3.4). The most common crystal size ranged from 20 μm at 30 rpm to 40 μm at 60 rpm, whereas the biggest crystals with around 70 μm were obtained at 45 rpm (Figure 3.3Bb). Ariyanto and co-workers studied the mechanisms of crystal formation using a di-hydrogen ammonium phosphate solution [258]. These authors clearly showed that the crystal size was not significantly affected by the stirring speeds tested (50-120 rpm) and obtained crystals with around 50 μm using the same Mg source ($MgCl_2$) and 50 rpm.

The quadratic model achieved for $Mg(OH)_2$ indicated that the significant model terms were A, B, AB and B^2 showing that both variables had an important effect on crystal size (Table 3.4). The crystals obtained with this Mg source were smaller than the obtained with the other Mg sources. Approximately 50 % of the crystals developed with 30 rpm and 45 rpm had around 30 μm. Crystals with around 60 μm, were achieved in the 60 rpm experiments (Figure 3.3Cc).

The effect of each variable on crystal size was described for MgO (F-value = 4.39), $MgCl_2$ (F-value = 3.99) and $Mg(OH)_2$ (F-value = 5.16) by following quadratic model equations, where $Crystal_{size}$ (µm) corresponds to the struvite crystal size:

$$Crystal_{size} = 0.28 - 0.02A - 7.67E\text{-}3B + 3.33E\text{-}4AB + 1.83E\text{-}3A^2 + 5.87E\text{-}5B^2 \quad \textbf{EQUATION 3.6}$$

$$Crystal_{size} = -0.28 + 0.09A + 0.01B - 6.26E\text{-}4AB - 0.02A^2 - 1.26B^2 \quad \textbf{EQUATION 3.7}$$

$$Crystal_{size} = 0.18 - 0.04A - 6.49E\text{-}3B + 1.39E\text{-}3AB - 1.41E\text{-}3A^2 + 5.12E\text{-}5B^2 \quad \textbf{EQUATION 3.8}$$

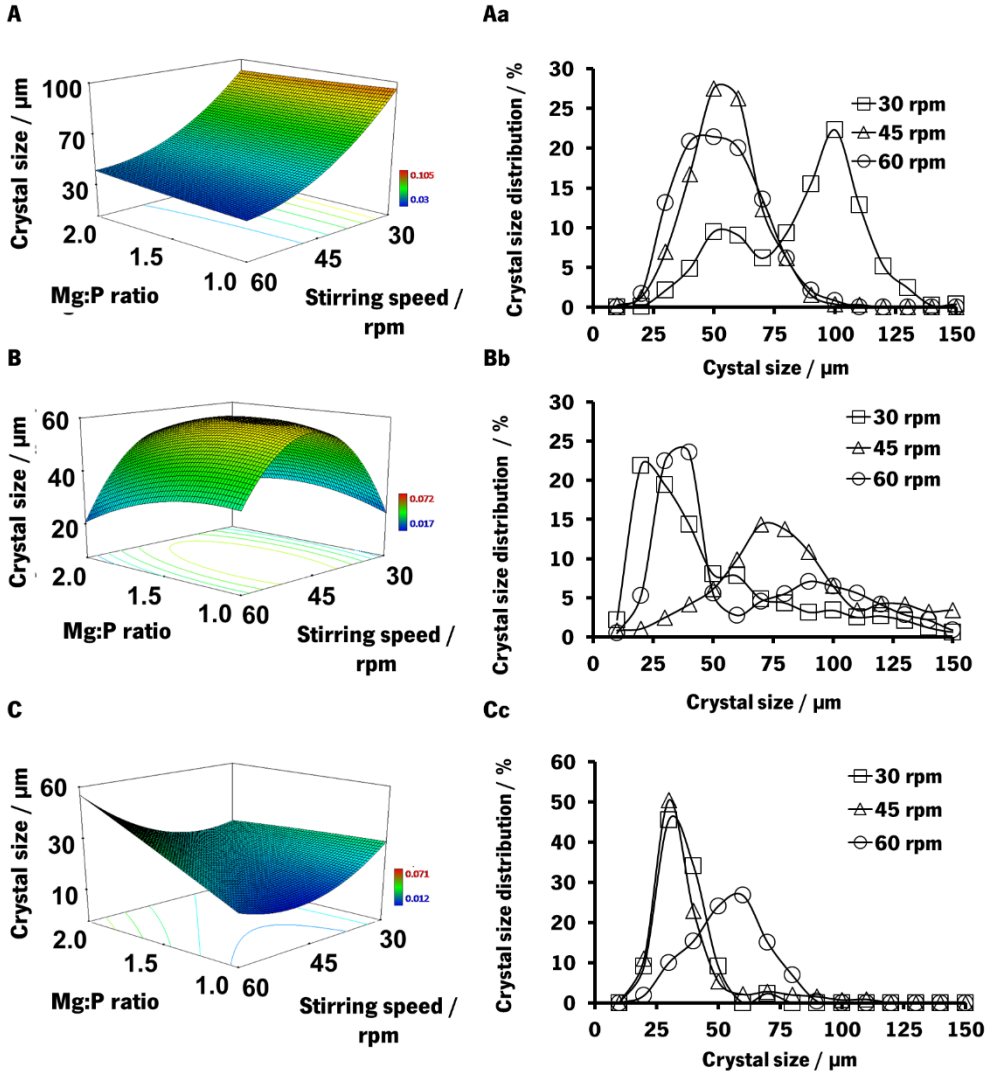


FIGURE 3.3 Graphs showing the effect of Mg:P ratio and stirring speed on crystal size (left) and particle size distribution (right) with **A)** MgO; **B)** $MgCl_2$ and **C)** $Mg(OH)_2$ as Mg sources.

ii. Characterization and identification of crystals - XRD and SEM-EDS

Microscopic image analysis showed that the crystals shape was non-uniform depending of the Mg source (Figure 3.4). Usual crystal morphologies include coffin-like [3], needle-like [8], x-shape [259] and rod shape [214]. Using MgO, the obtained precipitate exhibited an irregular shape, and some crystals with a typical x-shape. Using $MgCl_2$ and $Mg(OH)_2$, the morphology of the precipitated crystals were similar showing the typical prismatic pattern of the struvite crystals. Korchef *et al.* and Munch and Barr, reported similar crystals shape using $MgCl_2$ and $Mg(OH)_2$ as Mg sources [260, 261].

Samples of the collected precipitate obtained after P removal with Mg:P of 1.5:1 and 45 rpm for each Mg source were selected for crystals characterization. The content of struvite in the precipitates was confirmed by SEM-EDS and XRD techniques. SEM-EDS analyses of the crystals are shown in Figure 3.4. Chemical element composition showed the presence of Mg, P, N and O on the crystals precipitated with three different Mg sources, indicating that struvite was obtained with this process. The XRD patterns supports that the precipitates formed were a mixture of struvite with amorphous products. The prominent peaks of the precipitate matched very well with the standard model for struvite but a broad hump on the baseline was observed. According to the SEM images, when MgO or $MgCl_2$ were added, crystals of struvite were covered by other small amorphous precipitates (Figure 3.4A and Figure 3.4B), whereas, with $Mg(OH)_2$, two different types of precipitates could be observed (Figure 3.4C).

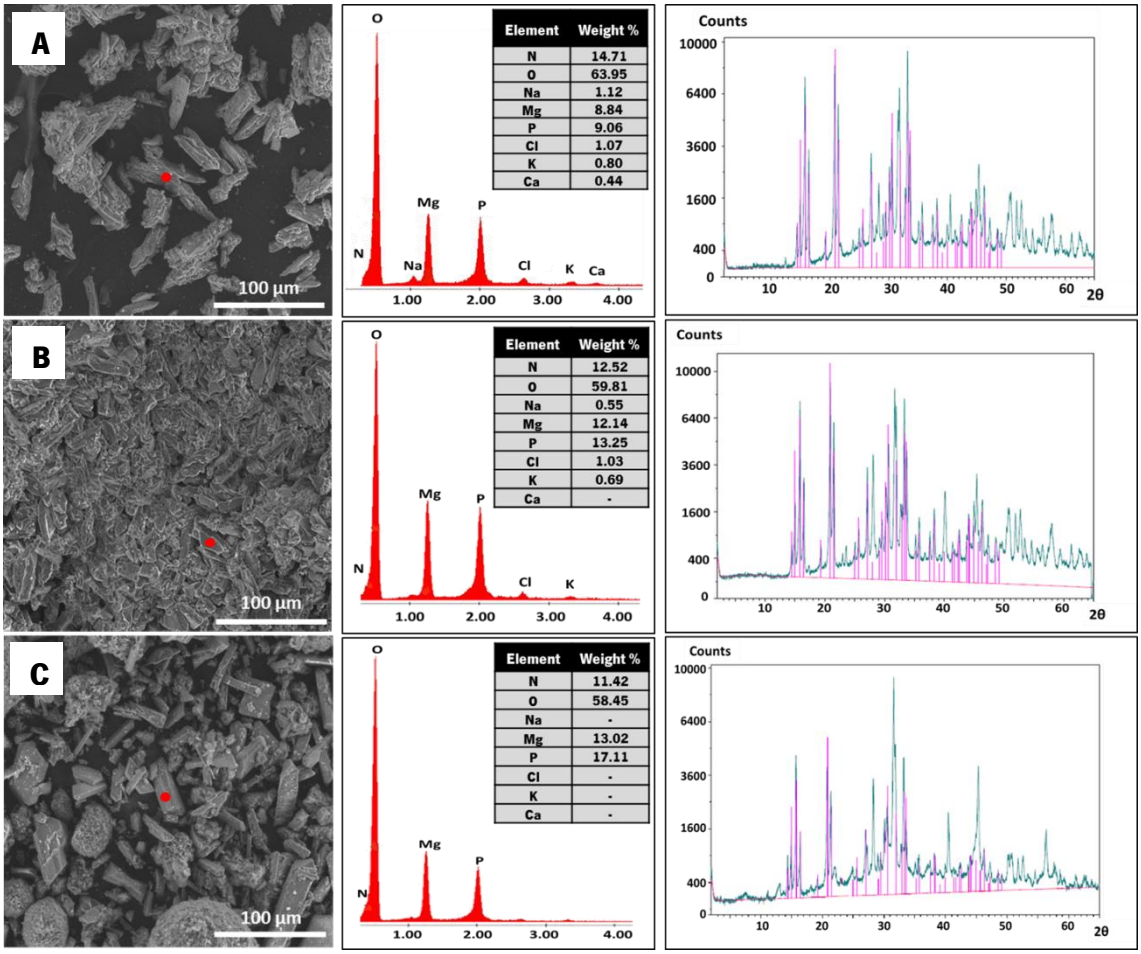


FIGURE 3.4 Scanning electron microscopy (SEM) picture, respective elemental analysis and X-ray diffraction (XRD) spectra of the precipitates (left to right) from batch experiments at 1.5:1 of Mg:P and 45 rpm with **A)** MgO; **B)** $MgCl_2$ and **C)** $Mg(OH)_2$ as Mg sources. Vertical lines (pink) at XRD analysis corresponds to standard struvite (Powder diffraction file (PDF) No. 15-0762).

3.3.3. Economic overview

P recovery by struvite precipitation is a promising and feasible process not only in terms of environmental benefits [262] but also from an economic point of view [263]. P recovery from urine has the potential to greatly reduce P loadings in wastewater treatment plants. Mihelcic and co-workers reported that P available from urine could account for 22 % of the total global phosphorus demand [212]. The economic viability of struvite precipitation includes not only the costs of the urine separation implementation and the effects on wastewater treatment process but also the costs of precipitation process and the economic value added of struvite. On the other hand, several studies reported that the efficiency of municipal wastewater treatment plants has been affected by precipitates, namely struvite, formed in the stench traps and pipes due to the high phosphate concentration in wastewater [3, 211, 220]. This may lead to an increase of operating and

maintenance costs for cleaning unwanted struvite formed in pipes. Whilst struvite is unwanted in municipal wastewater treatment facilities if precipitation is controlled and cost-effective, struvite might have potential as fertilizer [222].

The costs related to the struvite production have been reported by several studies as highly dependent of the P concentration. According to Dockhorn, the fixed costs (*e.g.* investment, labor and energy) decrease with P concentration, whereas the variable cost mainly related to the Mg source added, increase with P concentration [264]. Waste products containing Mg such as bittern [265] and wood ash [266] are less expensive Mg sources and can be an interesting alternative to produce Mg salts, thus saving costs. However, due to the heterogeneous composition, a reliable product is not always guaranteed and the marketability of the struvite may not be possible. For example, Krähenbühl and co-workers, reported that wood ash is not a very suitable precipitant for struvite production because the precipitate has a low phosphorus content and can contain high concentrations of heavy metals [267]. Therefore, due to the high influence of chemical´s price in P recovery economic feasibility, cost savings may be achieved through the choice of an appropriate Mg source as a struvite precipitant. The calculated input costs for producing struvite based on the market prices of different Mg sources is presented in Table 3.5. A comparative analysis shows that the cost of using MgO or $MgCl_2$ is similar. However, MgO presents some advantages due to the high Mg content that contributes for a less quantity of chemical added simplifying the logistic and reducing the transportation costs. Moreover, basic character in pH adjustment of MgO allows to achieve the optimal pH value (8.5) for struvite precipitation without any alkali addition.

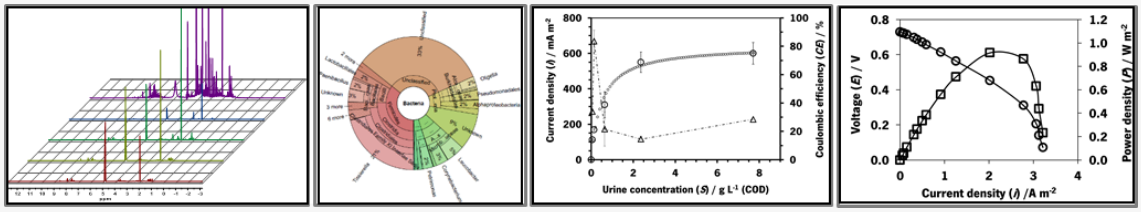
TABLE 3.5 Estimated struvite production costs using industrial grade magnesium salts.

		MgO	**$MgCl_2$**	**$Mg(OH)_2$**
Chemical formula		MgO	$MgCl_2 \cdot 6H_2O$	$Mg(OH)_2$
Product price[a]	€ kg^{-1}	29.40	5.35	12.12
Magnesium content	g kg^{-1}	534	119	407
Mg:P ratio		2:1	2:1	2:1
Required input	kg $kg_{struvite}^{-1}$	0.16	0.86	0.24
Input cost	€ $kg_{struvite}^{-1}$	4.62	4.62	2.82

[a] Price quoted by VWR International, for a 25 kg bag of technical grade material (January 2016).

3.4. CONCLUSIONS

A CCF centred design using a RSM allowed to optimize struvite precipitation from undiluted human urine. Statistical analysis revealed that the maximum P recovery was achieved using MgO as Mg source at 2:1 molar ratio and a stirring speed of 30 rpm. 99 % recovery of P and simultaneously formation of struvite crystals of 50 to 100 μm size were obtained. XRD and SEM-EDS analysis revealed that the precipitate formed was a mixture of struvite with amorphous products.



Chapter 4

INVESTIGATING BACTERIAL COMMUNITY CHANGES AND ORGANIC SUBSTRATE DEGRADATION IN MICROBIAL FUEL CELL OPERATING ON REAL HUMAN URINE

4. Investigating bacterial community changes and organic substrate degradation in Microbial Fuel Cell operating on real human urine

The work presented in this chapter corresponds to the following scientific article:

Barbosa, S.G., Peixoto, L., ter Heijne, A., Kuntke, P., Alves, M.M., Pereira, M.A., 2017 Investigating bacterial community changes and organic substrate degradation in MFC operating on real human urine. (submitted).

ABSTRACT

The present study investigates the changes in the microbial community and the degradation of organic compounds in microbial fuel Cells (MFC) operated on human urine. An anaerobic community was enriched in "urine-degrading" electroactive microorganisms by stepwise lowering the dilution factor of the anode media from 50 times diluted to undiluted urine. In a duplicated assay a current density of 495±16 mA m^{-2}, a chemical oxygen demand (COD) removal of 75.5±0.7 % and a Coulombic efficiency (CE) of 26.5±0.7 % were obtained during operation on undiluted urine. In a control assay, operated on undiluted urine without the microbial enrichment procedure, a current density of only 81±9 mA m^{-2} was obtained. The organic compounds commonly found in urine as well as the metabolic products associated to their degradation were analysed by proton nuclear magnetic resonance (^{1}H-NMR). The main compounds initially identified in the urine were urea, creatinine, glycine, trimethylamine N-oxide and acetate. Most of the organic compounds, except acetate, were depleted within 10 days of operation. The microbial community responsible for urine degradation in the anode of both MFCs was investigated using the Illumina MiSeq platform. Bacteria related with Firmicutes phyla were enriched in the anodic biofilms compared to the initial anaerobic inoculum, within which *Tissierella* and *Paenibacillus* were the dominant genus. *Tissierella* can metabolize creatinine producing acetate whereas several bacterial species belonging to the *Paenibacillus* genus demonstrated the ability to function as exoelectrogens. *Corynebacterium*, that comprise urea-hydrolysing bacteria were also amongst the main genera detected in the developed biofilms.

4.1. INTRODUCTION

Bio-electrochemical systems (BES), such as MFCs represent a new generation of technology that not only allows the production of energy but also the recovery of useful products with simultaneous wastewater treatment [11, 268]. MFCs allow the transformation of conventional wastewater treatment processes, which are characterized as energy-intensive and treatment-focused into integrated systems that allow the production of value added products while wastewater is treated [17]. MFCs are microbial fuel cells where substrate (*e.g.* wastewater) is oxidized by exoelectrogenic microorganisms. The released electrons are transferred to an electrode surface, as a result the chemical energy is converted into electrical energy [9].

Several artificial wastewater or synthetic growth media using defined organic substrates such as glucose [65] and acetate [269] have been successfully used as feedstocks for MFCs with an increase of power density by several orders of magnitude over the past decade. However, there are many challenges that limit BES application in real wastewater treatment. Among the major limitation for the BES is the wastewater complexity, the deviation of electrons into alternative electron acceptors, like SO_4^{2-} and NO_3^- or into non-electroactive biomass growth, or the substrate consumption via other competing metabolic pathways, such as methanogenesis. Additionally, technical challenges such as the high internal resistance of BES are also significant hurdles. Rabaey *et al.* reported a lower CE of the BES treating real wastewater compared to feed streams based on acetate and glucose [270]. The authors reported that the low efficiency was related to the presence of non-readily biodegradable compounds and the presence of alternative electron acceptors. Nevertheless, several wastewaters such as swine wastewater [170], brewery wastewater [61], human faeces wastewater [271], petroleum refinery wastewater [272] and domestic wastewater [273] have been tested for electricity production in MFCs.

Human urine, which is discharged with the domestic wastewater, is highly concentrated in nutrients (about 80 % of the nitrogen (N) and 45 % of the phosphorus (P) loads) [5]. Furthermore, urine can also provide a source of organic matter for energy production in BES since the concentration of organic compounds in urine is high (around 10 g L^{-1} of COD) and mainly composed by organic acids, creatinine, amino acids and carbohydrates [274]. Therefore, separation of urine from other wastewater streams would keep these organic compounds concentrated, and therefore, an interesting option to be used as a feedstock for MFC [244]. Several studies have evaluated the use of BES for current production from urine, however the performance of these BES in terms of CE,

COD removal and current density are rather poor. Ieropoulos *et al.* reported for the first time a MFC, which produced electricity from urine [204]. The authors of this study demonstrated an inverse relationship between the efficiency of conversion and the amount of urine to treat. Also Kuntke *et al.* developed a microbial fuel cell to simultaneously produce energy and recover ammonium from human urine [167]. Santoro *et al.* reported that raw human urine can be successfully oxidised in a membrane-less single chamber MFC showing a stable and relatively low, current generation [188].

Even though the removal of nutrients (N and P) and organic compounds (COD) were studied in MFCs treating urine, the anode performance has been significantly limiting the treatment efficiency due to the urea hydrolysis into carbon dioxide and ammonia, which increases the urine pH damaging the anodic biofilm. Although all existing efforts, the treatment of a real effluent, such as undiluted urine, using MFC systems is still not understood. Therefore, the main goal of this work was to develop a suitable strategy for microbial acclimation to undiluted urine in an MFC. The biological community developed was analysed by high throughput sequencing in order to identify the dominant bacterial and archaeal communities present in the anode biofilm. Additionally, ^{1}H-NMR spectroscopy was performed to study the course of the urine biodegradation. In addition, the kinetic relationship between substrate concentration and current generation was determined.

4.2. MATERIALS AND METHODS

4.2.1. Urine and inoculum source

Human urine collected from 5 male and 5 female individuals, was fed as anolyte after a phosphorus removal step according to Barbosa *et al.* [268] at decreasing dilution ratios (1/50, 1/25, 1/10, 1/3 and 1/1). The undiluted urine composition after pre-treatment is shown in Table 4.1. For each urine dilution, three successive batches were performed until a stable current density production was obtained (difference between two cycles <10 mV), after which the dilution of urine in the anodic chamber was decreased. Before each new cycle, the feed was flushed with nitrogen gas for 10 minutes to avoid oxygen in the anodic chamber. The anolyte was inoculated with anaerobic sludge collected from the wastewater treatment plant (WWTP) (Salgueiro, Portugal) for a final volume of 10 % (v/v). Before inoculation, the anaerobic sludge was filtered through a sieve (1 mm) to remove impurities. In order to focus on anodic chamber performance and to assure that the overall

performance was controlled by anodic chamber processes, potassium hexacyanoferrate (0.050 mol L^{-1}) in phosphate buffer (0.100 mol L^{-1}) at pH 7 was used as an unfailing catholyte.

TABLE 4.1 Composition of urine after phosphorus precipitation.

	Unit	Urine
pH		9.04±0.03
COD	g L^{-1}	7.55±2.00
TKN	g L^{-1}	5.6±2.2
NH_4^+-N	g L^{-1}	1.92±0.07
PO_4^{3-}-P	g L^{-1}	0.05±0.01
Conductivity	mS cm^{-1}	23.5±3.5

4.2.2. MFC experimental setup and operation

Three MFCs were used during the experiments. Two MFCs (duplicate run), were used to promote the gradual acclimation of bio-electroactive microorganisms to concentrated human urine (MFC A and MFC B). A closed circuit that comprise the working electrode and counter electrode connected across a resistor was used as acclimation system [275]. Additionally, a control assay (MFC C), in which the MFC was inoculated with anaerobic sludge and fed with undiluted urine as substrate was also performed. Each cell consisted in two plexiglass plates with an anode and a cathode chamber separated by a cation exchange membrane (CEM) (Ralex, Mega, Straz pod Ralskem, Czech Republic) (Figure 4.1). The MFCs were operated in batch mode at room temperature (20±3 °C). Anolyte and catholyte were recirculated via an external bottle at a flow rate of 1.00 mL min^{-1} and 1.25 mL min^{-1}, respectively, using a peristaltic pump (Sci Q 400, Watson Marlow, Cornwall, United Kingdom). Anode and cathode were connected with a 500 Ω resistor. Carbon felt (2 mm) in contact with carbon paper were used as anode and a modified graphite insert with flow channels (MAST Carbon International Limited, Basingstoke, United Kingdom) in contact with carbon paper as cathode. Flat graphite plates (Müller & Rössner GmbH & Co., Troisdorf, Germany) in contact with anode and cathode were used as current collectors. The cell voltage was recorded every 15 minutes by an Ecograph T data logger (RSG 30, Endress+Hauser B.V., Naarden, The Netherlands).

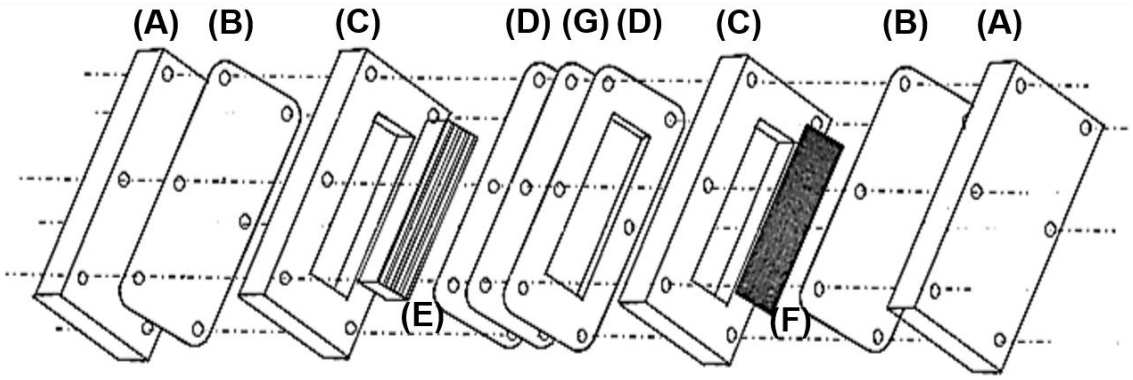


FIGURE 4.1 Schematic representation of the microbial fuel cells (MFCs) configuration: **A)** Flat graphite plates; **B)** carbon paper; **C)** plexiglass plates; **D)** silicone gaskets; **E)** graphite insert; **F)** carbon felt and **G)** cation exchange membrane (CEM).

4.2.3. Electrochemical characterization

Polarization and power curves were recorded to determine the performance and the internal resistance of the MFCs when a stable current density generation was achieved at maximum urine concentration. The polarization curves were performed by changing the external resistance of the cell. External resistance were decreased stepwise in the range of 6100 Ω to 10 Ω and was kept at each resistance for 5 minutes for current stabilization. The open circuit voltage was determined by disconnecting the electrodes for a period of 30 minutes (until stabilization) and before to perform the polarization and power curves. The internal resistance was determined from the slope of polarization curve.

4.2.4. Chemical analysis

Time course of urine degradation was assessed by monitoring the soluble chemical oxygen demand (COD) using Hach-Lange cuvette tests (Hach Lange, Düsseldorf, Germany) and a spectrophotometer DR 2800 (Hach Lange, Düsseldorf, Germany). All samples were previously centrifuged at 10 000 rpm for 5 minutes. Nuclear magnetic resonance (^{1}H-NMR) spectroscopy was used to study the course of the biodegradation of the organic matter. Samples from both MFCs working with undiluted urine were taken at different times (0, 10, 24, 46 and 59 days). The NMR measurements were performed using a Bruker Avance II 400 MHz spectrometer. The main functional groups were identified by liquid phase ^{1}H-NMR spectroscopy with D_2O as the solvent.

4.2.5. Calculation

The current density was obtained using $i = E \cdot (R \cdot A)^{-1}$, where i (A m^{-2}) corresponds to the current density, E (V) corresponds to the cell voltage, R (Ω) corresponds to the resistance and A (m^2) corresponds to the area of the anode (22 cm^2). Current generation as a function of substrate concentration was modelled according to Liu *et al.* [276] using an empirical Monod-type equation (Equation 4.1) where i (mA m^{-2}) is the current density production, i_{max} (mA m^{-2}) the maximum current density production, S (g L^{-1}) the concentration of substrate and K_S (g L^{-1}) the half-saturation constant.

$$i = \frac{i_{max} \cdot S}{K_S + S}$$ **EQUATION 4.1**

The CE was determined according to Equation 4.2, where CE (%) is the Coulombic efficiency, M (g mol^{-1}) is the molar mass of oxygen, Q (C) is the amount of produced charge calculated by integrating the current measured over time, F (C mol^{-1}) is the Faraday constant, b is the number of electrons produced per mole of O_2 (4), ΔCOD (g L^{-1}) is the change on COD concentration over time and V (L) is the volume of urine.

$$CE = \frac{M \cdot Q}{F \cdot b \cdot \Delta COD \cdot V}$$ **EQUATION 4.2**

The obtained results in terms of current production for assays with (MFC A and MFC B) and without (MFC C) acclimation to urine, were compared after a significance statistical analysis by using the Student's t-test with an established significance value of $p<0.05$.

4.2.6. Microbial community investigation

The biofilm developed at the anode from MFC A and MFC B was collected, concentrated (10 000 rpm, 5 minutes) and stored at -20 °C. In addition, the initial sludge inoculum and the urine used as substrate were also investigated for comparison of microbial community. DNA from the different samples was extracted according to the manufacturer's instructions using the FastDNA spin kit for soil (MP Biomedicals, USA) and the concentration of DNA extracted was checked using a nanodrop (Thermo Scientific, USA). Precipitation of DNA was performed by adding twice the solution volume of ethanol. The resulting extracted DNA was sent for high throughput sequencing using an Illumina

MiSeq platform (Research and Testing Laboratory-RTL, USA), in order to identify the dominant bacterial and archaeal communities present. The Illumina two-step was the MiSeq method developed by Caporaso and co-workers [277] and using universal primers for Bacteria, 28F and 388R, used for amplification of the variable regions V1-V3 and universal primers for Archaea, 517F and 909R, used for amplification of the variable regions V4-V5. Illumina sequencing data was submitted to the European Nucleotide Archive (ENA), under the study accession number PRJEB16750, and can be viewed by following the URL: http://www.ebi.ac.uk/ena/data/view/PRJEB16750.

4.3. Results and Discussion

4.3.1. Current generation as a function of urine concentration

Several successive batch assays of MFC fed with human urine were operated to study this substrate suitability for current generation. For start-up, MFCs were inoculated with 10 % of suspended anaerobic sludge from the biological reactors of the municipal WWTP of Salgueiro (Portugal). MFC A and MFC B were used for acclimation assay and were fed with 1/50 of urine as substrate whereas a MFC C, performed as a control assay, was fed with undiluted urine (Figure 4.2).

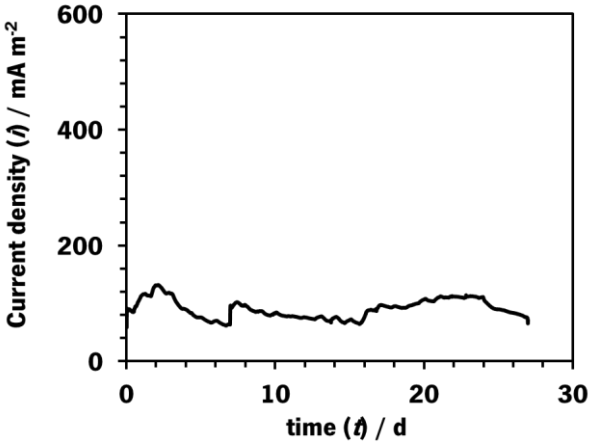


Figure 4.2 Measured current density over time with undiluted urine as substrate without any acclimation strategy.

Figure 4.3A and Figure 4.3B show the time-course of the cell voltage taken across a 500 Ω load during the start-up process for MFC A and MFC B, respectively. For both MFCs (A and B) a lag phase was observed with approximately 6 days with a subsequent current density increase after

which the current decreased as a consequence of organic matter depletion. The anolytes were replaced with a fresh batch each time the cell voltage decreased to less than 100 mV. The maximum voltage achieved was approximately 500 mV for both MFCs (A and B), which corresponds to a current density of 455 mA m^{-2} and to a power density of 227 mW m^{-2}. Compared to the control assay with undiluted urine, the acclimation method allowed to obtain a significantly higher current density (455 mA m^{-2}) that corresponds to approximately 5-fold the current obtained on the control assay (81±9 mA m^{-2}, Figure 4.2) (p<0.05). When reproducible current densities were observed for different batches, the anolyte was removed and replaced by new anolyte with stepwise decreased urine dilution.

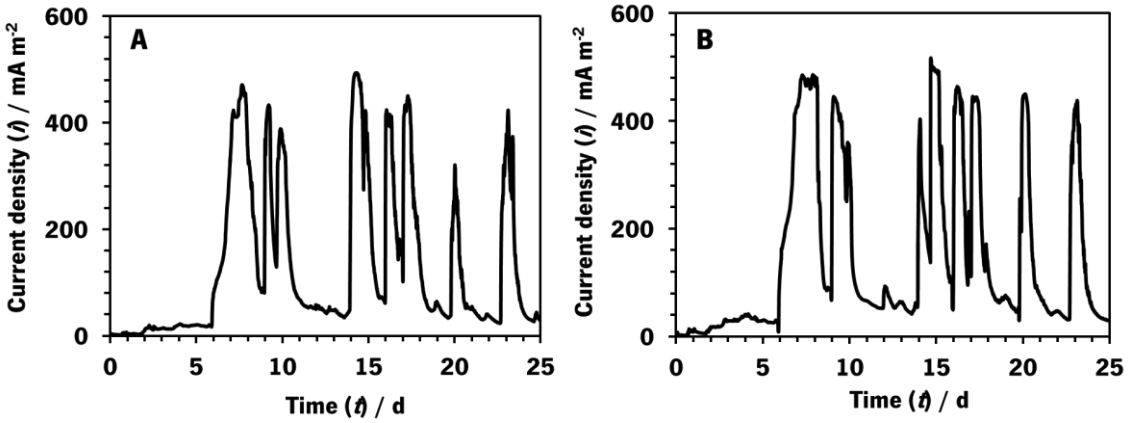


FIGURE 4.3 Measured current density during the start-up period with anaerobic sludge and 50x diluted urine **A)** MFC A and **B)** MFC B.

The current generation as a function of decreasing urine dilution for MFC A and MFC B is shown in Figure 4.4A and Figure 4.4B, respectively. The current generation in the MFCs was monitored at urine dilution ranging from 1/50 (0.06 g L^{-1} of COD) and 1/1 (7.71 g L^{-1} of COD). For each urine dilution, several batches were performed until a stable current production was obtained. Each batch corresponds to anolyte removal and replacement by fresh anolyte. Figure 4.4 shows that the anolyte replacement had no impact on current production as the current always increased immediately after the anolyte replacement. This suggests that the current generation resulted from the attached bacteria on the electrode, and was independent from the planktonic bacteria, thus the direct electron transfer mechanism is the major responsible for current generation [55, 126]. The results also showed that the increasing urine concentration does not seem to affect the development of the biofilm since the current generation also gradually increased. Using undiluted urine, a stable current density of approximately 501±14 mA m^{-2} (314±18 mW m^{-2}) for MFC A and

489±18 mA m^{-2} (299±22 mW m^{-2}) for MFC B was reached. A significance statistical analysis showed that MFC A and MFC B can be considered as a duplicate since no significant differences were observed (p<0.05). The acclimation process also allowed to obtain higher current than the reported in earlier experiments using real and synthetic urine [167] and real urine [278] without acclimation step.

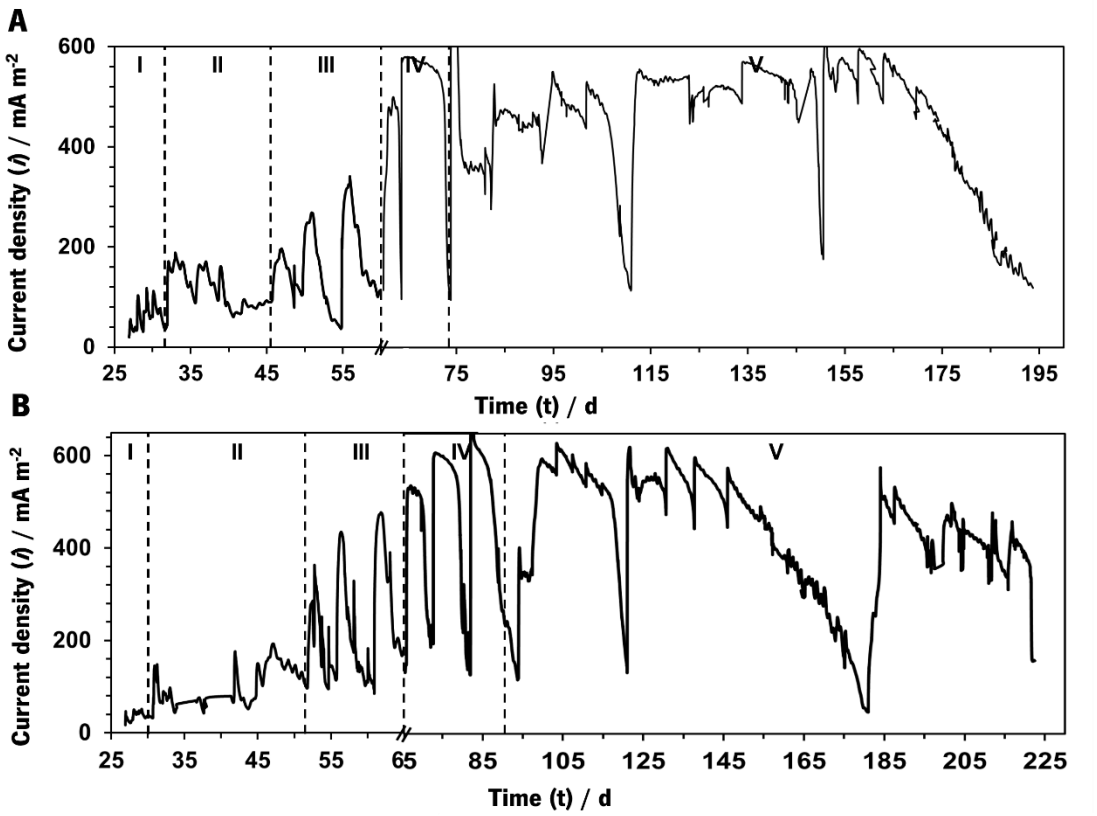


FIGURE 4.4 Measured current density during the experimental period with urine concentration increase: **A)** MFC A and **B)** MFC B. I: dilution 1/50 (0.06 g L^{-1} (COD)); II: dilution 1/25 (0.14 g L^{-1} (COD)); III: dilution 1/10 (0.64 g L^{-1} (COD)); IV: dilution 1/3 (2.37 g L^{-1} (COD)) and V: dilution 1/1 (7.71 g L^{-1} (COD)).

Current generation as a function of substrate concentration was modelled using an empirical Monod-type equation. According to the Figure 4.5, the current output at each urine concentration appeared to follow a saturation-type relationship. A i_{max} of 642 mA m^{-2} and K_s of 0.5 mg L^{-1} (R^2 = 0.979) were obtained for MFC A whereas a i_{max} of 592 mA m^{-2} and K_s of 0.4 mg L^{-1} (R^2 = 0.994) were obtained for MFC B. Previous reports demonstrated that MFC performance is affected by the substrate concentration. Sleutels and co-workers reported that low substrate load in combination with a sufficiently high anode overpotential plays a key-role in favourable growth kinetics of electrogens compared to methanogens and results in a high CE [279]. Furthermore, the

relationship between substrate concentration and power generation have been reported to demonstrate a saturation kinetic behaviour for different substrates namely xylose [280], lactate [281], nitrate [282] and swine wastewater [170].

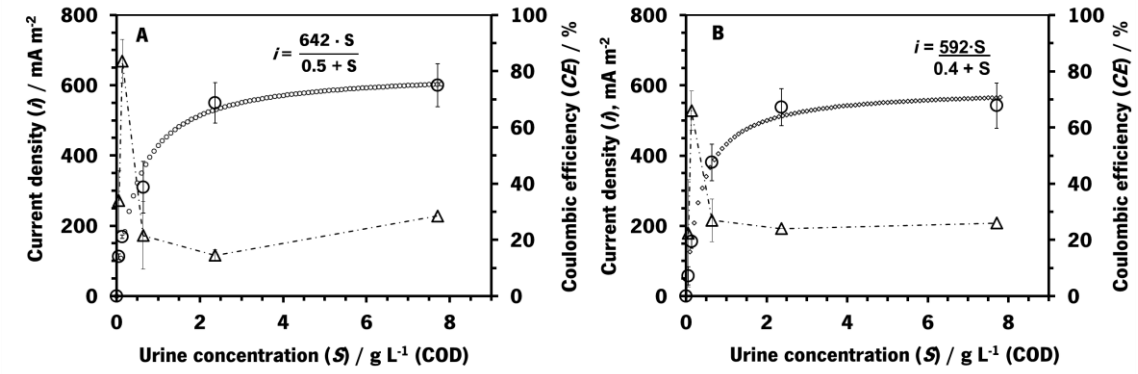


FIGURE 4.5 Correlation between maximum current density and coulombic efficiency (CE) with urine concentration for **A)** MFC A and **B)** MFC B.

Using undiluted urine, the average COD concentration of the effluent for both MFCs ranged between 1.72 g L^{-1} and 1.87 g L^{-1}, which corresponds to an average removal efficiency of 75 % and 76 % for MFC A and MFC B, respectively. It is important to note that this high removal is due to the high duration of each batch, between 40 and 60 days. The CE during the batches using undiluted urine was determined when a stable current density was obtained. The obtained CE at different urine concentrations is shown in Figure 4.5. A CE of 27 % and 26 % were achieved for MFC A and MFC B, respectively. The operation time of the batches increased with the increase of COD concentration (1±0.5 days for 0.06 g L^{-1} and 65±30 days for 7.71 g L^{-1}), which implied more chances for other processes to happen such as fermentation. Therefore, the CE decreased when the urine dilution decreased which means that less available electrons were used for current production. Several articles reported the decrease of CE with the increase of substrate concentration [166, 282, 283]. The low efficiency obtained, using undiluted urine, suggest that the electrons released from the substrate oxidation may have been used for gas production (H_2 or CH_4) or lost to alternative electron acceptors (*e.g.* sulphur or nitrogen compounds) [44, 185]. Furthermore, the presence of CH_4 was detected in the external bottle used for recirculation. Nevertheless, the CEs obtained in this work are in accordance with previous reports using wastewater containing fermentable substrates [120, 270, 284].

The anode potential of the MFCs was estimated from the theoretical cathode potential for a 50 mM $K_3Fe(CN)_6$ in 100 mM PO_4 buffer (pH 7) (0.215 V vs. Ag/AgCl) [285] subtracting the measured cell potential. The estimated average anode potential shows a decrease with the increase of urine concentration. This decrease in anode potential can be explained by the increase of the anode pH due to ammonia concentration increase. This observation is in accordance with earlier published work [167].

For further investigation of the MFCs performance, polarization curves at different external resistances were recorded. The polarization and power curves for both MFCs were performed during stable current generation with undiluted urine (Figure 4.6). The open circuit voltage measured in the stable phase for both MFC was 0.730 V. In the power curves, the highest power density reached in MFC A and MFC B were 0.9 W m^{-2} and 1.0 W m^{-2}, which corresponds to a current density of 2.0 A m^{-2} and 2.1 A m^{-2}, respectively. Based on the polarization curves, the internal resistances of 66 Ω for MFC A and 59 Ω for MFC B were determined from the slope of the curve in the region dominated by ohmic losses, which were close to the external resistance that produced maximum power densities (100 Ω) in the power curve.

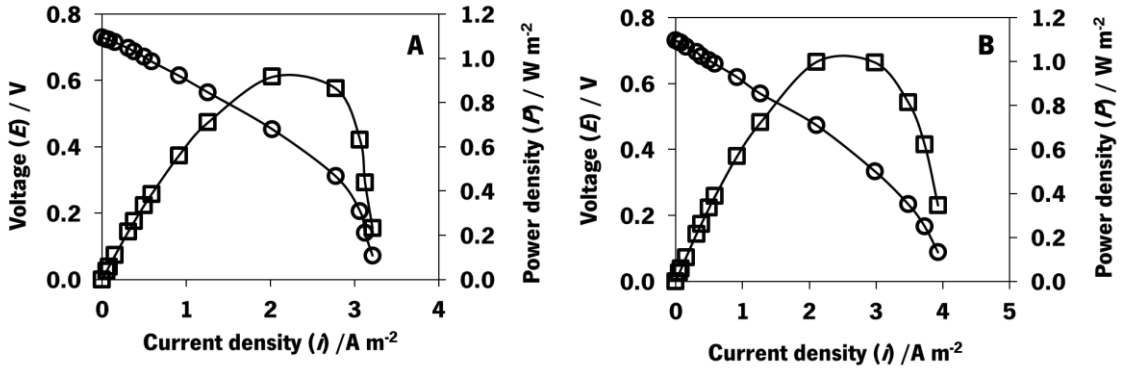


FIGURE 4.6 Polarization (○) and power curves (□) obtained by varying the external resistance between the electrodes for: **A)** MFC A and **B)** MFC B.

4.3.2. ^{1}H-NMR analysis

NMR spectra of MFC A and MFC B anolytes were taken to study degradation of organic compound found in urine, and are shown in Figure 4.7. The spectra were initially dominated by signals in the aliphatic region ascribed to protons on methyl groups of aliphatic chains, protons located in methylene chains (0 to 3 ppm) and protons attached to O or N (1.5 to 6.5 ppm). Furthermore, signals in the aromatic region were also detected (6.5 to 8 ppm). The signal at 4.79 ppm

corresponds to D_2O. According to the results, in the aliphatic region the following main signals were observed: δ = 5.79, 4.08, 3.58, 3.29, 3.07 and 1.94 ppm. The signal centred at 5.79 ppm corresponds to the urea molecule and the signals centred at 4.08 and 3.07 ppm correspond to creatinine. Urea and creatinine have been reported as two of the most abundant organic metabolites found in urine [274] and according to results, they were depleted during the first 10 days of operation. Urea is hydrolysed by an enzyme (urease) produced by many bacteria, however urea cannot be utilized as carbon source by the anode microbial community [213, 286]. Therefore, urea does not contribute for electricity production.

The 3.58 and 3.29 ppm signals correspond to glycine and trimethylamine N-oxide (TMAO) compounds, respectively, whereas the signal at 1.94 ppm corresponds to acetate. According to the Figure 4.7 it is possible to observe that the peak correspondent to acetate increase in the beginning of the batch due to the conversion of other organic compounds such as, creatinine into acetate, and decrease in the end of the operation due to the conversion of acetate into energy.

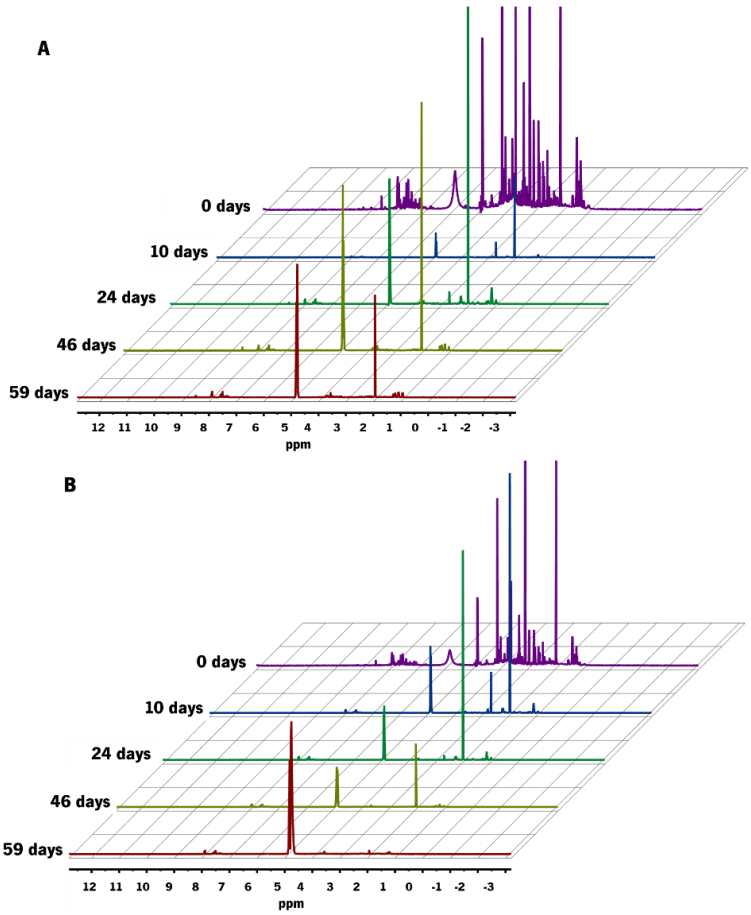


FIGURE 4.7 ^{1}H-NMR spectral data of anolyte from **A)** MFC A and **B)** MFC B.

4.3.3. Microbial communities

Microbial community of the initial inoculum sludge, as well as the community present in the urine used as substrate and the community developed at the anode from both MFCs, were investigated. The data generated from Illumina sequencing is displayed by Krona® charts (Hierarchical Data Browser) in Figure 4.8. The charts represent, 52, 41, 90 and 83 % of the total sample, since the remain percentage was classified as "no hit", which means that there were no matches with the software database that meet the minimum criteria to be considered a good match. Furthermore, about 30 % of the sequences retrieved from the samples collected from the anodes were classified as "unknown", which means that the taxonomic information provided by NCBI contains missing information.

A clear variation in the community composition was observed when comparing the original anaerobic inoculum with the anode biofilms, with Firmicutes phyla being largely enriched in the anodic communities (9 % in the initial inoculum, 22 % in the MFC A and 33 % in the MFC B) (Figure 4.8). On the other hand, the Proteobacteria phyla percentage was reduced from 53 % in the initial inoculum, to 24 % in the MFC A and 10 % in the MFC B. These shifts were similar to the reported in MFCs operated at alkaline pH values [287]. Furthermore, it is possible to observe that several groups of bacteria identified in MFCs anodes are also detected in the urine (Figure 4.8D), suggesting its contribution to the microbial community developed in the anodes. According to Figure 4.8B and Figure 4.8C, the taxonomic profiles of MFC A and MFC B are highly similar. The two main bacteria taxa commonly found in both MFCs were Proteobacteria (24 % and 10 %, for MFC A and MFC B, respectively, assigned to the orders Burkholderiales, Caulobacterales, Desulfobacterales, Rhizobiales, Rhodobacterales and Pseudomonadales) and Firmicutes (22 % and 33 %, for MFC A and MFC B, respectively, assigned to the orders Clostridiales and Bacillales, Bacteroidetes and Actinobacteria).

Assigned to the Proteobacteria phylum, *Paracoccus, Desulfobulbus* and *Pseudomonas* are three dominant genera detected on the anodes. Several microorganisms of *Paracoccus* genus have been demonstrating the ability to reduce nitrate even in MFCs [288]. *Desulfobulbus* genus, belonging to the class Deltaproteobacteria, comprise sulphate-reducing bacteria and was also identified. According to Tice and Kim the high SO_4^{2-} concentration (350 mg L^{-1} to 1500 mg L^{-1}) in fresh human urine promotes the growth of SO_4^{2-} reducing bacteria [289]. *Pseudomonas* belonging to the class Gammaproteobacteria have been reported as an electroactive bacteria since most microorganisms

affiliated with this class are reported as exoelectrogens. Pham and co-workers reported the capacity of *Pseudomonas* to transfer electrons to the electrode via self-produced metabolites functioning as soluble mediators [290].

Paenibacillus, Clostridium, Atopostipes and *Tissierella* are the four main genera identified belonging to the Firmicutes phylum. Several bacterial species belonging to the *Paenibacillus* and *Clostridium* genera demonstrated the ability to function as exoelectrogen and were found under different operation conditions generating current in MFCs [291, 292, 293]. *Atopostipes* have been known as carbohydrates fermenting such as glucose to lactate, acetate, and formate [294]. *Tissierella* species have been identified as able to grow on urine, metabolizing creatinine as sole carbon source producing acetate, methylamine, ammonia and carbon dioxide [295]. The ^{1}H-NMR spectra (Figure 4.7) showed that both peaks corresponding to creatinine compound (δ=4.08 ppm and δ=3.07 ppm) disappeared during the first 10 days of operation, possibly due to the presence of species assigned to the genus *Tissierella*. *Petrimonas* and *Corynebacterium* genus, assigned to the Bacteroidetes and Actinobacteria phyla were also identified. *Petrimonas* is known as a fermentative bacteria, which can use carbohydrates and some organic acids and reduce nitrate to ammonium [278]. *Corynebacterium* have been associated to microorganisms that have the ability to produce urease that catalyses the hydrolysis of urea into carbon dioxide and ammonia [213]. Likely, *Corynebacteria* is responsible for the degradation of urea, as ^{1}H-NMR spectrum (Figure 4.7) demonstrated that until the day 10, urea is depleted.

The archaea community composition was dominated by Methanomicrobiales, with significantly lower percentage of Methanosarcinales (Figure 4.9). *Methanolinea* sp., belonging to the Methanomicrobiales order is characterized as a hydrogenotrophic methanogen and *Methanolobus* sp. belonging to the order *Methanosarcinales* is characterized as a methylotrophic methanogen.

In spite of high free ammonia concentration present in urine (around 200 mg L^{-1}), Schnürer and Nordberg demonstrated that the methane production is also possible due to the shift from the acetoclastic mechanism to the syntrophic pathway [296]. Syntrophic acetate oxidation involves acetate oxidation to H_2 and CO_2 by an acetate oxidizing bacteria, followed by the reduction of CO_2 to CH_4 by a hydrogenotrophic methanogen that can tolerate higher levels of ammonia than acetoclastic methanogens. Westerholm and co-workers reported a decrease in the acetoclastic methanogens and an increase in hydrogenotrophic methanogens in response to increasing ammonia levels, most likely caused by a higher tolerance of Methanomicrobiales to ammonia [297]. The results obtained in this experiment also showed the prevalence of Methanomicrobiales

in the anode biofilm suggesting that the methane produced may have been by a syntrophic pathway.

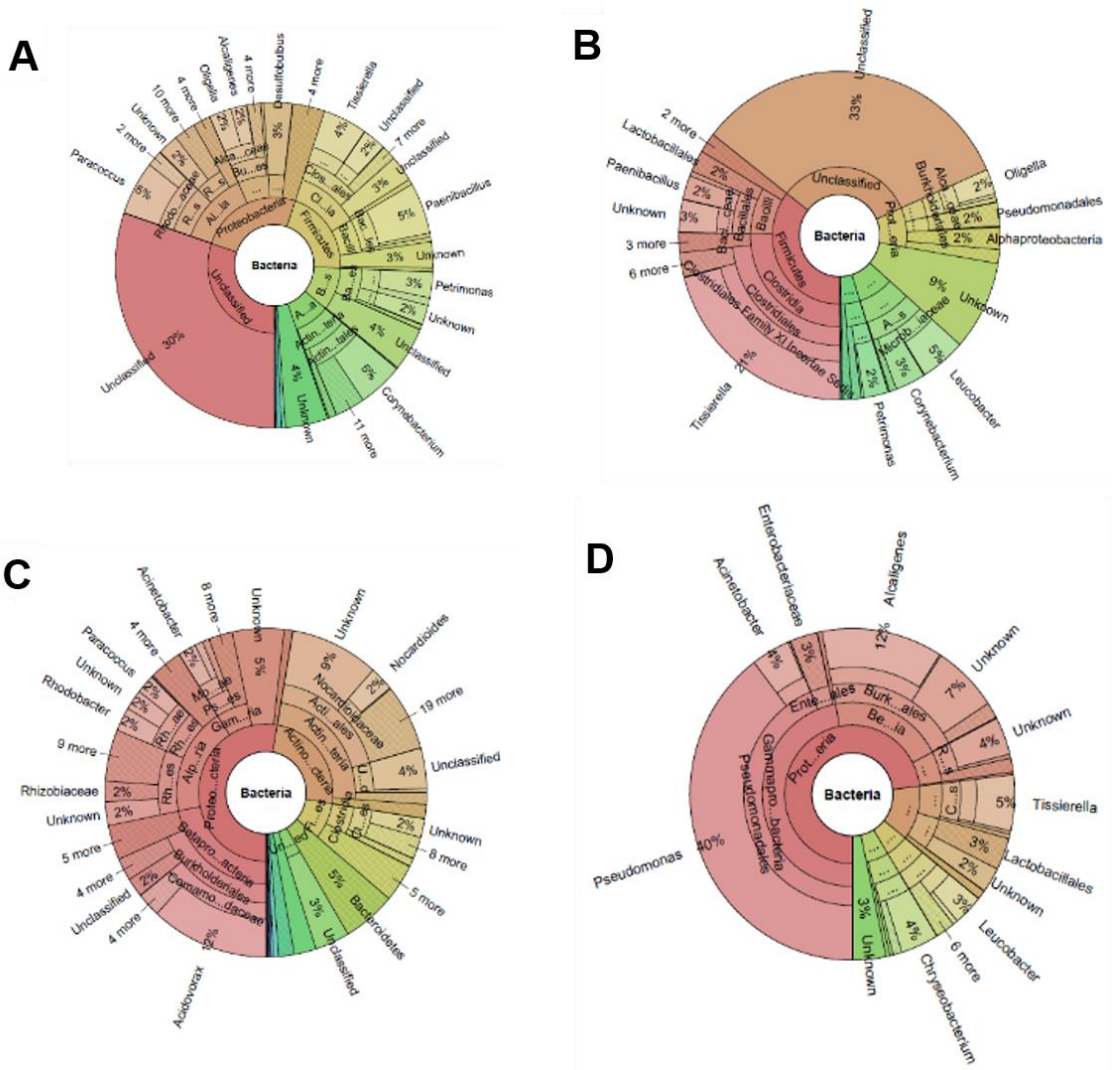


FIGURE 4.8 Bacterial community distribution at genus level for biofilms developed in **A)** anode of the MFC A; **B)** anode of MFC B as well as for the bacterial community present in **C**) initial sludge inoculum and **D)** urine used as substrate.

Several *Methanolobus* species such as *Methanolobus profundi* [298] *Methanolobus taylorii* [299] and *Methanolobus psychrophilus* [300] that use methylated compounds for methane production have been reported. Besides, Winfrey and Ward demonstrated that in the presence of high concentrations of sulphate, that is the case of urine, methane may be resultant from different substrates such as methylamine [301]. ^{1}H-NMR spectra (Figure 4.7) demonstrated that methylamine signal (δ=2.60 ppm) decreases over time possibly due to the methane formation from methylamine by *Methanolobus s*pecies. Similar to the previous compound, the signal of TMAO

(δ=3.25 ppm) identified in both MFCs disappear during the first 10 days of operation possibly due to the TMAO reduction to trimethylamine (TMA). In turn, TMA signal is reduced over time since TMA may stimulate and can be used as substrate for methane production [302].

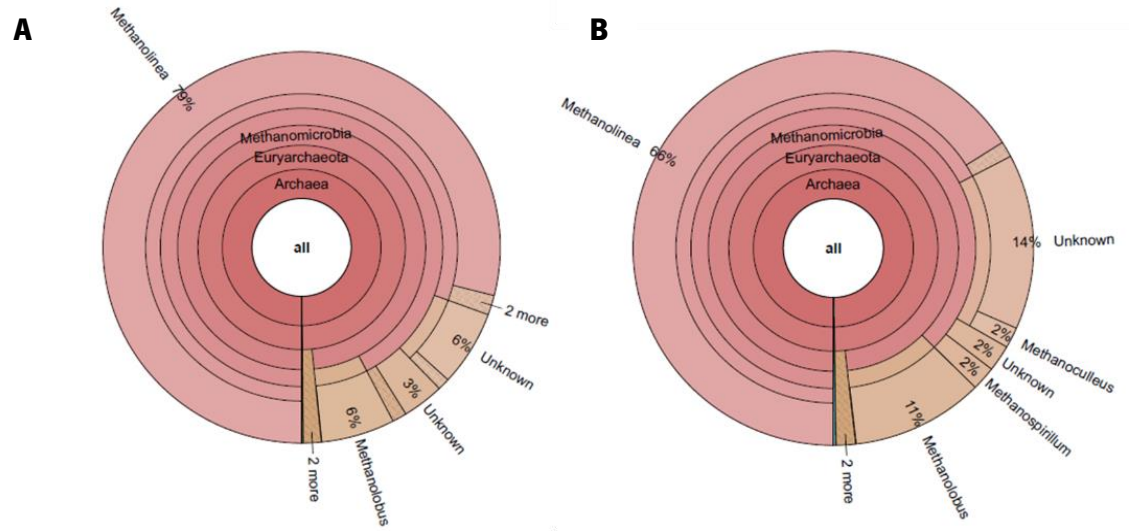
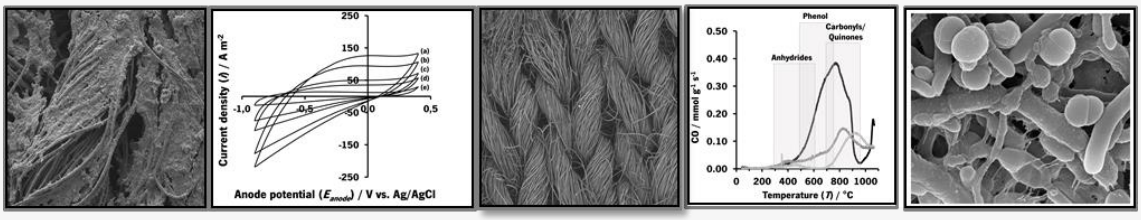


FIGURE 4.9 Archaea community distribution at genus level for biofilms developed in the anode of the **A)** MFC A and **B)** MFC B.

4.4. CONCLUSIONS

The present study demonstrated that MFCs can be operated with undiluted human urine. In general, there was no difference between the two MFCs, both of which achieved similar CE (27 % for MFC A and 26 % MFC B) and current density production (545 mA m^{-2} for MFC A and 591 mA m^{-2} for MFC B). According to the microbial community analysis, Firmicutes phyla was enriched in the anodic biofilms compared to the initial anaerobic inoculum, within which *Tissierella* and *Paenibacillus* were the dominant genera in the MFC A and MFC B anodes, respectively. The presence of these species was related to the degradation products of urine, as analysed by ^{1}H-NMR. *Tissierella* is responsible for metabolize creatinine producing acetate whereas several bacterial species belonging to the *Paenibacillus* genus demonstrated the ability to function as exoelectrogen. These results demonstrated that high strength wastewater such as undiluted urine can be used for power generation in MFCs using an adapted microbial community, generating approximately 80 % higher current density than the control assay fed with undiluted urine without any microbial acclimation.



Chapter 5

EFFECT OF DIFFERENT CARBON MATERIALS ON THE PERFORMANCE OF MICROBIAL ELECTROLYSIS CELLS OPERATED ON URINE AND THEIR MICROBIAL COMPOSITION

5. Effect of different carbon materials on the performance of Microbial Electrolysis Cells operated on urine and their microbial composition

The work presented in this chapter corresponds to the following scientific article:

Barbosa, S.G., Peixoto, L., Soares, O.S.G.P., Pereira, M.F.R., ter Heijne, A., Kuntke, P., Alves, M.M., Pereira, M.A., 2017. Effect of different carbon materials on the performance of MECs operated on urine and their microbial composition. (submitted).

ABSTRACT

In this study, the anode performance of microbial electrolysis cells (MEC) fed with urine using three different carbon anodes, Keynol (phenolic-based), C-Tex (cellulose-based) and PAN (polyacrylonitrile-based) was compared. Two strategies were used to supply energy to MECs; cell potential control (1st assay) and anode potential control (2nd assay). In both assays, the MEC using C-Tex outperformed MECs using Keynol and PAN. The MEC with the C-Tex under anode potential control at -0.300 V generated the highest current density of 904 mA m^{-2}, which was almost 3-fold higher than the MEC with Keynol, and almost 8-fold higher than the MEC with PAN at identical operational conditions. The microbial composition on each anode and its correlation with the generated current were investigated. Results showed that the different anodes studied had no effects on the microbial diversity developed on each anode. Nonetheless, C-Tex had higher percentage of bacteria belonging to Lactobacillales and Enterobacteriales suggesting that microbes assigned to these order may be correlated with the higher current generation.

5.1. INTRODUCTION

Microbial Electrolysis Cells (MECs) are a specific type of Bioelectrochemical Systems (BESs), which combines the biological oxidation of organic substrate to the electrochemical reduction of water to produce hydrogen gas (H_2) [19]. Several studies have shown that H_2 production can be successfully coupled to wastewater treatment in MECs [193, 303, 304]. Recently, urine was proposed an ideal wastewater for bioelectrochemical systems [244]. Urine is a liquid waste that accounts for 1 % of the total volume of domestic wastewater produced. Even though, approximately 75 % of the nitrogen (N) load and 50 % of the phosphorus (P) loads found in domestic wastewater originate from urine [197]. Furthermore, urine contains a wide range of organic compounds, such as acetate that can be biologically oxidised. MECs efficiently convert chemical energy stored in organic substrate into H_2, and are therefore a promising technology for renewable and sustainable H_2 production. Kuntke and co-workers investigated the use of MEC for H_2 production from diluted urine [235]. The authors demonstrated that MEC can be a promising technology for H_2 production with simultaneous ammonium (NH_4^+) and chemical oxygen demand (COD) removal from diluted urine. Nonetheless, further research is necessary to improve the conversion of the chemical energy to electrical energy [235]. Thus, an efficient biological transfer of electrons between bacteria and anode surface is essential.

The development of the biofilm and electron transfer are strongly dependent on the anode characteristics, namely surface charge, surface wettability (hydrophobicity/hydrophilicity), surface area and conductivity [305]. Several anode materials have been used in MECs such as graphite brush [306], plain carbon cloth [32] and graphite granules [307]. As a general trend, it has been reported that increasing the surface area available for bacteria attachment of the anode materials improves the current output [66, 308, 309]. Further, Guo and co-workers showed that positively charged and hydrophilic surfaces improved electroactive biofilm growth and development. In order to improve the performance of the MECs, a better understanding how electrode properties affect biofilm performance is, therefore, necessary [12].

The aim of this study was to evaluate the performance of electrochemically active biofilms fed with urine on three different carbon anode materials. These carbon anodes produced from different sources, phenol-based (Keynol), cellulose-based (C-Tex) and polyacrilonitrile (PAN) were investigated for the textural, chemical and electrochemistry characterization. The performance of the MEC was assessed by the current density, the coulombic efficiency and the COD removal

efficiency. The biological community developed was investigated by high throughput sequencing and the relationship between the identified microorganisms and the generated current was analysed.

5.2. MATERIALS AND METHODS

5.2.1. Urine and inoculum source

MECs were fed with urine collected from 5 male and 5 female individuals. Urine was pre-treated by adding a magnesium source in order to remove phosphorus (P) as a precipitate, namely struvite according to Barbosa *et al.* [268]. Urine composition after pre-treatment is shown in Table 5.1. The MECs were inoculated with an anaerobic community previously enriched in "urine-degrading" electroactive microorganisms in a MFC (Chapter 4).

TABLE 5.1 Composition of urine after phosphorus precipitation.

	Unit	Urine
pH		9.04±0.03
COD	g L^{-1}	7.55±2.00
TKN	g L^{-1}	5.6±2.2
NH_4^+-N	g L^{-1}	1.92±0.07
PO_4^{3-}-P	g L^{-1}	0.05±0.01
Conductivity	mS cm^{-1}	23.5±3.5

5.2.2. Electrodes characterization

In this study three types of carbon electrodes, C-Tex, Keynol and PAN (MAST Carbon International Limited, United Kingdom) were tested as anode material in MECs. Textural and electrochemical characterizations were performed before their application in the MECs.

i. Chemical and textural characterization

A scanning electron microscope (SEM) (Nova NanoSEM 200, FEI, USA) integrated with an energy dispersive spectrometer (EDS) (Pegasus X4M, EDAX, USA) was used to investigate the surface morphology of the different electrode materials. Elemental analysis was carried out on a vario MICRO cube analyser from Elemental GmbH (Germany) in CHN mode. Each element (carbon (C), hydrogen (H) and nitrogen (N)) was determined by combustion of the sample at 1050 °C and

calculated by the mean of three independent measurements, using a calibration with a standard compound. Also the elemental content of oxygen (O) on the different electrodes was carried out on a rapid OXY cube analyser from Elemental GmbH (Germany). The content of O was determined by pyrolysis of the sample at 1450 °C and calculated by the mean of three independent measurements, using calibration with a standard compound.

The surface chemistry was characterized by temperature programmed desorption (TPD). The carbon monoxide (CO) and carbon dioxide (CO_2) TPD profiles were obtained with a fully automated AMI 300 Catalyst characterization apparatus (Altamira Instruments, USA) connected to a Dycor Dymaxion Mass Spectrometer. Each sample (0.100 g) was heated up to 1100 °C at 5 °C min^{-1} using a constant flow rate of helium equal to 25 $cm^3 min^{-1}$.

The textural characterization of the samples was based on the nitrogen (N_2) adsorption isotherm, determined at -196 °C with Quantachrome NOVA 4200e instrument (Quantachrome, USA). The samples (0.100 g) were outgassed at 150 °C for 3 h under vacuum. The specific surface area (S_{BET}) of the samples was calculated by the Brunauer-Emmett-Teller (BET) equation. The external surface area (S_{ext}) and the volume of micropores (V_{micro}) were calculated by the t-method using the standard isotherms proposed by Rodriguez-Reinoso *et al.* [310]. The total specific pore volume (V_p) was determined from the amount adsorbed at $P/P_0 = 0.95$.

The wettability (hydrophobicity/hydrophilicity) of the dry electrodes was determined through their contact angle at room temperature. Sessile drop technique was performed in an OCA20 (DataPhysics, Germany) instrument by depositing ultrapure water drops (3 μL) on the sample surface and the contact angle was analysed with the SCA20 software. At least three different spots of each material were measured to provide an average contact angle measurement. The thermal stability of the electrodes were investigated by thermogravimetric analysis (TGA) using a thermogravimetric analyser (TGA 4000, PerkinElmer, USA) starting from room temperature to 800 °C with a heating rate of 10 °C min^{-1} under a N_2 flux (3 mL min^{-1}). The surface functional groups of different materials was analysed by Fourier transform infrared (FTIR) spectroscopy (Spotlight 300, PerkinElmer, USA) at room temperature in the range of 400 cm^{-1} to 4000 cm^{-1}.

ii. Bacterial attachment capacity

The biomass attachment was quantitatively measured by assessed dry weight measurements. Mixed urine collected from 5 female and 5 male individuals was used as the inoculum. Small pieces of the electrodes (Keynol: 140±41 mg; C-Tex: 117±35 mg and PAN: 90±31 mg) were

immersed in urine for 2 weeks (room temperature and 45 rpm). After this period, the electrodes were dried in a drying oven at 105° C until a stable weight. For each electrode material, the assays were performed in triplicate. The final weight of electrodes were measured to determine the extents of bacterial attachment, biofilm formation and other aggregates [93]. The amount of attached biomass was calculated based on the difference of the weight before and after the biofilm development per amount of electrode used.

iii. Electrochemical characterization

The electrochemical performance of the different materials was studied in a three-electrode test cell using a potentiostat (VSP, Biologic, France). Platinum foil (2 cm x 2 cm) was used as the counter electrode and an Ag/AgCl electrode was used as the reference electrode. The electrochemical measurements were carried out in 50 mL of KOH 1M at room temperature.
Cyclic voltammetry measurements were carried out between −0.9 and 0.4 V at different scan rates (1, 5, 10, 30, and 50 mV s^{-1}). The galvanostatic charge/discharge tests were performed at the same potential range used for cyclic voltammetry at a current of 1 mA. The specific capacitance of the various electrodes was determined from the charge-discharge curves using Equation 5.1, where C is the capacitance per unit of the electrode surface (mF cm^{-2}), I is the current density (mA cm^{-2}), Δt is the time of discharge (s), ΔV is the potential window (V) and m is the mass of electrode [311]:

$$C = \frac{I\,\Delta t}{\Delta V\, m} \qquad \textbf{EQUATION 5.1}$$

5.2.3. Reactor set up

An experimental set-up with three simultaneously running MECs was assembled to study the influence of the three different anode materials (Keynol, C-Tex and PAN) on anode performance and the developed microbial community. The set-up consisted of three identical dual-chambers plexiglass MECs operated at room temperature (20±3 °C). The different anode materials connected to a graphite insert (MAST Carbon International Limited, United Kingdom) were used as anode and NiMo (MAST Carbon International Limited, United Kingdom) connected to a graphite insert as a cathode. The graphite inserts were designed to fit in the anode compartments and contained parallel flow channels to direct the flow. At the same time, they ensured good contact

between electrode material and current collector. Flat graphite plates connected to each graphite insert (Müller & Rössner GmbH & Co., Germany) were used as current collectors. A cation exchange membrane CMH-PP (Ralex, Mega, Czech Republic) was placed directly between the two-chambers. Urine after phosphorus removal was fed as anolyte whereas NaCl (0.1 M) was supplied as catholyte.

In the first assay, the MECs were operated under cell potential control by setting the cell potential with a potentiostat. The applied cell potential was step wise increased (100 mV), during almost 6 weeks (38 days), from 0.4 V to 0.9 V. The anode potential that allow to obtain the highest current density was selected for the next assay with anode potential control. In the second assay, new electrodes were used and the anode potential was controlled at -0.300 V vs. Ag/AgCl using a potentiostat. The electrochemical instrumentation consisted of a potentiostat (VSP, Biologic, France) used to control potential and a data acquisition software (EC-Lab software) to record data such as current density. All voltages are reported vs. Ag/AgCl (+0.210 V vs. NHE).

5.2.4. Chemical analysis and measurements

During the experiments, samples were taken from the anode effluent compartment and were analysed for soluble chemical oxygen demand (sCOD) concentration using Hach-Lange cuvette tests (Hach Lange, Düsseldorf, Germany) and a spectrophotometer DR 2800 (Hach Lange, Düsseldorf, Germany). All samples were previously centrifuged at 10 000 rpm for 5 minutes. pH was also measured using a portable pH meter (HI 83141, Hanna, Italy).

Current density was determined dividing the current obtained by the area of each anode (25 cm^2). Coulombic efficiency (CE) which was determined from the measured current and the removed COD as described by Logan and co-workers [19]. Cyclic voltammetry was used to characterize electron transfer mechanism at the surface of the different anodes. The current density in response to the anode potential, in a range from −0.900 V to 0.800 V, was recorded directly from the potentiostat output at a scan rate of 0.15 mV s^{-1}.

5.2.5. Microbial community investigation

The biofilm attached at each anode was collected by cutting small pieces of electrode. In addition, the initial inoculum was also investigated for comparison of the microbial community. The samples were preserved at -20 °C until analysis. DNA from the different biofilms was extracted using the FastDNA spin kit for soil (MP Biomedicals, USA) according to the manufacturer's guidelines. The

concentration of the extracted DNA was checked using a nanodrop equipment (Thermo Scientific, USA). The DNA samples were sent for high throughput sequencing using an Illumina MiSeq platform (Research and Testing Laboratory-RTL, USA). The MiSeq method used was the Illumina two-step [277]. Specific primer sets (Bakt_341F/Bakt_805R) for the amplification of bacterial domain were used. Illumina sequencing data was submitted to the European Nucleotide Archive, under the study accession number PRJEB20142, and can be viewed by following the URL: http://www.ebi.ac.uk/ena/data/view/ PRJEB20142.

5.3. RESULTS AND DISCUSSION

5.3.1. Electrodes characterization

i. Chemical and textural characterization

Figure 5.1 shows SEM images of the carbon fibers of the different carbon electrodes at 160x and 1000x magnification. These SEM images shows that all three electrodes present uniform morphology over the whole sample. The fibers cross sections represent a circular shape with an average diameter of 6.5±1.2 µm for Keynol, 7.3±1.2 µm for C-TEX and 6.9±0.8 µm for PAN. The elemental analysis showed that Keynol is composed of 78.9 % C, 9.1 % O and 2.0 % H. C-Tex is mainly composed of 74.6 % C, 11.1 % O, 1.2 % H and 1.15 % N. PAN is composed of 88.2 % C, 1.2 % O, 0.6 % H and 7.1% N. The sum of CHNO for each anode material was not 100 %, suggesting that other compounds mainly inorganics can be present in the sample.

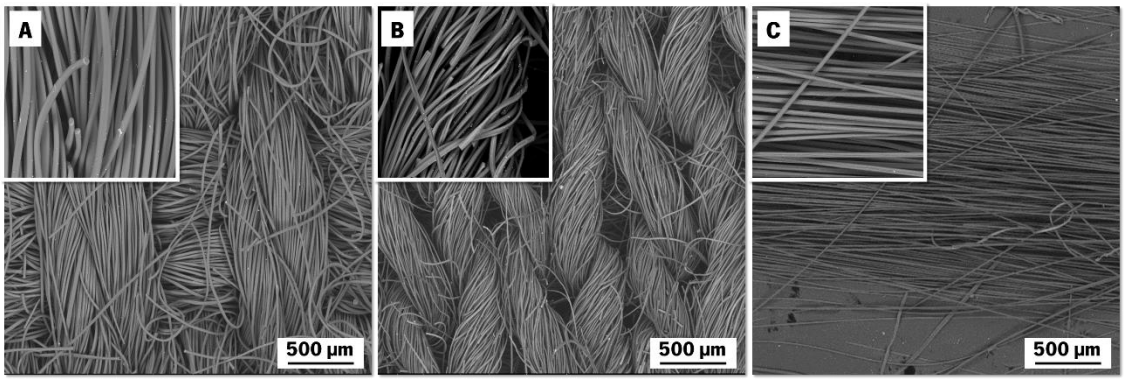


FIGURE 5.1 Scanning electron microscopy (SEM) images of different carbon anode materials (160 x): **A)** Keynol **B)** C-Tex and **C)** PAN. The insets show a higher magnification image of the electrodes (1000 x).

Figure 5.2 shows the TPD profiles of the different electrodes in study. An increase of the CO and CO_2 peaks corresponds to an increase in the amount of functional groups containing oxygen. The TPD peaks were assigned to the different oxygen functional groups by comparison with the data exhibited in [312,313]. According to Chen and co-workers, oxygen-containing groups on carbon surface improve the surface hydrophilicity and improve the contact between the electrode surface and electrolyte [314]. The polarity of the oxygen functional groups promote the reaction between the oxygen, at the carbon surface, and water molecules in the electrolyte by hydrogen bonds, increasing the hydrophilicity of the electrode surface [315]. The TDP profile of C-Tex showed larger CO and CO_2 peaks which corresponds to higher amount of oxygen functional groups, compared With the other materials (Keynol and PAN), suggesting that the cell adhesion is promoted on the C-Tex surface.

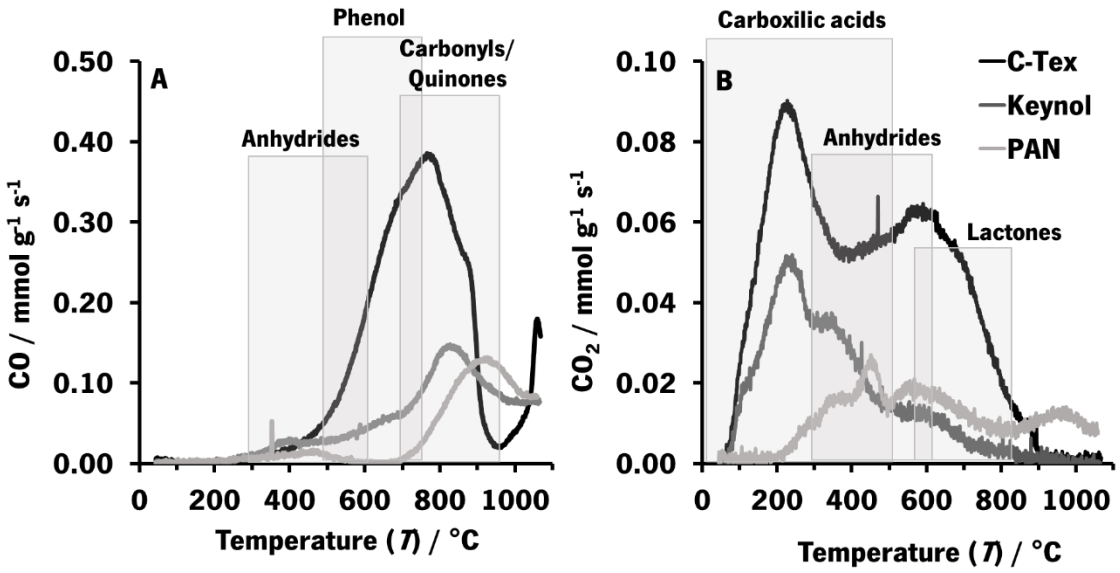


FIGURE 5.2 Temperature programmed desorption curves profile of different anodes, corresponding to the evolution of **A)** CO and **B)** CO_2 upon decomposition of the various types of oxygen functional groups.

The results of textural characterisation resulting from the N_2 equilibrium adsorption isotherms are presented in Table 5.2. The shape of Keynol and C-Tex N_2 sorption isotherms (Figure 5.3) is of type I according to IUPAC demonstrating that the pores present in these electrodes are essentially micropores (d<2 nm) [316]. Table 5.2 shows that on Keynol 90 % of the total pore volume are micropores, whereas on C-Tex the micropores volume corresponds to 55 %. The shape of PAN N_2 sorption isotherms is of type II, which is typical for multi-layer adsorption in non-microporous materials (Figure 5.3). Table 5.2 shows that the volume of pores on PAN is insignificant compared

with the other electrodes. According to these results, Keynol showed a slightly higher S_{BET} (1234 m^2 g^{-1}) compared to C-Tex (1090 m^2 g^{-1}) and a largely higher S_{BET} compared to PAN (13 m^2 g^{-1}). High S_{BET} of Keynol and C-Tex can be attributed to their high amount of micropores (d<2 nm). However, given the size of a typical bacteria (1 μm to 3 μm), high S_{BET} does not necessarily increase the surface area available for bacterial attachment [71]. According to Lu and co-workers, only pores with a large diameter, such as macropores (50 nm<d<1000 nm) and pores introduced by material assembly contribute to the surface area available for biofilm formation [69]. The S_{ext} was also determined, which corresponds to the surface area of the materials excluding the contributing of micropores. C-Tex present the highest S_{ext} (305 m^2 g^{-1}) compared to the other electrodes (70 m^2 g^{-1} for Keynol and 13 m^2 g^{-1} for PAN).

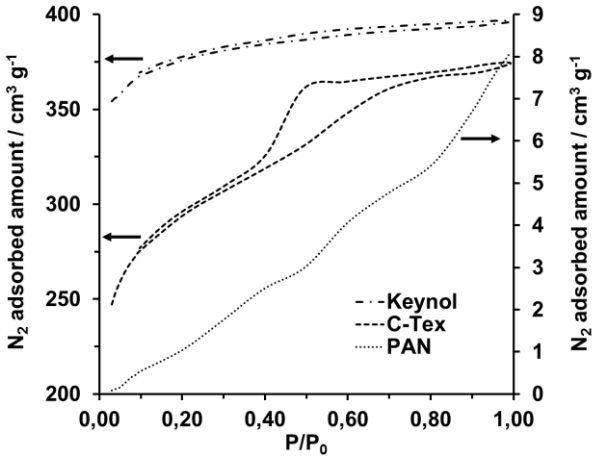


FIGURE 5.3 N_2 adsorption/desorption isotherms measured at 77 K for different anodes.

Biofilm attachment to the different electrodes was determined quantitatively by measuring the "dry mass" of the materials before and after biofilm development. The amount of microorganisms attached was normalized to the anode weight. The results showed that biofilm amount per weight of electrode was higher in the C-Tex (648±210 mg g^{-1}) compared with Keynol (334±96 mg g^{-1}) and PAN (518±57 mg g^{-1}). A positive relation between the S_{ext} of the C-Tex and the amount of biofilm attachment was found, suggesting that C-Tex presented higher surface area available for biofilm development. Possibly the high amount of micropores (90 % of the total pore volume) on Keynol was responsible for the lower biofilm attachment.

TABLE 5.2 Textural characterisation of the different anode materials.

Anode material	S_{BET} $m^2\ g^{-1}$	S_{ext} $m^2\ g^{-1}$	V_{micro} $cm^3\ g^{-1}$	V_P* $cm^3\ g^{-1}$
C-Tex	1090	305	0.319	0.574
PAN	13	13	0.000	0.012
Keynol	1234	70	0.553	0.610

*P/P_o=0.95

The wettability of the electrode surfaces also influences biofilm development and can lead to significant differences in MECs performance. Water contact angles between 60° and 80° have been described as an adequate level of surface wettability for optimal biofilm formation [317]. The hydrophilic property of electrodes surface was determined by measuring the contact angle between the water droplet and the electrode surface. If the contact angle is higher than 90°, the surface can be considered hydrophobic. If the contact angle is less than 90°, the surface can be considered hydrophilic [318]. At time zero, C-Tex and Keynol demonstrated a contact angle equal to 0° indicating that these materials can be considered hydrophilic, while PAN demonstrated a contact angle of 124±6° indicating his hydrophobic behaviour. The hydrophobic character of PAN is possibly due to the presence of the nitrile group at the PAN surface. Nitrile groups are polar however polyacrilonitrile polymer structures are insoluble in water. The hydrophilic properties of C-Tex is possible due to the higher amount of oxygen functional groups identified at their surface (Figure 5.2). According to Guo and co-workers, hydrophilic surfaces improve the electroactive biofilm formation [12].

The thermal stability of the electrode materials was evaluated by TGA analysis. Figure 5.4 shows the thermogravimetric (TG) and derivative thermogravimetric (DTG) curves for electrodes under N_2 atmosphere from room temperature to 800 °C. According to the results, Keynol and C-Tex exhibited a similar TG and DTG curves with a characteristic region of weight loss (about 25 %) up to 100 °C. This level of weight loss is attributed to the evaporation of the water, as expected due to the hydrophilic behaviour displayed by these electrodes. DTG curve of PAN shows a weight loss occurring between 300 °C and 400 °C mainly caused by the cyclization reaction (Figure 5.4B). During the cyclization, nitrile group form the conjugate C=N group leading to the formation of an aromatic ring [318]. Cyclization does not cause any substantial weight loss (Figure 5.4A). According

to the results obtained all the electrode materials tested demonstrated thermal stability under inert atmosphere.

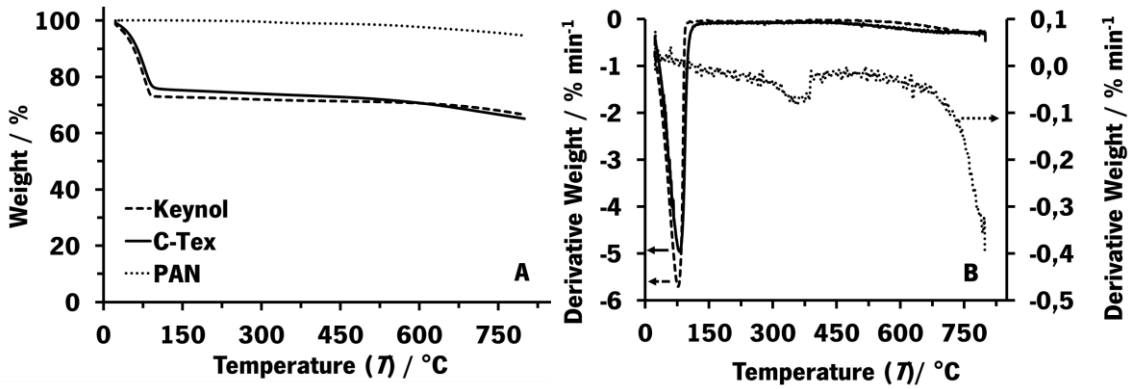


FIGURE 5.4 **A)** Thermogravimetric (TG) and **B)** derivative thermogravimetric (DTG) curves under N_2 atmosphere from room temperature to 800 °C for different electrode materials.

ii. Electrochemical characterization

Electrochemical measurements (abiotic) were performed in a 250 mL glass electrochemical cell using a potentiostat. Using a three-electrode setup, the reference electrode was Ag/AgCl and the counter electrode was a platinum foil. Cyclic voltammograms of Keynol, C-Tex and PAN, performed at different scan rates, are presented in the Figure 5.5A, Figure 5.5C and Figure 5.5E, respectively. As observed in the results, Keynol and C-Tex curves shows a quasi-rectangular shape indicating a strong capacitive behaviour [100]. The capacitive profile is mainly a consequence of the large surface area of the electrodes [319]. At higher scan rates (>10 mV s^{-1}) the shape of the cyclic voltammogram of Keynol change from quasi-rectangular to elliptical. The change of the curve shape could be due to the lower electrical conductivity and the slower diffusion rate inside the available pores [100]. For PAN the area limited by the curve is very small compared with the other electrodes, showing its low electrochemical activity (Figure 5.5E). By comparison, Keynol exhibited higher catalytic activity than C-Tex and PAN electrodes.

The galvanostatic charge-discharge curves of Keynol, C-Tex and PAN recorded at various current densities (0.75, 1.25, 1.90, 2.50 and 5 mA cm^{-2}) are shown in Figure 5.5B, Figure 5.5D and Figure 5.5F, respectively. The shape of all charge-discharge curves is almost triangular, which suggest a capacitive behaviour of the electrodes [320]. The specific capacitance of the various electrodes was determined from the charge-discharge curves during the discharge process. The capacitance was determined at current density of 2.5 mA cm^{-2}. The specific capacitance of Keynol and C-Tex

was 2885 mF cm^{-2} and 615 mF cm^{-2}, respectively. PAN shows a lower capacitance of 38 mF cm^{-2} at the same current density. As expected, Keynol demonstrated a higher capacitance mainly because of the higher S_{BET}.

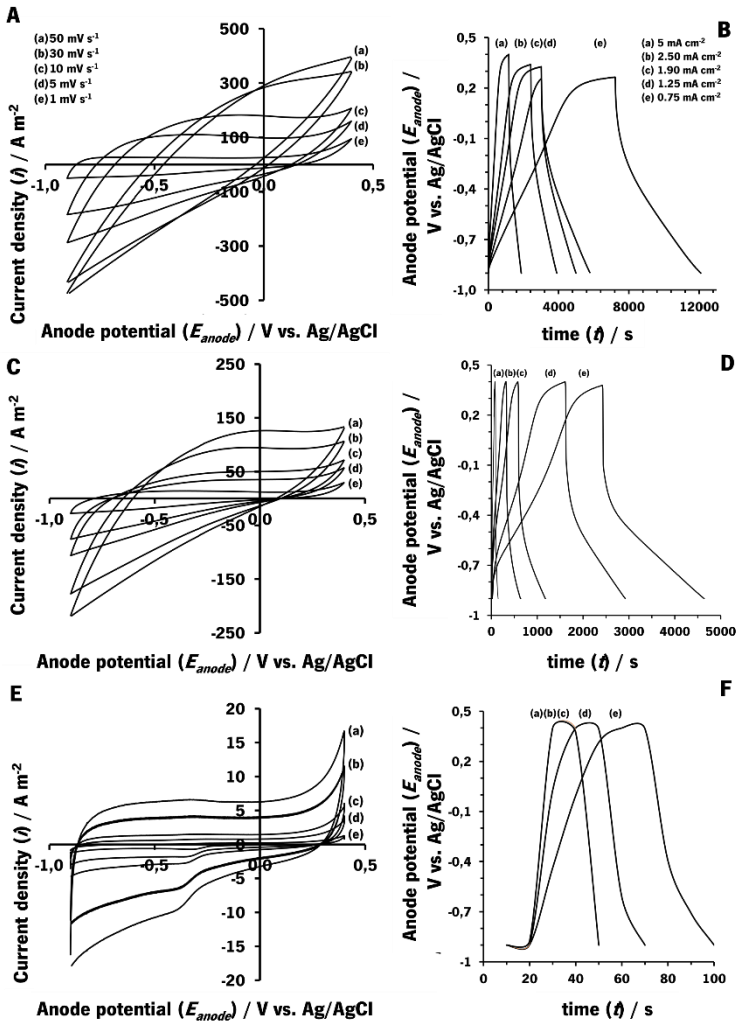


FIGURE 5.5 Electrochemical properties of different electrodes in 1M KOH aqueous electrolyte: **A)** and **B)** cyclic voltammetry and charge-discharge curves of Keynol, **C)** and **D)** cyclic voltammetry and charge-discharge curves of C-Tex and **E)** and **F)** cyclic voltammetry and charge-discharge curves of PAN.

5.3.2. Effect of different anodes on the performance of a MEC under cell potential control versus anode potential control

i. Current generation

Urine-fed MECs were operated under cell potential control to study the effect of three different anodes on the anode performance. Over a period of almost 6 weeks (38 days) the applied cell

potential was step wise (100 mV) increased from 0.4 V to 0.9 V (Figure 5.6A). During this process, anode potential of the MEC using C-Tex went up from -0.418 V to -0.200 V while cathode potential went down from -0.939 V to -1.136 V. The potential difference between anode and cathode increased with applied voltage, and simultaneously current density was increased in MEC. However when the applied cell potential was increased to 0.900 V, anode potential increased (to -0.200 V) and current density decreased, suggesting that the biofilm was negatively affected. For this reason, applied cell voltage was decreased again to 0.800 V. Figure 5.6A shows that for MEC using C-Tex, setting the applied cell potential at 0.800 V a current density of 229 mA m^{-2} was produced. Wang and co-workers also demonstrated the increase of current density with the increase of cell potential using carbon cloth as anode [321]. On the other hand, the increase of applied cell potential in the MECs using Keynol and PAN does not seem to affect the current density generated (Figure 5.6A). Thence, the applied cell potential of the MECs using Keynol and PAN was decreased and maintained at 0.400 V. At this applied cell potential, MEC using Keynol produced an average current density of 109 mA m^{-2}, whereas the MEC using PAN produced 60 mA m^{-2}.

Figure 5.6B shows the development of current density under anode potential control setting at -0.300 V. This potential was chosen according to the 1st assay, where the highest current density was obtained at a cell potential of 0.800 V, corresponding to an anode potential of -0.288 V. The MEC using C-Tex developed current density more quickly and to higher values than MECs using the other anodes. With the anode potential set at -0.300 V, an average current density of 904 mA m^{-2} was obtained using C-Tex, a value around 4-fold higher than that obtained with the applied cell potential at 0.800 V (229 mA m^{-2}). Similar tendency was observed for Keynol and PAN. An average current density of 338 mA m^{-2} and 118 mA m^{-2} was achieved for Keynol and PAN, respectively that is around 3-fold (109 mA m^{-2}) and 2-fold (60 mA m^{-2}) higher than the current density obtained under cell potential control (0.400 V). More positive anode potential was also tested and showed a diminishment of the current density generated. At an anode potential of -0.200 V, current densities of 369 mA m^{-2} and 258 mA m^{-2} were achieved from the MECs using C-Tex and Keynol, respectively. Torres and co-workers also observed that increasing the anode potential (-0.150 V vs. SHE (standard hydrogen electrode) to +0.370 V vs. SHE) decreased the current density [322]. For the MEC using PAN, increasing the anode potential to -0.200 V did not influence the generated current (115 mA m^{-2}).

By comparison, the results showed that both under cell and anode potential control the current density production was higher using C-Tex compared to the other anode materials. The highest

current densities obtained in our experiments were 904 mA m^{-2} on C-Tex, 338 mA m^{-2} on Keynol and 118 mA m^{-2} on PAN. The S_{ext} of the anodes also in the similar way as the current densities (C-Tex 305 m^2 g^{-1}, Keynol 70 m^2 g^{-1} and PAN 13 m^2 g^{-1}). This indicated that the current density and the S_{ext} showed a positive relation. Since high S_{ext} facilitates the microbial attachment and biofilm formation, this suggest that C-Tex demonstrated higher surface area available for biofilm attachment.

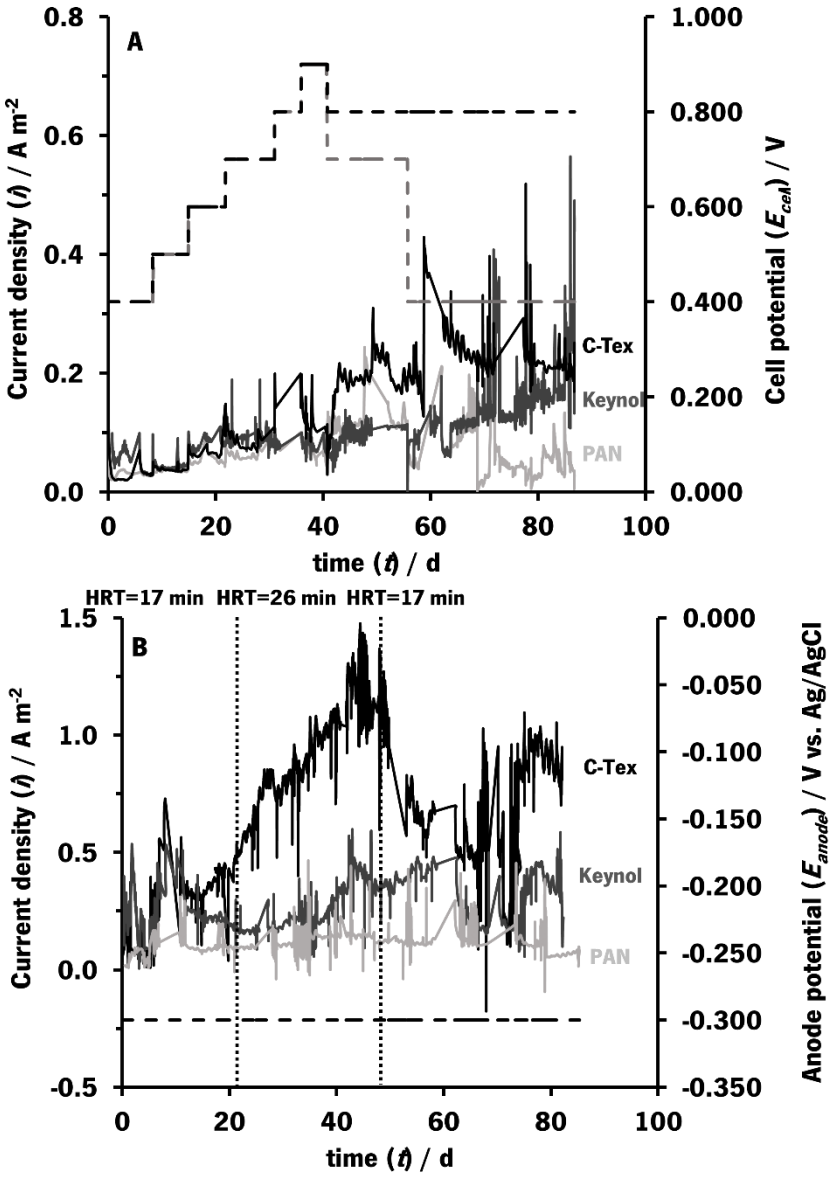


FIGURE 5.6 Measured current density for different anodes under **A)** cell potential control (**- - -** represents the cell potential for C-Tex and - - - represents the cell potential for PAN and Keynol) and **B)** anode potential control (**- - -** represents the anode potential).

ii. MEC treatment efficiency

Higher current densities were obtained at optimum anode potential control (-0.300 V) (Figure 5.6B). Under this operation mode, sCOD removal were similar for all anodes studied ranged from 39 % to 42 % at a HRT of 17 minutes and from 41 % to 46 % at a HRT of 26 minutes. These results suggest that the anodes tested do not influence the biodegradability of the urine since the COD removal is similar in all MECs, however appear to influence the current density generated. Since the COD removal was similar for all anode materials, the difference in the current density obtained was possibly due to the higher efficiency of chemical energy conversion to electrical energy on C-Tex.

The CE was determined for both HRT when a stable current density was achieved. CE results seemed to be dependent of the anode material used. For both HRT tested, MEC using C-Tex demonstrated higher CE compared with MECs using Keynol and PAN. At a HRT of 17 minutes, a CE of 12 % was determined in the MEC with C-Tex, while a CE of 4 % and 2 % was determined in MECs with Keynol and PAN, respectively. At a HRT of 26 minutes, a CE of 20 % was obtained in the MEC with C-Tex, whereas a CE of 6 % and 4 % were obtained for MECs with Keynol and PAN, respectively.

Fermentation and electricity generation are competitive processes for fermentable substrates in MECs which can explain the low CEs obtained [16]. Furthermore, the electrons released from the substrate oxidation can be used for gas production (H_2 or CH_4) or lost to alternative electron acceptors (*e.g.* sulphur or nitrogen compounds), resulting in a lower CE [193]. The CEs obtained in this work are in same range of CE reported in previous studies using wastewater containing fermentable substrates such as food processing wastewater [190] and pig slurry [323].

iii. Electrochemical characterization

Voltammograms of anode-respiring biofilm show a sigmoidal profile when the electron is direct transferred, whereas mediated electron transfer can be identified by simple oxidation and reduction peaks [68]. The voltammograms of each anode were performed at 0.15 mV s^{-1} between -0.900 V and 0.800 V (Figure 5.7). Sigmoidal shaped voltammograms were observed for all anodes suggesting that the current was produced by direct electron transfer from the biofilm. Torres and co-workers [322] demonstrated that the electroactive microorganisms that grown at low anode

potentials (-0.150 V vs. SHE) carried out extracellular electron transfer exclusively by conducting electrons through the biofilm.

Furthermore, the voltammograms of the different anode materials demonstrate the same shape varying only in the magnitude of the current production. Therefore, the difference in current density obtained can be explained by the difference in the surface area available for microbial growth [68].

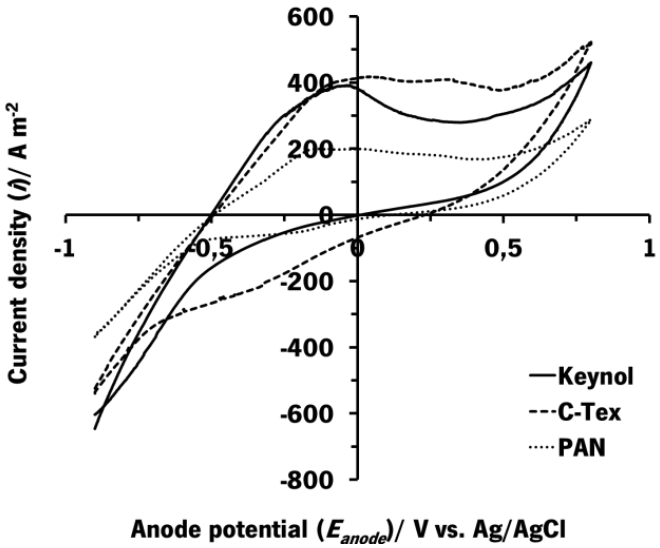


FIGURE 5.7 Cyclic voltammograms of biofilms developed in the different anodes. The scanning rate was 0.15 mV s^{-1} and Ag/AgCl was used as the reference electrode.

5.3.3. Microbial community analysis

SEM inspection of the biofilm developed on the different anodes showed that the surfaces were covered with a dense biofilm composed of microorganisms with different morphologies and size (Figure 5.8). Rods and cocci shape microorganisms were observed in all biofilms. SEM images show that microorganisms not just colonizing the carbon fibers but also form a multilayer and compact biofilm structure. As a consequence, most cells were not in direct contact with the anode. Furthermore, some mineral deposits were also observed when Keynol was used. EDS analysis revealed that the crystals observed on the Keynol surface were mainly composed by Ca (67 %), O (21 %) and C (11 %). Tilley and co-workers reported the precipitation of calcite ($CaCO_3$), among other crystals, in collection and storage systems of urine due to the increase of pH as a consequence of urea hydrolysis [324].

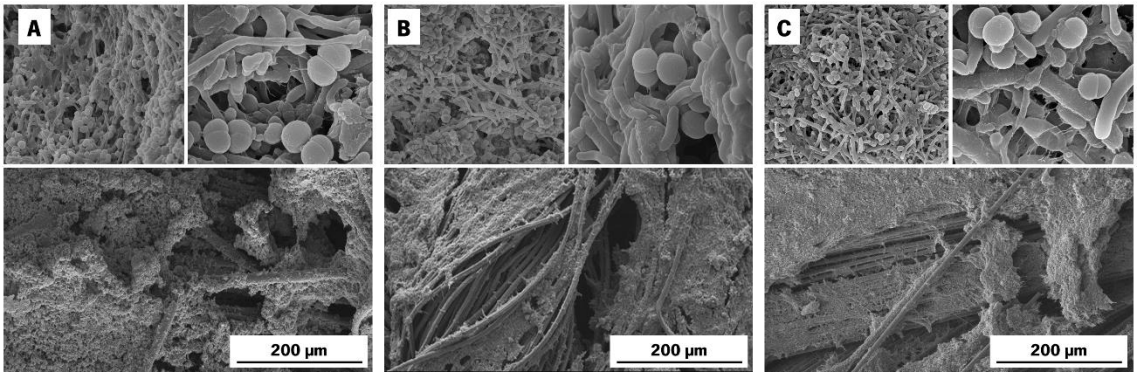


FIGURE 5.8 Scanning electron microscopy images (500 X) of biofilms grown under anode potential control on MECs using **A)** Keynol, **B)** C-Tex and **C)** PAN anodes. The insets show a higher magnification image of the biofilm (left: 10 000x, and right: 50 000x).

The microbial community composition of the biofilm developed in both assays, under cell and anode potential control, in each electrode material was analysed by 16S rDNA high throughout sequencing and compared with the anaerobic inoculum (Figure 5.9).

Figure 5.9A shows that microorganisms identified in the urine adapted sludge used to inoculate all MECs could be assigned into four groups. Firmicutes was the dominant bacterial phylum representing 27 % of the total analysed population, whereas Proteobacteria was the second most abundant phylum identified representing 18 % of the total population followed by Actinobacteria and Bacteroidetes phyla with 12 % and 7 %, respectively. By comparison with initial inoculum it is possible to observe that a process of enrichment and selection occurred during the operation in the MECs using different anode materials both under cell potential control and anode potential control.

Under cell potential control, Firmicutes and Proteobacteria accounted for more than 80 % of the total population in MECs using C-Tex and PAN and 65 % of the total population in MEC using Keynol. Assigned to the Firmicutes phylum, the anodic biofilm was dominated by Lactobacillales and Tissierellales orders. Lactobacillales specifically occurred in the anode biofilm of the MEC using C-Tex (70 %), while in the MECs using Keynol and PAN Lactobacillales are in similar percentage (35 % and 28 %, respectively) with Tissierellales (33 % and 35 %, respectively). *Atopostipes* sp. representing 17 % to 34 % of the Lactobacillales order is known as a fermentative bacteria, which can use carbohydrates such as glucose to lactate, acetate, and formate [294]. The remaining percentage of Lactobacillales was classified as “unknown” which means that the taxonomic information provided by NCBI contains missing information. Takahashi and co-workers suggest

that *Trichococcus* bacteria, assigned to the Lactobacillales order, is capable of utilizing electrodes as extracellular electron acceptors producing electricity from rice bran [325]. *Tissierella creatinhophila* representing 41 % to 53 % of the Tissierellales order, has the ability to grow on urine, metabolizing creatinine as sole carbon source to acetate, methylamine, ammonia and carbon dioxide [326]. Relatively to the Proteobacteria phylum, microorganisms assigned to Betaproteobacteria and Gammaproteobacteria classes were the most abundant in biofilm developed in all electrodes. Burkholderiales belonging to Betaproteobacteria class largely dominated the anodic biofilm representing 75 % of the sample taken from the MEC using Keynol; 83 % using C-Tex and 90 % using PAN (Figure 5.9B). *Oligella ureolytica* was identified in the biofilms developed on MECs using C-Tex and PAN representing more than 70 % of the total population assigned to Burkholderiales order and more than 20 % of the total sequences analysed, while the biofilm developed in MEC using Keynol these bacteria represent only 10 %. *Oligella ureolytica* have been described as a non-fermentative bacteria capable to reduce nitrate to nitrite [327]. *Oligella* also has been reported to as urease-positive which means that it has the capability to hydrolyse urea [328]. Pseudomonadales and Enterobacteriales are the most abundant orders belonging to the Gammaproteobacteria class. Most bacterial species affiliated with class Gammaproteobacteria are considered electrochemically active bacteria suggesting that *Pseudomonas* and *Enterobacter* sp. identified can be considered the most likely exoelectrogens present. Several authors have reported the ability of *Pseudomonas* sp. to produce electricity by producing electron shuttles to enhance electron-transfer rate [146] as well as the capability of *Enterobacter* sp. of using a wide range of substrates such as cellulose, sucrose and glycerol to generate electricity [329].

Under anode potential control, a clear selection in the community composition was observed when compared the original anaerobic inoculum with the anode biofilms. These results show that Firmicutes phyla was largely enriched in the anodic communities accounting from 79 % to 88 % of the total population (Figure 5.9A). Lactobacillales was the dominant order assigned to the Firmicutes phylum, specifically in the biofilm developed on C-Tex (68 % of the total Firmicutes population and 54 % of the total sequences analysed) (Figure 5.9B). Similarly to the results obtained under cell potential control, *Atopostipes* sp. represent 9 % to 14 % of the total Lactobacillales identified, being the remaining percentage of the Lactobacillales order classified as “unknown”. Bacteria assigned to the Lactobacillales order have been described to produce lactic acid as the major metabolic end product of carbohydrate fermentation. Bacteroidetes was the second most abundant phyla identified in the anodic biofilms representing 5 % to 12 % of the total

bacteria population (Figure 5.9A). For all anodes studied, more than 90 % of the total Bacteroidetes community was composed by *Petrimonas* sp. which can ferment carbohydrates such as glucose to acetate, H_2 and CO_2 using nitrate as electron acceptor [330]. Even though the Proteobacteria phylum only represents 1 % of the total population identified in all anodic biofilms, Enterobacteriales order represent around 70 % of the total Proteobacteria population in the biofilm developed on C-Tex. On the other hand, the biofilm developed on C-Tex under cell potential control showed that Enterobacteriales order represent only 6 % of the Proteobacteria population. *Enterobacter* sp. representing 73 % of the Enterobacteriales order may have important influence on current production, since several species belonging to the Enterobacteriales order have been described as electrochemically active bacteria [143, 331, 332]. This suggests that higher percentage of Enterobacteriales detected in the biofilm developed under anode potential control can be the responsible for the higher current density generated. Several authors have reported current generation by species belonging to the Enterobacteriales such as, *Enterobacter cloacae* in mediator-less microbial fuel cell [333]. This evidence is in accordance with the cyclic voltammograms obtained suggesting that current was produced by DET from the biofilm. Furthermore, *Geobacter* sp. assigned to the Desulfuromonadales order was identified in the biofilm developed on the C-Tex under anode potential control. *Geobacter* have been designated as electrogenic bacteria that have the ability to transfer electrons for an insoluble electron acceptor [64, 334].

By comparison of the obtained results, it can be concluded that the different anode materials studied have no effects on the microbial diversity developed. Figure 5.9 demonstrates there are no visible differences in the diversity of bacteria identified in the different biofilms obtained whether under cell or anode potential control. However, the different anodes appear to promote the growth of some microorganisms to the detriment of others. In general, compared with biofilms developed on Keynol and PAN, the biofilm developed on C-Tex presented a higher percentage of microorganisms assigned to Lactobacillales order. Furthermore, the biofilm developed on C-Tex with controlled anode potential presented a higher percentage of microorganisms assigned to Enterobacteriales order. The biofilm developed under this condition also generated a higher current density.

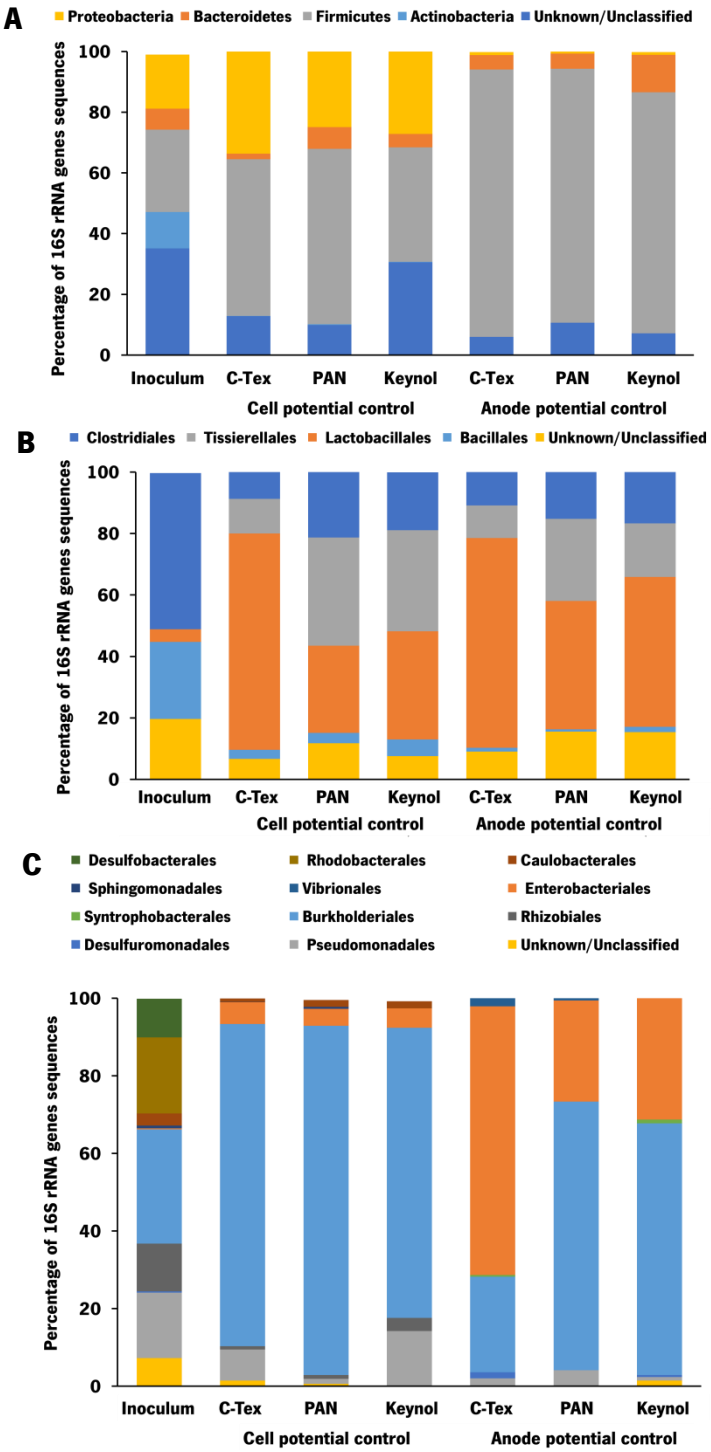
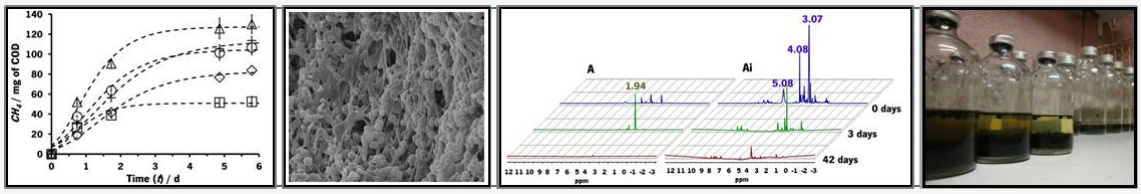


FIGURE 5.9 Bacterial community distribution of biofilm grown on different anodes tested (C-Tex, Pan and Keynol) under cell and anode potential control at **A)** phylum level, **B)** order lever assigned to Firmicutes phyla and **C)** order level assigned to Proteobacteria phyla.

5.4. CONCLUSIONS

This study, demonstrated that urine feed MEC with C-Tex as anode produced higher current density than MECs using Keynol or PAN. After accounting for differences in the anodes textural, chemical and electrochemical characteristics, the results suggest that the higher S_{ext} of the C-Tex, which corresponds to the surface area excluding the micropores contribution, enabled the higher current density generation compared to Keynol and PAN. Different anode materials had no differences on microbial diversity. The microbes belonging to Firmicutes and Proteobacteria were the dominant phyla in the all anode materials. Lactobacillales assigned to Firmicutes phyla and Enterobacteriales assigned to Proteobacteria phyla were the order identified in the biofilm developed on C-Tex, suggesting that microbes assigned to these order may be related with the higher current generation. *Enterobacter* sp. of Gammaproteobacteria may be related with current density generation.



Chapter 6

PRE-ACIDIFICATION OF URINE AS A STRATEGY TO ENHANCE THE PERFORMANCE OF A MICROBIAL ELECTROLYSIS CELL

6. Pre-acidification of urine as a strategy to enhance the performance of a Microbial Electrolysis Cell

ABSTRACT

This study investigated the effect of pre-treated urine on anode performance of a two chambered microbial electrolysis cells (MECs) compared to raw urine. Pre-treatment of urine (acidification) was performed by anaerobic digestion batch assays. The effect of pre-treatment of urine on anode performance was assessed by measuring the current density, chemical oxygen demand (COD) removal, ammonium nitrogen (NH_4^+-N) removal, and Coulombic efficiency (CE). The MEC using acidified urine achieved the highest average current density (218±6 mA m^{-2}) and the highest CE (17±1 %). Although no significant differences were observed in the COD removal efficiency between both urines, the MEC using acidified urine displayed the highest COD removal rate (0.14±0.02 g L^{-1} d^{-1}). The lowest effluent NH_4^+-N concentration (678±127 mg L^{-1}) which corresponds to an NH_4^+-N removal of 87±3 % was also obtained for the MEC using acidified urine. The organic compounds initially found, as well as the metabolic products associated to the biodegradation of the organic matter were analysed by proton nuclear magnetic resonance (^{1}H-NMR). The main compounds initially identified in the raw urine were urea, creatinine and acetate whereas the main compounds identified in the acidified urine were methylamine, acetate and propionic acid demonstrating the effectiveness of anaerobic digestion pre-treatment.

Finally, bioaugmentation with *Geobacter sulfurreducens* further improved the performance of both MECs. Under this condition an average current density of 289 mA m^{-2} which corresponds to a CE of 21 % was obtained for MEC fed with acidified urine.

6.1. INTRODUCTION

Around 75 % of the total amount of nitrogen (N) and with around 50 % of the total amount of phosphorus (P) present in domestic wastewater originates from urine [197]. At the same time, urine accounts with only 1 % of the total volume of wastewater, which indicate that urine is highly concentrated. In fresh urine most of the N is mainly found as urea [5]. During storage, the urea is hydrolysed due to microbial urease activity into ammonia (NH_3)/ammonium (NH_4^+) and carbonate [214]. Stored urine, after urea hydrolysis, contains a COD concentration of 9.3 g L^{-1} and approximately 1.9 g L^{-1} of NH_4^+-N [268]. Thus, urine can be considered as a valuable resource for N recovery and energy production in bioelectrochemical systems (BESs) [167].

BES are fuel cells commonly composed by two compartments, an anode and a cathode chamber with a membrane between both with coupled microorganisms that catalyses biological reactions [26]. BES can be operated in a microbial fuel cell mode (MFC) if electrical energy is produced or in a MEC if energy is supplied to promote non-spontaneous reactions, namely hydrogen (H_2) production [27]. H_2 production instead of electricity production present several advantages. The use of a MEC in alternative of a MFC eliminates the need of aeration at the cathode, which is necessary in a MFC concept [235]. Further, H_2 gas has a higher economic value than electricity [335]. Kuntke and co-workers demonstrated that MEC revealed to be a viable technology for diluted urine treatment with NH_4^+ recovery and energy production simultaneously [235]. However, in this work only 34 % of the NH_4^+-N was removed suggesting that further increase of the current output is necessary to improve the NH_4^+ recovery. According to the authors, a special focus on conversion of the chemical energy (COD) to electrical energy is essential [235].

In general, MECs fed with fermentable substrates are outperformed (in terms of the Coulombic efficiency) by MECs using non-fermentable substrates [335]. Several studies have shown the efficient conversion of volatile fatty acids (VFAs) such as, acetate and butyrate [336] and propionate [337] directly into electricity. However, urine is a complex substrate that contains fermentable compounds, such as glucose. Chae *et al.* investigated the effect of four different substrates (acetate, butyrate, propionate and glucose) on MFC performance [338]. Glucose-fed-MFC showed the lowest CE due to glucose consumption by diverse non-electricity-generating microorganisms by several metabolic pathways including fermentation and methanogenesis [338].

Therefore, a two-stage bioconversion processes (TSBPs) may be a suitable option to improve MEC performance using urine. In a TSBP the complex biodegradable compounds that are not directly

used by the electrochemically active bacteria are firstly converted in a preliminary anaerobic acidification step to simple compounds namely VFAs [339]. Cerrillo and co-workers investigated BES operation in combination with anaerobic digestion [323]. Pig slurry was firstly submitted to a process of anaerobic digestion in a lab-scale continuous stirred tank reactor. The effluent of the anaerobic digestion was used as fed for a subsequent MEC. MEC operated with digested pig slurry shown higher CE compared with MEC fed with raw pig slurry [323].

The present work aimed to evaluate the effect of anaerobic pre-treated urine on the anode performance of a MEC, compared to raw urine. Urine acidification by anaerobic digestion was performed in order to convert complex organic compounds found in urine into simpler compounds. A preliminary anaerobic biodegradability assay was performed in order to assess the anaerobic biodegradability of urine. Furthermore, the organic compounds found in raw and acidified urines as well as the metabolic products associated to urine degradation were analysed with NMR. Finally, the effect of bioaugmenting the microbial community with *G. sulfurreducens* on the anode performance was also assessed.

6.2. MATERIAL AND METHODS

6.2.1. Urine source

Human urine was collected and mixed from 5 male and 5 female individuals. After storage over 6 days at room temperature, a magnesium source (MgO) was added to promote phosphorus recovery by struvite precipitation according to Barbosa and co-workers [268]. Following the precipitation process, the urine was submitted to two distinct downstream processes. A portion of this urine (herein referred as raw urine) was used as feed for a first MEC (MEC A). The remaining urine was submitted to an anaerobic digestion to promote the acidification of organic compounds present in urine (herein referred as acidified urine) and then used as feed for a second MEC (MEC B). Both urines were stored at -80 °C before use.

6.2.2. Anaerobic biodegradability of urine

Anaerobic biodegradability batch assays were used to evaluate the anaerobic biodegradability of raw urine. During the anaerobic biodegradability assays the biochemical methane production (BMP) and the methane production rate (R_m) from urine were determined. Biodegradability assays were performed according to Angelidaki and co-workers [340]. Batch tests were prepared by adding

the substrate (urine), 30 % (v/v) of inoculum (anaerobic granular sludge) and basal medium to a final volume of 50 mL. All batches were performed in triplicate and incubated at 37 °C. Anaerobic biodegradability of urine was tested using different concentrations of COD 0 g L^{-1}; 0.5 g L^{-1}; 1 g L^{-1}; 2 g L^{-1}; 5 g L^{-1}; 8 g L^{-1}.The COD concentrations in study were obtained by dilution urine with basal medium. A blank assay without the addition of urine was also performed to discount methane production from residual substrate present in the inoculum.

The specific acetoclastic activity (SAA) and specific hydrogenotrophic methanogenic activity (SHMA) analysis were performed according to Costa *et al.* [341]. The methanogenic activity values were corrected to the standard temperature and pressure conditions (STP). Anaerobic granular sludge from a brewery industry plant (volatile solids (VS) = 0.06±0.01 g g^{-1}) was used as inoculum. SAA was 213.7±16.9 mL (CH_4) g^{-1} (VS) d^{-1} and SHMA was 389.3±16.3 mL (CH_4) g^{-1} (VS) d^{-1}.

Methane production was monitored by gas chromatography and BMP was expressed in L of CH_4 per kg of COD added to each vial and determined according to the Equation 6.1 [342]. Where, COD_{CH4} (kg) is the amount of COD of urine converted into CH_4, also called cumulative methane production, determined by the theoretical methane production (350 L of CH_4 per 1 kg of COD). The amount of COD of urine added to each vial is represented by COD_{added} (kg).

$$BMP = \frac{COD_{CH_4} \times 350}{COD_{added}}$$ **EQUATION 6.1**

Methanation percentage (MP) (%) was defined as the amount of methane produced during the batch assays in relation to the theoretical BMP (*i.e.* 350 L kg^{-1} of COD) and was determined according to the Equation 6.2 [342]. Where COD_{CH4} (mg) is the amount of COD of urine converted into CH_4 and COD_{added} (mg) is the amount of COD of urine added to each vial.

$$MP = \frac{COD_{CH_4}}{COD_{added}} \times 100$$ **EQUATION 6.2**

The progress of cumulative methane production during batch assays was described by the modified Gompertz according to the Equation 6.3 [342]. Where M(t) is the methane cumulative production (mg), P is the maximum methane production (mg), R_m is the maximum methane production rate (mg d^{-1}), e equals to 2.7182818, λ is the lag-phase (d) and t is the time (d).

$$M(t) = P\ exp\left[-exp\left[\frac{R_m{}^e}{p}(\lambda - t) + 1\right]\right]$$ **EQUATION 6.3**

6.2.3. Anaerobic acidification of urine

Urine acidification was performed by anaerobic digestion in order to promote volatile fatty acids formation (*i.e.* acetate and propionate) from anaerobic microbial conversion of organic compounds. Anaerobic digestion was performed in batch assays, at 37 °C, by adding the substrate (raw urine) and 30 % (v/v) of inoculum (anaerobic granular sludge) to a final volume of 500 mL. To avoid urine dilution no basal medium was added. Batch assays were performed in triplicate and were conducted until reach a steady state in terms of sCOD. Centrifugation was the process used to separate the acidified urine from granular sludge. After the first centrifugation at 5000 rpm for 30 minutes at room temperature, the supernatant was carefully collected and was submitted to a second centrifugation step using the same parameters. The acidified urine was frozen at -80 °C to avoid the presence of methanogenic microorganisms.

6.2.4. MEC experimental setup and operation

The experimental setup was composed by a dual-chamber MEC to study the effect of a preliminary anaerobic digestion of urine in the performance of the system. Additionally, a control assay in which a second MEC was fed with raw urine was also performed. The set was operated at room temperature (25±3 °C). Cellulose-based carbon (C-Tex) (MAST Carbon International Limited, United Kingdom) pressed to a graphite insert (MAST Carbon International Limited, (United Kingdom) was used as anode and a graphite insert as a cathode. Flat graphite plates (Müller & Rössner GmbH & Co., Germany) glued using epoxy with each graphite insert were used as current collectors. A cation exchange membrane (Ralex, Mega, Czech Republic) was placed directly between the two-chambers. Based on previous findings (Chapter 5), MECs were performed setting the anode at −300 mV vs. Ag/AgCl using a potentiostat (VSP, Biologic, France). Potassium hexacyanoferrate (0.050 mol L^{-1}) in phosphate buffer (0.100 mol L^{-1}) at pH 7 was used as catholyte. For each urine, three sequential batches were performed until a stable current density was obtained. The urine fed in each new cycle, was previously flushed with N_2 gas for 10 minutes to avoid oxygen in the anodic chamber. The anode chambers were inoculated with an anaerobic

community previously enriched in "urine-degrading" electroactive microorganisms in a microbial fuel cell (MFC) (Chapter 4) for a final volume of 5 % (v/v).

i. Bioaugmentation with *Geobacter sulfurreducens*

G. sulfurreducens (DSM 12127) acquired from DSMZ (Braunschweig, Germany) was used for augmenting the native microbiology of the anode compartment of each MEC. *G. sulfurreducens* was grown at 35 °C with sodium acetate as electron donor and sodium fumarate as electron acceptor as suggested by Caccavo and co-workers [343]. *G. sulfurreducens* was pre-grown in a medium adapted from the DSMZ medium 826. The composition of the medium was (per L): NH_4Cl, 1.5 g; Na_2HPO_4, 0.6 g; NaH_2PO_4, 1.5 g; KCl, 0.1 g; Na-acetate, 0.8 g; Na_2-fumarate, 8.0 g; $NaHCO_3$, 2.5 g; vitamins solution, 10 mL; trace metals solution, 10 mL and selenio-tungstate solution (per L: NaOH, 0.5 g; $Na_2SeO_3 \cdot 5H_2O$; 3 mg and $Na_2WO_4 \cdot 2H_2O$, 4.0 mg), 1 mL. The vitamins solution contained (per L): biotin, 2.0 mg; folic acid, 2.0 mg; pyridoxine HCl, 10.0 mg; thiamine $HCl \cdot 2H_2O$, 5.0 mg; riboflavin, 5.0 mg; nicotinic acid, 5.0 mg, d-Ca-pantothenate, 5.0 mg; vitamin B_{12}, 0.1 mg, p-aminobenzoic acid, 5.0 mg and lipoic acid, 5.0 mg. The trace metals solution contained (per L): nitrilotriacetic acid, 1.5 g; $MgSO_4 \cdot 7H_2O$, 3.0 g; $MnSO_4 \cdot H_2O$, 0.5 g; NaCl, 1.0 g; $FeSO_4 \cdot 7H_2O$, 0.1 g; $CoSO_4 \cdot 7H_2O$, 0.18 g; $CaCl_2 \cdot 2H_2O$, 0.1 g; $ZnSO_4 \cdot 7H_2O$, 0.18 g; $CuSO_4 \cdot 5H_2O$, 0.01 g; $KAl(SO_4)_2 \cdot 12H_2O$, 0.02 g; H_3BO_3, 0.01 g; $Na_2MoO_4 \cdot 2H_2O$, 0.01 g; $NiCl_2 \cdot 6H_2O$, 0.025 g and $Na_2SeO_3 \cdot 5H_2O$, 0.3 mg.

The growth of *G. sulfurreducens* was done in 120 mL bottles sealed with butyl rubber septa and aluminium crimp caps. The headspace was flushed with N_2/CO_2 (80/20) to ensure anaerobic microenvironment. To inoculate the MECs, 10 mL of the previously homogenised cultures were taken from the bottle and injected into the anode compartment of each MEC. MECs were inoculated with an optical density (OD_{600}) of 0.110.

6.2.5. Chemical analysis and measurements

Methane in the bottles headspace was analysed in a gas chromatograph (Chrompack 9000) equipped with a FID detector and a Chromosorb 101 (80e120 mesh, 2 m x 1/8") column, using N_2 as carrier gas (30 mL min^{-1}). Column, injector, and detector temperatures were 35 °C, 110 °C, and 220 °C, respectively.

VFAs were determined by HPLC (Jasco, Japan) equipped with a UV detector (210 nm) and a Chrompack column (6.5 x 30 mm^2) at 60°C and using sulphuric acid (0.5 mol L^{-1}) as mobile phase at a flow rate of 0.6 mL min^{-1}.

The MECs performance was assessed by monitoring, total chemical oxygen demand (tCOD) soluble chemical oxygen demand (sCOD), ammonium nitrogen (NH_4^+-N), nitrate (NO_3-N) and sulphate (SO_4^{2-}) concentrations using Hach-Lange cuvette tests (Hach Lange, Düsseldorf, Germany) and a spectrophotometer DR 2800 (Hach Lange, Düsseldorf, Germany). All samples were previously centrifuged at 10 000 rpm for 5 minutes. The sCOD removal efficiency (%) was calculated from the difference in measured COD of the influent and effluent of the anode chamber. The COD removal rate (g L^{-1} d^{-1}) was determined from the difference in the measured COD of the influent and effluent of the anode chamber normalized to the hydraulic retention time (d). The NH_4^+-N removal efficiency (%) was calculated from the difference in measured NH_4^+-N concentration of the influent and effluent of the anode chamber. The NH_4^+-N removal rate (g L^{-1} d^{-1}) was determined from the difference in the measured NH_4^+-N of the influent and effluent of the anode chamber normalized to the hydraulic retention time (d). Ammonia nitrogen (N-NH_3) was calculated based on NH_4^+-N concentration, temperature (T) (°C) and pH according to the Equation 6.4 [344]. Where NH_3-N and NH_4^+-N were expressed in mg L^{-1}.

$$NH_3 - N = \frac{NH_4{}^+ - N \times 10^{pH}}{\exp\left(\frac{6344}{273+T}\right) + 10^{pH}} \qquad \textbf{EQUATION 6.4}$$

Current density was determined based on projected surface area of the anode (25 cm^2). CE was determined from the measured current and the removed COD as described by [19].

Nuclear magnetic resonance (^{1}H-NMR) spectroscopy was used to study the course of the biodegradation of the organic matter during MECs operation. Samples from both MECs were taken at different times (0, 3 and 42 days) and analysed by ^{1}H-NMR using a Bruker Avance II 400 MHz spectrometer. The main functional groups were identified by liquid phase ^{1}H-NMR spectroscopy. Deuterated water (D_2O) was used as the solvent.

Significance statistical analysis by using a single factor analysis of variance (ANOVA) was used to compare the results obtained for the different urines, raw and acidified urine. Statistical significance was established at the $p<0.05$ level.

6.3. RESULTS AND DISCUSSION

6.3.1. Anaerobic biodegradability of urine

Anaerobic biodegradability batch tests were used to assess the BMP potential of human urine. Human urine used in anaerobic biodegradability assays had a tCOD of 10.43±0.06 g L^{-1} and a sCOD of 8.74±0.56 g L^{-1}. NH_4^+-N and NH_3-N concentrations were 3.32±0.08 g L^{-1} and 1.88±0.05 g L^{-1}, respectively, which represents a total ammonia nitrogen (TAN) concentration of 5.20 g L^{-1}. Initial pH of urine was 9.01±0.03. This characterisation resulted from an average of 3 measurements.

The profile of cumulative methane production is shown in Figure 6.1. The best scenario in terms of specific methane production was observed for COD concentration of 0.5 g L^{-1} with a specific methane production of 299±43 L kg^{-1} (COD) which corresponds to a MP of 86±12 %. A specific methane production of 160±51 L kg^{-1} (COD) and 165±33 L kg^{-1} (COD) which corresponds to a MP of 46±14 % and 47±9 % were obtained for COD concentrations of 1 and 2 g L^{-1}, respectively (Table 6.1). In this experiment, a decrease of almost 50 % in methane production was observed for assay with 1 g L^{-1} of COD, which exhibited a final TAN concentration of 1 g L^{-1}. Complete methane production inhibition was observed for assay with 5 g L^{-1} of COD which showed a final TAN concentration of 4.3 g L^{-1}. Colón and co-workers, reported a specific methane production of 437 L kg^{-1} (COD) at a TAN concentration of 3 g L^{-1} using undiluted simulant human excreta [345]. The same authors reported a strong inhibition of methane production with the increase of TAN concentration; a decrease of 66, 86 and 90 % was detected for 5, 8 and 10 g L^{-1}, respectively. According to Yenigün and co-workers, TAN concentrations between 1.7 g L^{-1} to 1.8 g L^{-1} can cause anaerobic digestion failure [346].

For all concentrations of COD tested an increase of the TAN concentration at the end of the batch assay was observed. This increase was mainly due to the urea hydrolysis by an enzyme (urease) into carbon dioxide and NH_3/NH_4^+. Furthermore, NH_3-N concentration detectable at the end of the batch assays reached inhibitory levels. Around 1 g L^{-1} of NH_3-N was obtained for the assays with 5 g L^{-1} of COD. According to Hansen *et al.*, NH_3-N concentrations between 0.100 g L^{-1} and 1.100 g L^{-1} have been reported for initial inhibition of unadapted microorganisms [347]. Simultaneously, it is possible to observe that the pH value increased during the assay from 7 to 8.5 at 5 g L^{-1} of COD (Table 6.1).

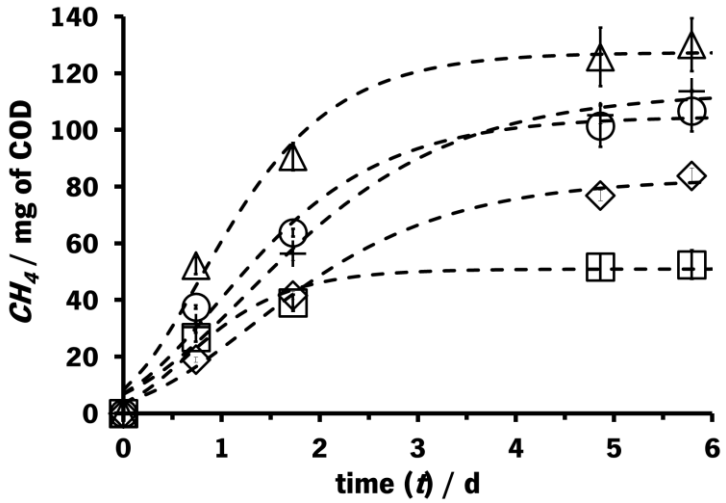


FIGURE 6.1 Cumulative methane production during anaerobic biodegradability assays of urine at COD concentrations of: (◊) 0 g L^{-1} (Blank); (+) 0.5 g L^{-1}; (O) 1 g L^{-1}; (Δ) 2 g L^{-1}; (□) 5 g L^{-1}; (x) 8 g L^{-1}. The symbols represent the experimental data with respective standard deviation (n = 3 points). The lines represent the predicted data by the modified Gompertz equation.

With the increase of COD concentration, an increase of the inhibition effects was observed. This inhibition was seen not only by the decreasing values of BMP and MP and by the high concentration of TAN but also by the VFA accumulation. In this experiment, the VFA identified was mostly acetic acid with concentration of 2.55 g L^{-1} for batch assay with 5 g L^{-1} of COD (Table 6.1). Franke-Whittle and co-workers demonstrated that acetic acid concentrations above 0.78 g L^{-1} could indicate process instability [348]. Further, sCOD accumulation was also observed during batch operation with 5 g L^{-1} of COD. Urea is not completely oxidized during COD measurement analysis, thus urea does not contribute to the measured COD [349, 350]. However, its hydrolysis during the anaerobic digestion may explain the higher final sCOD concentration observed.

Although methane production was inhibited for high concentrations of COD, VFA accumulation, mainly acetate, during batch assays suggested that urine was acidified during the anaerobic digestion. Thus, anaerobic batch digestion was used as a pre-treatment for urine acidification.

TABLE 6.1 Methane production parameters predicted by the modified Gompertz equation and experimental results obtained at the end of anaerobic biodegradability batch assays.

		0.5 g L^{-1}	**1 g L^{-1}**	**2 g L^{-1}**	**5 g L^{-1}**
TAN	g L^{-1}	0.25	0.50	1.00	2.50
P	mg	113	105	127	51
BMP	L kg^{-1}	299±43	160±51	165±33	-
MP	%	86±12	46±14	47±9	-
R_m	mg d^{-1}	34.7	40.7	61.2	31.0
R^2	-	0.990	0.984	0.987	0.973
pH	-	7.55	7.70	8.00	8.45
$sCOD_{end}$	g L^{-1}	0.81	0.87	0.98	7.83
NH_4^+-N	g L^{-1}	0.50±0.12	0.98±0.06	1.85±0.12	3.39±0.30
NH_3-N	g L^{-1}	0.02±0.04	0.06±0.02	0.21±0.04	0.91±0.01
VFA	g L^{-1}(COD)	n.d.	0.53±0.11	0.45±0.05	2.67±0.55
Acetic acid	g L^{-1} (COD)	n.d.	0.53±0.11	0.43±0.02	2.55±0.55

n.d. not determined

6.3.2. MECs performance using raw versus acidified urine

The anodic chamber of each MEC were fed with raw urine (non-acidified) and acidified urine. Table 6.2 shows the chemical composition of the fed urines. The results showed that acidified urine presents higher sCOD and TAN concentrations compared with raw urine. Concentration of TAN increase in the acidified urine possibly due to urea hydrolysis during the anaerobic digestion pre-treatment process into NH_3/NH_4^+ and carbamate followed by the subsequent carbamate decomposition into NH_3/NH_4^+ and bicarbonate (HCO_3^-) [213]. As a result of the decomposition of urea, the pH of the urine increased from 7.8 to 9.0 (Table 6.2). Simultaneously, it was observed an increase on sCOD concentration in acidified urine possibly due to urea hydrolysis. As previous mentioned, it is well established that urea does not contribute to the measured COD since urea is not completely oxidized during COD measurement analysis. Therefore, urea cannot be utilized as carbon source by the anode microbial community [213, 286]. Thus, the higher COD observed in the acidified urine can maybe be explained by the hydrolysis of urea during the anaerobic digestion pre-treatment. A control assay without urine, showed that the sCOD contribution from inoculum was insignificantly. Furthermore, compared to raw urine, acidified urine showed higher

concentration of VFAs, namely acetic acid due to the conversion of other, more complex organic compounds into acetate.

TABLE 6.2 Characterization of raw and acidified human urine used as feedings in the MECs (n=3).

		Raw urine	Acidified urine
sCOD	g L^{-1}	5.17±0.71	10.70±0.36
NH_4^+-N	g L^{-1}	0.44±0.11	5.17±0.43
NH_3-N	g L^{-1}	0.03±0.00	2.78±0.38
SO_4^{2-}	g L^{-1}	0.87±0.06	0.26±0.01
NO_3^--N	mg L^{-1}	7.78±0.11	11.15±1.20
pH	-	7.76±0.05	8.95±0.05
VFA	g L^{-1} (COD)	3.15±0.44	5.72±0.75
Acetic acid	g L^{-1} (COD)	2.78±0.27	4.70±0.75

i. Current generation

The current density generated in the MECs during three sequential batches using raw and acidified urine are shown in Figure 6.2A and Figure 6.2B, respectively. The shape of the current density profiles was very similar for both MECs. An initial current density peak was observed, with a visible difference between maximum current density between both MECs. Current density peaks of 826±202 mA m^{-2} and 1411±553 mA m^{-2} were observed for MEC fed with raw and acidified urine, respectively. These current density peaks occurred immediately after the urine replacement, suggesting that the electron transfer is independent from the planktonic bacteria and bacterial attached to the electrode are responsible for current generation [126]. After the initial current peaks, a plateau in current density was observed. VFA analysis suggest that the initial current peaks were related to the consumption of easily biodegradable compounds such as acetate. Until 13±2 days of operation, an acetate removal rate of 0.15±0.02 g L^{-1} d^{-1} was observed for both MECs which corresponds to an acetate removal of 50 % for MEC with raw urine (3.70±0.66 g L^{-1} to 1.84±0.06 g L^{-1}) and 40 % for MEC with acidified urine (4.71±0.28 g L^{-1} to 2.83±0.04 g L^{-1}). The remaining 47 % of acetate removed on MEC with raw urine (1.84±0.06 g L^{-1} to 0.37±0.19 g L^{-1}) and 26 % on MEC with acidified urine (2.83±0.04 g L^{-1} to 1.60±0.14 g L^{-1}) occurred during more 25±5 days of operation. Significantly higher average current density was generated from acidified urine (218±6 mA m^{-2}) compared with average current density produced from raw urine (107±1 mA m^{-2}) (p<0.05).

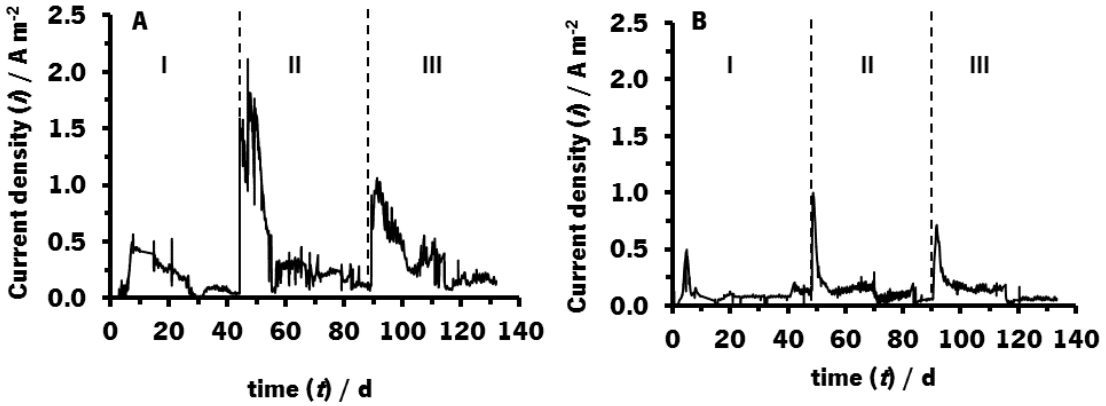


FIGURE 6.2 Current density during experiment on microbial electrolysis cells fed with **A)** raw and **B)** acidified urine for three sequential batches (I, II and III).

ii. MECs efficiency

Figure 6.3A and Figure 6.3B shows the removal efficiencies obtained during the MECs operation. No significant differences on COD removals between both MECs were observed (p<0.05). COD removals were 65±10 % in MEC using raw urine and 54±3 % in MEC using acidified urine. However, MEC using acidified urine displayed a significantly higher COD removal rate (0.14±0.02 g L^{-1} d^{-1}) compared with the MEC using raw urine (0.08±0.02 g L^{-1} d^{-1}) (p<0.05).

Although, no significant differences were observed for COD removal between both MECs, the higher current density production on MEC using acidified urine was a result of the higher CE obtained. CE was determined during the operation at the stable current density generation. CEs of 14±2 % and 17±1% were obtained for MECs using raw and acidified urine, respectively. For both MECs the CE obtained was low, although are in the same range as in other studies that also used complex wastewaters with fermentable substrates. Cerrillo and co-workers reported a CE of 18 % using digested pig slurry in a MEC at an anode potential of -100 mV vs. SHE [323] whereas Kuntke and co-workers described a CE of 10 % using raw urine in a MFC [167].

The NH_4^+-N removal efficiency for the MEC using acidified urine was 89±2 % which corresponds a NH_4^+-N removal rate of 0.12 g L^{-1} d^{-1} and to an effluent NH_4^+-N concentration of 678±127 mg L^{-1}. This NH_4^+-N removal efficiency was higher than the NH_4^+-N removal reported by Kuntke and co-workers who reported an ammonium removal efficiency of 34±2 % using 5x diluted raw urine at an applied cell voltage of 1.0 V vs. Ag/AgCl [235]. The MEC using raw urine demonstrated a negative NH_4^+-N removal efficiency and an effluent NH_4^+-N concentration of 1496±420 mg L^{-1}. The negative NH_4^+-N

removal efficiency can be explained by the urea hydrolysis which increase the NH_4^+-N concentration in the anode chamber (Figure 6.3A). Urea is hydrolysed by an enzyme, namely urease, into carbon dioxide and ammonia increasing the urine pH from 7.7 to 9 during the first 7 days of operation (Figure 6.3A). Kuntke and co-workers also reported a negative NH_4^+-N removal rate (-60 g m^{-2} d^{-1}) [235]. Further, considering the day 5 for MEC with raw urine, where maximum NH_4^+-N concentration was observed (5.12±0.17 g L^{-1}) a lower NH_4^+-N removal efficiency (68±12 %) was obtained in comparison to MEC with acidified urine. MEC using acidified urine demonstrated an effluent concentration of NH_4^+-N (678±127 mg L^{-1}.) significantly lower than the effluent NH_4^+-N concentration on MEC using raw urine (1496±420 mg L^{-1}) (p<0.05).

The concentration of NO_3^--N (Table 6.2) decrease over time, with a final concentration of 4.66±0.14 mg L^{-1} and 5.90±0.76 mg L^{-1}, which corresponds to a NO_3^--N removal of 40 % and 46 % for MECs using raw and acidified urine, respectively. Nitrate is an alternative electron acceptor that might be reduced by denitrifying bacteria, thus reducing the CE of the system. The low CE obtained for both MECs demonstrated that further improvements are needed in order to improve the conversion of the chemical energy into electrical energy efficiency.

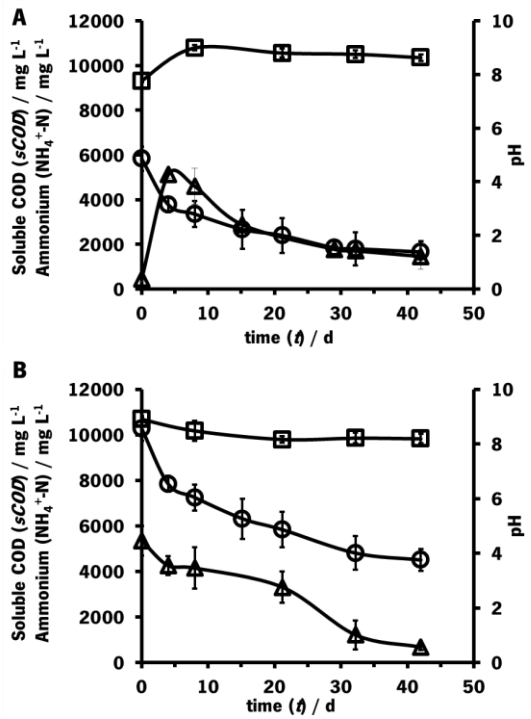


FIGURE 6.3 Average COD removal (○), NH_4^+-N removal (Δ) and pH (□) for three different batches during experiment on microbial electrolysis cells fed with **A)** raw and **B)** acidified urine.

iii. ^{1}H-NMR analysis

The degradation of organic compounds during the second batch was studied. Samples from both MECs working with raw and acidified urine were taken at different times (0, 3 and 42 days) and ^{1}H-NMR were performed to study the course of the urine biodegradation. The NMR spectra of samples taken from MEC using raw urine and from MEC using acidified urine are shown in Figure 6.4A and Figure 6.4B, respectively. Figure 6.4Ai and Figure 6.4Bi shown the NMR spectra of raw urine and acidified urine, respectively, after suppression of acetate peak (1.94 ppm). D_2O (used as the solvent) peak region (4.8 ppm) was excluded from all the spectra.

The spectra of initial raw urine, which corresponds to day 0 was dominated by signals in the aromatic region (6.5 to 8 ppm) and in the aliphatic region ascribed to protons attached to O or N (2.5 to 6.5 ppm). Furthermore, some signals were detected in the aliphatic region (0 to 3 ppm). Conferring to the Figure 6.4A, the main signals initially detected were at 5.80, 4.08, 3.07 and 1.94 ppm (aliphatic region). According to Bouatra and co-workers urea and creatinine two of the principal compounds present in urine [274]. In the ^{1}H-NMR analysis both compounds were identified (urea at 5.08 ppm and creatinine at 4.08 ppm and 3.07 ppm). The signal attributed to urea compound disappear until day 3 of operation corroborating the hypothesis that ammonium concentration increase in the anode chamber due to the urea hydrolysis. Furthermore, the signals attributed to creatinine decrease during the first 3 days of operation. The reduction in the urea and creatinine peaks were possibly due to the presence of microorganisms assigned to *Corynebacterium* and *Tissierella* genus identified in the acclimated sludge used to inoculate the MECs (Figure 4.8, Chapter 4). Some *Corynebacterium* species have been described as urease positive that catalyses the hydrolysis of urea into carbon dioxide and ammonia [351] whereas some species of *Tissierella* genus are responsible for metabolize creatinine producing acetate, methylamine, ammonia and carbon dioxide [326]. Simultaneously an increase in the acetate peak was observed (1.94 ppm) until day 3 due to the conversion of complex organic compounds with a subsequent decrease during the operation due to the consumption of acetate.

The spectra of initially acidified urine, which corresponds to day 0, was dominated by signals in the aromatic region (6.5 to 8 ppm) and in the aliphatic region (0 to 3 ppm) (Figure 6.4B). The presence of numerous peaks in the aliphatic region indicates a high biodegradability of the organic compounds found in acidified urine. The principal signals initially detected were at 2.60, 1.92 and 1.06 ppm (aliphatic region). Urea and creatinine that are two of the main compounds present in

urine were not identified in acidified urine, suggesting that during the anaerobic digestion these compounds were hydrolysed. These statement is in accordance with the increase of ammonia concentration during anaerobic digestion. Furthermore, methylamine (2.60 ppm) identified in acidified urine is a result of creatinine hydrolysis. According to the spectra data, its peak almost disappear after 3 days of operation In comparison with raw urine, the peak corresponding to acetate (1.92 ppm) is higher demonstrating that the complex organic compounds where converted to acetate during acidification process. Similar to the spectra of MEC using raw urine, the acetate peak decrease over time due to its consumption. Furthermore, contrary to the raw urine, propionate (1.06 ppm) was identified in the acidified urine demonstrating the success of the acidified process. According to the spectral data, also the propionate peak decrease demonstrating its consumption over batch operation. Electricity production from propionate oxidation in a MFC was previously reported by Jang and co-workers [337].

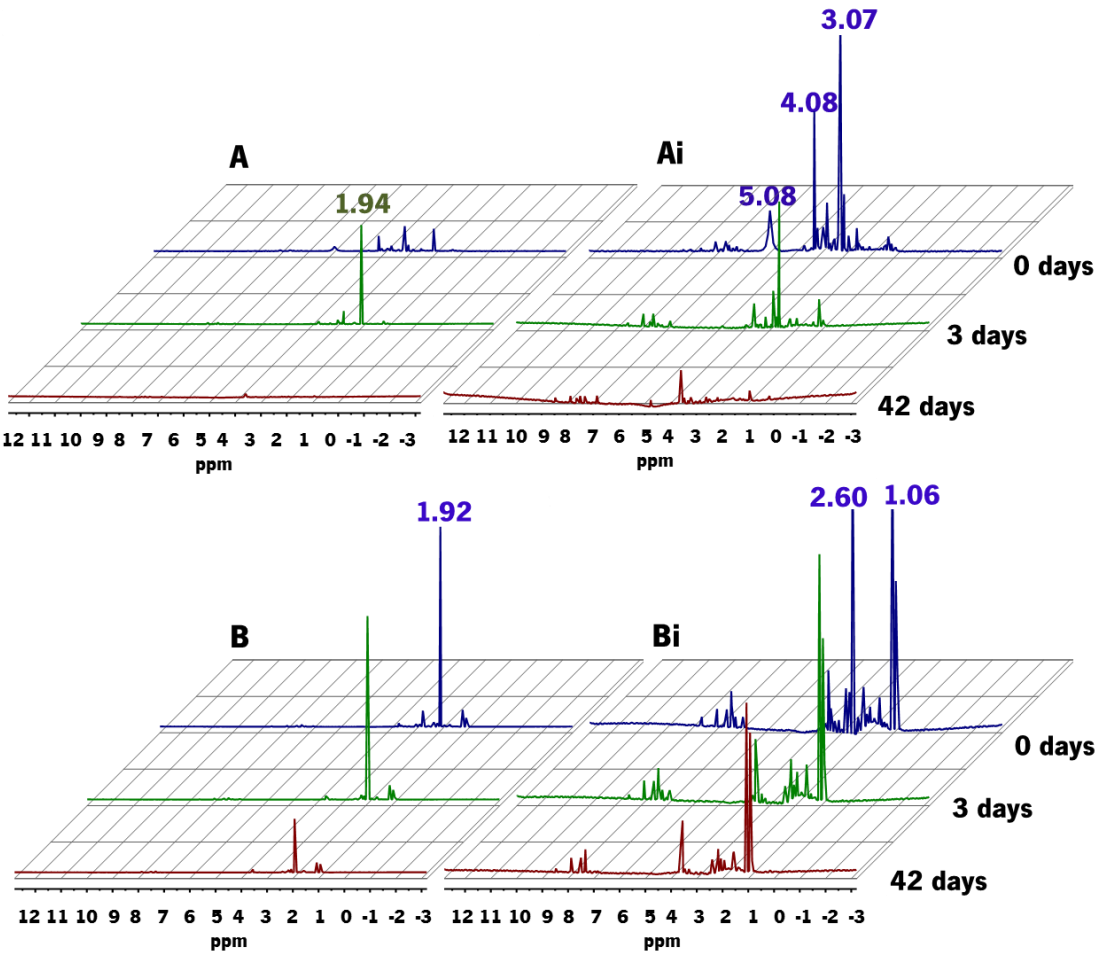


FIGURE 6.4 Proton nuclear magnetic resonance (^{1}H-NMR) spectral data of **A)** raw urine; **Ai)** raw urine after suppression of acetate peak; **B)** acidified urine and **Bi)** acidified urine after suppression of acetate peak.

6.3.3. MECs performance after bioaugmentation with *Geobacter sulfurreducens*

A new batch was operated after bioaugmenting the anodic native microflora with *G. sulfurreducens* as biocatalyst to enhance MECs current output. The current density generated using raw and acidified urine after bioaugmentation are shown in Figure 6.5A and Figure 6.5B, respectively. Similarly to the current density curves obtained before bioaugmentation, an initial current density peak was observed for both MECs. A maximum current density of 380 mA m^{-2} and 981 mA m^{-2} were achieved for MEC operating with raw and acidified urine, respectively, after which the current density production stabilized. During stable phase operation, the MECs fed with raw and acidified urine produced an average current of 157 mA m^{-2} and 289 mA m^{-2}, respectively. In comparison with current density obtained before bioaugmentation (107±1 mA m^{-2} and 218±6 mA m^{-2} for MECs using raw and acidified urine, respectively), the addition of *G. sulfurreducens* to the MECs presented a positive impact on the performance, showing that activity of electroactive microorganisms was one of the limiting factors.

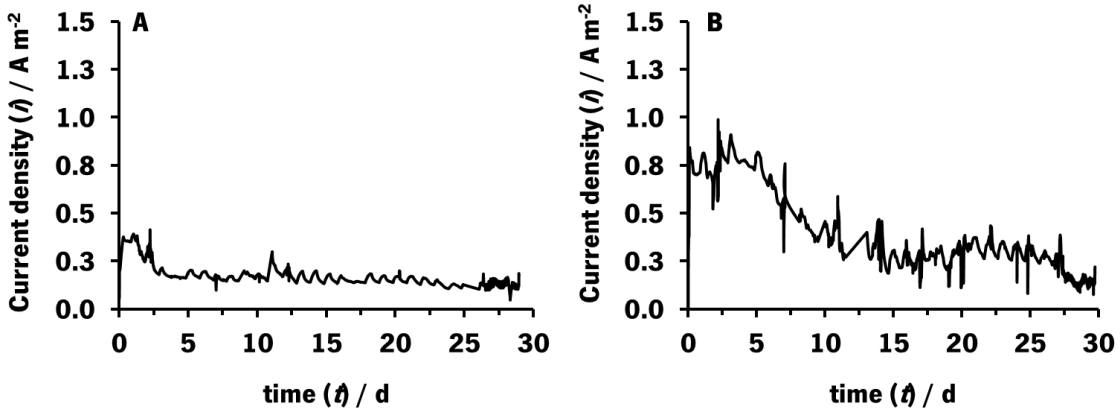


FIGURE 6.5 Current density during experiment after bioaugmentation with *Geobacter sulfurreducens* on microbial electrolysis cells fed with **A)** raw and **B)** acidified urine.

Removal efficiencies obtained during the MECs operation are presented in Figure 6.5A and Figure 6.5B. MEC fed with raw urine demonstrated higher COD removal efficiency (63 %) in comparison with the COD removal efficiency obtained on MEC fed with acidified urine (47 %). However, no differences were observed for both MEC when compared the COD removal rate observed before bioaugmentation. MEC using raw urine displayed a COD removal rate of 0.10 g L^{-1} d^{-1} whereas the MEC using acidified urine demonstrated a COD removal rate 0.16 g L^{-1} d^{-1}.

Mostly important, bioaugmentation with *G. sulfurreducens* had a positive impact on CE compared to the CE obtained before bioaugmentation. Nevertheless, bioaugmentation of the microbial community developed on the anode surface with *G. sulfurreducens* at the stable stage operation did not increase significantly the CE (a CE of 18 % and 21 % were obtained for MECs using raw and acidified urine, respectively). This may be explained by limitations on the direct contact between the *G. sulfurreducens* and the anode surface imposed by the biofilm already developed at the anode surface. Nevertheless, CE improvement contributed to increase the current density generation.

The increase on current density of MEC fed with acidified urine after bioaugmentation allowed to increase the NH_4^+-N removal rate. A NH_4^+-N removal rate of 0.17 g L^{-1} d^{-1}, which corresponds to a NH_4^+-N removal efficiency of 77 % and to an effluent NH_4^+-N concentration of 1346 mg L^{-1}, was observed (Figure 6.6B). According to Kuntke and co-workers the transport of electrons through the external electrical circuit, induces an ion transport through the cation exchange membrane to maintain the electroneutrality of the MEC [235]. Similarly to the previous observed, MEC fed with raw urine displayed a negative NH_4^+-N removal efficiency with an effluent NH_4^+-N concentration of 2480 mg L^{-1} (Figure 6.6A). The hydrolysis of urea during the MEC operation with raw urine was demonstrated not only by the increase of NH_4^+-N concentration but also by the increase of pH from 7.6 to 8.6 (Figure 6.6A).

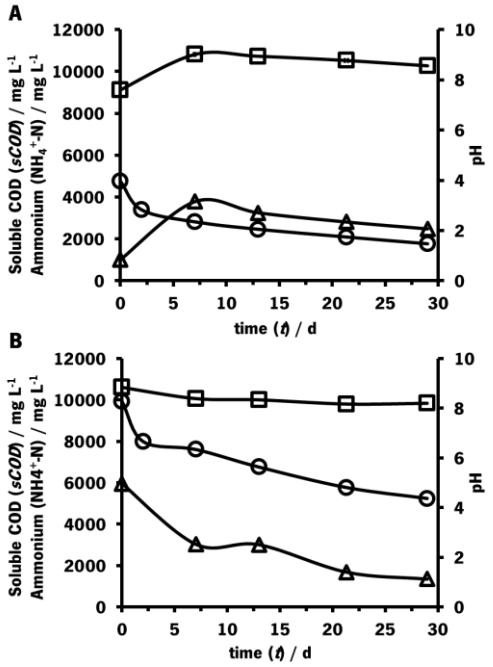


FIGURE 6.6 Average COD removal (○), NH_4^+-N removal (Δ) and pH (□) during experiment on microbial electrolysis cells fed with **A)** raw and **B)** acidified urine.

6.4. Conclusions

In this study, MEC fed with urine pre-treated by anaerobic digestion produced higher current density compared to MEC fed with raw urine. Anaerobic digestion was performed to increase the concentration of VFAs in the urine by converting the complex organic compounds. ^{1}H-NMR analysis demonstrated the differences between the two different urines. The main compounds identified in raw urine was urea, creatinine and acetate whereas in the acidified urine the main compounds identified were acetate, propionate and methylamine. Furthermore, higher NH_4^+-N removal was observed on MEC fed with acidified urine. Finally, the enhancement of current production and CE following bioaugmentation with *G. sulfurreducens* to the native microbial population suggest that prior to bioaugmentation, the MEC performance was limited by the concentration of anode-respiring bacteria. In conclusion, this study demonstrated that integrating a urine acidification pre-treatment with MECs is an interesting alternative for the treatment of urine. Further, NH_4^+-N can be removed for its reuse as fertilizer.

Chapter 7

General conclusions and future perspectives

7. General conclusions and future perspectives

The exhaustion of fossil fuel resources due to the increase of energy demand in combination with several environmental concerns contribute to the development of sustainable and renewable energy sources. In addition, the development of innovative electricity generating systems, are imperative in remote areas. Over the past years, bioelectrochemical systems (BESs) has emerged as a promising technology to produce bioenergy from renewable carbon sources including wastewaters. Several types of wastewaters have been described to work as fuel source for energy in BESs, including urine which is highly concentrated in nutrients, namely phosphorus and nitrogen, as well as biodegradable compounds. Furthermore, its separation from other wastewater streams contribute to reduce the operational costs associated to operational problems caused by struvite accumulation in wastewater treatment plants.

In this thesis, phosphorus (P) recovery in the form of struvite (magnesium ammonium phosphate, $NH_4MgPO_4 \cdot 6H_2O$) precipitation was analysed by adding three different Mg sources ($MgCl_2$, $Mg(OH)_2$ and MgO) (Chapter 3). A statistical design of experiments was used to assess the combined effect of Mg:P molar ratio (1:1, 1.5:1 and 2:1) and stirring speed (30, 45 and 60 rpm) for each Mg source tested. The efficiency of the non-spontaneous precipitation was assessed by the P recovery efficiency and size of the struvite crystals formed. MgO demonstrated to be the best Mg source for non-spontaneous P recovery from urine. The highest P recovery efficiency and highest struvite crystals size were achieved using MgO at 2:1 molar ratio and a stirring speed of 30 rpm. Further, MgO has the highest Mg content that contributes for a less quantity of chemical added and a basic character in pH adjustment, which is, optimal for struvite precipitation.

The fact that organic matter was present in urine after P recovery demonstrated that urine could be used as a fuel source for BESs. Although, urine has been described as a fuel source for electricity production in a microbial fuel cell (MFC), the performance of the system has been compromised due to the presence of fermentable compounds in urine. In this thesis, several strategies were tested in order to improve the anode performance of a BES fed with urine.

A MFC with increasing urine concentration (by lowering the dilution factor) was operated to promote the microbial acclimation to undiluted urine (Chapter 4). The effect of the microbial acclimation process on the MFC performance was assessed by current density production, chemical oxygen demand (COD) removal and coulombic efficiency (CE). The results showed that a microbial community enriched in “urine-degrading” electroactive bacteria was successfully developed by an

enrichment process, using anaerobic granular sludge as inoculum. When compared with a control assay fed with undiluted urine without any microbial acclimation, the adapted microbial community displayed 80 % higher current density. Further, the identification of several dominant genus in the adapted microbial community showed that different microorganisms were competing for the substrate. The enriched community was mainly composed by creatinine-degrading bacteria belonging to *Tissierella* genus and bacteria belonging to *Paenibacillus* genus, known for their ability to function as exoelectrogens. *Corynebacterium* that include urea-hydrolysing bacteria was the third main genera detected.

Urine application as fuel in BESs has been studied for electricity production in MFC. On the other hand, urine can also be used as fuel for hydrogen (H_2) production in microbial electrolysis cell (MEC). H_2 has been considered as an important energy fuel as it has the highest energy content per unit weight.

In this study, the performance of MECs operated with urine with three different carbon anode materials was evaluated (Chapter 5). Furthermore, the relation between the microbial communities developed on each anode material and the current produced was investigated. The results demonstrated that no differences on microbial diversity were identified for different anode materials. However, higher percentage of bacteria belonging to Lactobacillales and Enterobacteriales order were identified on cellulose-based carbon material (C-Tex). MEC current production values was determined in the following decreasing order: C-Tex, phenol-based (Keynol) and polyacrilonitrile-based (PAN). The highest current density displayed by C-Tex was possibly influenced by the high percentage of *Enterobacter* sp. identified. *Enterobacter* sp. belonging to Enterobacteriales order is known for their ability to produce electricity from a wide range of substrates. Considering that the microbial diversity was similar in all anode materials, the higher external surface area (S_{ext}) displayed by the C-Tex appears to be the main reason for the higher MEC performance.

Finally, the effect of submitting urine to an anaerobic pre-treatment on the anode performance of a MEC was also evaluated (Chapter 6). Anaerobic digestion showed to be an efficient method to promote the conversion of complex organic compounds present in urine into volatile organic acids, mainly acetate. The main compounds identified in pre-treated urine were acetate, propionate and methylamine whereas in the raw urine urea, creatinine and acetate were the major elements detected. When used as feed in a MEC, pre-treated urine exhibited a higher current density as well as higher ammonium removal, than raw urine. Additionally, bioaugmentation of the adapted

microbial community used as inoculum with *Geobacter sulfurreducens* further improve the MEC performance.

The work presented in this thesis significantly broadened the knowledge on BESs use for energy production, using urine as feed and with its simultaneous treatment. Although bio-H_2 production in MECs is emergent and visible progresses have been made in this subject, there are still several challenges to overcome for the treatment of complex substrates such as urine. Therefore, further research is essential mainly to improve the CE of the system. Future perspectives and recommendations resulting from this thesis include:

- Considering that 70 % to 80 % of the microbial community analysed after the acclimation step was classified as "no hit" or "unknown", further research on microbial community identification must be performed to elucidate about the microorganisms developed on the anode surface and their function. Further, the diversity and complexity of organic compounds found in urine requires a microbial consortium with fermentative and electrochemically active bacteria to allow the utilization of complex organic matter in urine. From a fundamental perspective, proteomic techniques should be used to identify which proteins are expressed during biofilm formation and their possible relation with electron transfer mechanisms.
- Bioaugmentation using electrochemically active bacteria (EAB), which have the ability to produce their own electron mediators (*e.g. Shewanella oneidensis*) should be thoroughly analysed in order to study the effect of electron mediators on current production when a biofilm is already established on the anode surface (during stable stage operation). In addition, bioaugmentation of the adapted microbial community with an EAB that are not able to self-secrete electron mediators (*e.g. Geobacter sulfurreducens*) should also be performed at an early stage (prior to the inoculation on MEC). Bioaugmentation at a start-up stage will allow the physical contact between the EAB and the anode surface.
- Methanogenesis and electricity production are processes competing for the same substrate in BESs. Several strategies could be applied to supress or minimize methanogenic activity. Namely, pH value control, anode potential control, exposure the biofilm to oxygen, addition of chemical inhibitors and changes in the substrate concentration.
- Further work exploring the connection between biofilm formation and electrode surface should be undertaken. The microbial adhesion to the electrode surface may be promoted

by using an electrode with a positive surface charge, to allow electrostatic interactions with negatively charged bacteria. Ammonia gas treatment of the electrode can be used to increase the positive surface charge.

- Integration of the 3D macroporous electrode material with nanocomposite materials such as conducting polymers (*e.g.* polyaniline) may also promote the microbial adhesion.
- The use of the MEC to recover ammonium should also be tested. This implies that an efficient NH_3 stripping concept should be integrated at the cathode of the MEC to remove NH_3 thus promoting ammonium diffusion through the membrane from the anode to the cathode. The removed ammonium may be reused as fertilizer.

References

[1] D. Cordell, J.O. Drangert, S. White, The story of phosphorus: Global food security and food for thought, Glob. Environ. Chang. 19 (2009) 292–305.

[2] M. Maurer, P. Schwegler, T.A. Larsen, Nutrients in urine: Energetic aspects of removal and recovery, in: Water Sci. Technol., 2003: pp. 37–46. d

[3] J.D. Doyle, S.A. Parsons, Struvite formation, control and recovery, Water Res. 36 (2002) 3925–3940.

[4] R.W. Howarth, R. Marino, Nitrogen as the limiting nutrient for eutrophication in coastal marine ecosystems : Evolving views over three decades, Limnol. Oceanogr. 51 (2005) 244–257.

[5] J.A. Wilsenach, M.C.M. van Loosdrecht, Impact of separate urine collection on wastewater treatment systems, Water Sci. Technol. 48 (2003) 103–110.

[6] Z. Liu, Q. Zhao, K. Wang, D. Lee, W. Qiu, J. Wang, Urea hydrolysis and recovery of nitrogen and phosphorous as MAP from stale human urine, J. Environ. Sci. 20 (2008) 1018–1024.

[7] M. Maurer, W. Pronk, T.A. Larsen, Treatment processes for source-separated urine, Water Res. 40 (2006) 3151–3166.

[8] J.A. Wilsenach, C.A.H. Schuurbiers, M.C.M. van Loosdrecht, Phosphate and potassium recovery from source separated urine through struvite precipitation, Water Res. 41 (2007) 458–466.

[9] B.E. Logan, B. Hamelers, R. Rozendal, U. Schröder, J. Keller, S. Freguia, P. Aelterman, W. Verstraete, K. Rabaey, Microbial fuel cells: Methodology and technology, Environ. Sci. Technol. 40 (2006) 5181–5192.

[10] P. Clauwaert, P. Aelterman, T.H. Pham, L. De Schamphelaire, M. Carballa, K. Rabaey, W. Verstraete, Minimizing losses in bio-electrochemical systems: The road to applications, Appl. Microbiol. Biotechnol. 79 (2008) 901–913.

[11] J. Babauta, R. Renslow, Z. Lewandowski, H. Beyenal, Electrochemically active biofilms: facts and fiction. A review, Biofouling. 28 (2012) 789–812.

[12] K. Guo, S. Freguia, P.G. Dennis, X. Chen, B.C. Donose, J. Keller, J.J. Gooding, K. Rabaey, Effects of surface charge and hydrophobicity on anodic biofilm formation, community composition, and current generation in bioelectrochemical systems, Environ. Sci. Technol. 47 (2013) 7563–7570.

[13] M. Mashkour, M. Rahimnejad, Effect of various carbon-based cathode electrodes on the performance of microbial fuel cell, Biofuel Res. J. 2 (2015) 296–300.

[14] Z. He, Y. Huang, A.K. Manohar, F. Mansfeld, Effect of electrolyte pH on the rate of the

anodic and cathodic reactions in an air-cathode microbial fuel cell, Bioelectrochemistry. 74 (2008) 78–82.

[15] M.A. Rodrigo, P. Cañizares, H. García, J.J. Linares, J. Lobato, Study of the acclimation stage and of the effect of the biodegradability on the performance of a microbial fuel cell, Bioresour. Technol. 100 (2009) 4704–4710.

[16] D. Pant, G. Van Bogaert, L. Diels, K. Vanbroekhoven, A review of the substrates used in microbial fuel cells (MFCs) for sustainable energy production, Bioresour. Technol. 101 (2010) 1533–1543.

[17] H. Wang, Z.J. Ren, A comprehensive review of microbial electrochemical systems as a platform technology, Biotechnol. Adv. 31 (2013) 1796–1807.

[18] B.E. Logan, B. Hamelers, R. Rozendal, U. Schröder, J. Keller, S. Freguia, P. Aelterman, W. Verstraete, K. Rabaey, Microbial fuel cells: methodology and technology., Environ. Sci. Technol. 40 (2006) 5181–5192.

[19] B.E. Logan, D. Call, S. Cheng, H.V.M. Hamelers, T.H.J.A. Sleutels, A.W. Jeremiasse, R.A. Rozendal, Microbial electrolysis cells for high yield hydrogen gas production from organic matter, Environ. Sci. Technol. 42 (2008) 8630–8640.

[20] S. Cheng, D. Xing, D.F. Call, B.E. Logan, Direct biological conversion of electrical current into methane by electromethanogenesis., Environ. Sci. Technol. 43 (2009) 3953–3958.

[21] R.A. Rozendal, E. Leone, J. Keller, K. Rabaey, Efficient hydrogen peroxide generation from organic matter in a bioelectrochemical system, Electrochem. Commun. 11 (2009) 1752–1755.

[22] D. Majumder, J.P. Maity, M. J. Tseng, V.R. Nimje, H.-R. Chen, C.C. Chen, Y.F. Chang, T.C. Yang, C.Y. Chen, Electricity generation and wastewater treatment of oil refinery in microbial fuel cells using *Pseudomonas putida*, Int. J. Mol. Sci. 15 (2014) 16772–16786.

[23] M.C. Potter, Electrical Effects Accompanying the decomposition of organic compounds, Proc. R. Soc. London. 84 (1911) 260–276.

[24] H.J. Kim, H.S. Park, M.S. Hyun, I.S. Chang, M. Kim, B.H. Kim, A mediator-less microbial fuel cell using a metal reducing bacterium, *Shewanella putrefaciens*, Enzyme Microb. Technol. 30 (2002) 145–152.

[25] D.R. Bond, D.R. Lovley, Electricity production by *Geobacter sulfurreducens* attached to electrodes, Appl. Environ. Microbiol. 69 (2003) 1548–1555.

[26] M. Rahimnejad, A. Adhami, S. Darvari, A. Zirepour, S. E. Oh, Microbial fuel cell as new technology for bioelectricity generation: A review, Alexandria Eng. J. 54 (2015) 745–756.

[27] H.V.M. Hamelers, A. Ter Heijne, T.H.J.A. Sleutels, A.W. Jeremiasse, D.P.B.T.B. Strik, C.J.N. Buisman, New applications and performance of bioelectrochemical systems., Appl.

Microbiol. Biotechnol. 85 (2010) 1673–1685.

[28] I.K. Kapdan, F. Kargi, Bio-hydrogen production from waste materials, Enzyme Microb. Technol. 38 (2006) 569–582.

[29] H.S. Lee, W.F.J. Vermaas, B.E. Rittmann, Biological hydrogen production: Prospects and challenges, Trends Biotechnol. 28 (2010) 262–271.

[30] H. Liu, H. Hu, J. Chignell, Y. Fan, Microbial electrolysis: novel technology for hydrogen production from biomass, Biofuels. 1 (2010) 129–142.

[31] R. Rozendal, H.V.M. Hamelers, G.J.W. Euverink, S.J. Metz, C.J.N. Buisman, Principle and perspectives of hydrogen production through biocatalyzed electrolysis, Int. J. Hydrogen Energy. 31 (2006) 1632–1640.

[32] H. Liu, S. Grot, B.E. Logan, Electrochemically assisted microbial production of hydrogen from acetate., Environ. Sci. Technol. 39 (2005) 4317–4320.

[33] T.H.J.A. Sleutels, R. Lodder, H.V.M. Hamelers, C.J.N. Buisman, Improved performance of porous bio-anodes in microbial electrolysis cells by enhancing mass and charge transport, Int. J. Hydrogen Energy. 34 (2009) 9655–9661.

[34] B.E. Logan, K. Rabaey, Conversion of wastes into bioelectricity and chemicals by using microbial electrochemical technologies, 337 (2012) 686–690.

[35] A. Kundu, J.N. Sahu, G. Redzwan, M. a. Hashim, An overview of cathode material and catalysts suitable for generating hydrogen in microbial electrolysis cell, Int. J. Hydrogen Energy. 38 (2013) 1745–1757.

[36] E. Croese, M.A. Pereira, G.J.W. Euverink, A.J.M. Stams, J.S. Geelhoed, Analysis of the microbial community of the biocathode of a hydrogen-producing microbial electrolysis cell, Appl. Microbiol. Biotechnol. 92 (2011) 1083–1093.

[37] J. Hu, Q. Zhang, D. Lee, H.H. Ngo, Feasible use of microbial fuel cells for pollution treatment, Renew Energy. (2017) *in press*.

[38] K.Y. Cheng, G. Ho, R. Cord-Ruwisch, Affinity of microbial fuel cell biofilm for the anodic potential, Environ. Sci. Technol. 42 (2008) 3828–3834.

[39] T.H. Pham, P. Aelterman, W. Verstraete, Bioanode performance in bioelectrochemical systems: recent improvements and prospects, Trends Biotechnol. 27 (2009) 168–178.

[40] V.B. Oliveira, M. Simões, L.F. Melo, A.M.F.R. Pinto, Overview on the developments of microbial fuel cells, Biochem. Eng. J. 73 (2013) 53–64.

[41] T.H.J.A. Sleutels, L. Darus, H.V.M. Hamelers, C.J.N. Buisman, Effect of operational parameters on Coulombic efficiency in bioelectrochemical systems, Bioresour. Technol. 102 (2011) 11172–11176.

[42] K. Rabaey, W. Verstraete, Microbial fuel cells: novel biotechnology for energy generation, Trends Biotechnol. 23 (2005) 291–298.

[43] T.H.J.A. Sleutels, A. Ter Heijne, C.J.N. Buisman, H.V.M. Hamelers, Bioelectrochemical systems: an outlook for practical applications, ChemSusChem. 5 (2012) 1012–1019.

[44] B.E. Logan, J.M. Regan, Electricity-producing bacterial communities in microbial fuel cells, Trends Microbiol. 14 (2006) 512–518.

[45] H.V.M. Hamelers, A. Ter Heijne, T.H.J. a Sleutels, A.W. Jeremiasse, D.P.B.T.B. Strik, C.J.N. Buisman, New applications and performance of bioelectrochemical systems, Appl. Microbiol. Biotechnol. 85 (2010) 1673–1685.

[46] R.A. Rozendal, T.H.J.A. Sleutels, H.V.M. Hamelers, C.J.N. Buisman, Effect of the type of ion exchange membrane on performance, ion transport, and pH in biocatalyzed electrolysis of wastewater, Water Sci. Technol. 57 (2008) 1757–1762.

[47] R.A. Rozendal, H.V.M. Hamelers, R.J. Molenkamp, C.J.N. Buisman, Performance of single chamber biocatalyzed electrolysis with different types of ion exchange membranes, Water Res. 41 (2007) 1984–1994.

[48] J.M. Sonawane, A. Yadav, P.C. Ghosh, S.B. Adeloju, Recent advances in the development and utilization of modern anode materials for high performance microbial fuel cells, Biosens. Bioelectron, 90 (2016) 558–576.

[49] A. Kadier, M.S. Kalil, P. Abdeshahian, K. Chandrasekhar, A. Mohamed, N.F. Azman, W. Logrono, Y. Simayi, A.A. Hamid, Recent advances and emerging challenges in microbial electrolysis cells (MECs) for microbial production of hydrogen and value-added chemicals, Renew. Sustain. Energy Rev. 61 (2016) 501–525.

[50] Y. Hindatu, M.S.M. Annuar, A.M. Gumel, Mini-review: Anode modification for improved performance of microbial fuel cell, Renew. Sustain. Energy Rev. 73 (2017) 236–248.

[51] M. Ghasemi, W.R.W. Daud, N. Mokhtarian, A. Mayahi, M. Ismail, F. Anisi, M. Sedighi, J. Alam, The effect of nitric acid, ethylenediamine, and diethanolamine modified polyaniline nanoparticles anode electrode in a microbial fuel cell, Int. J. Hydrogen Energy. 38 (2013) 9525–9532.

[52] C. Li, L. Zhang, L. Ding, H. Ren, H. Cui, Effect of conductive polymers coated anode on the performance of microbial fuel cells (MFCs) and its biodiversity analysis, Biosens. Bioelectron. 26 (2011) 4169–4176.

[53] R. Rozendal, H.V.M. Hamelers, K. Rabaey, J. Keller, C.J.N. Buisman, Towards practical implementation of bioelectrochemical wastewater treatment, Trends Biotechnol. 26 (2008) 450–459.

[54] D. Pant, G. Van Bogaert, C. Porto-Carrero, L. Diels, K. Vanbroekhoven, Anode and cathode materials characterization for a microbial fuel cell in half cell configuration, Water Sci.

Technol. 63 (2011) 2457–2461.

[55] J.R. Kim, B. Min, B.E. Logan, Evaluation of procedures to acclimate a microbial fuel cell for electricity production, Appl. Microbiol. Biotechnol. 68 (2005) 23–30.

[56] E. Croese, K.J. Keesman, (Aura) H C A Widjaja-Greefkes, J.S. Geelhoed, C.M. Plugge, T.H.J.A. Sleutels, A.J.M. Stams, G.J.W. Euverink, Relating MEC population dynamics to anode performance from DGGE and electrical data, Syst. Appl. Microbiol. 36 (2013) 408–416.

[57] P. Aelterman, S. Freguia, J. Keller, W. Verstraete, K. Rabaey, The anode potential regulates bacterial activity in microbial fuel cells, Appl. Microbiol. Biotechnol. 78 (2008) 409–418.

[58] F. Zhang, X. Xia, Y. Luo, D. Sun, D.F. Call, B.E. Logan, Improving startup performance with carbon mesh anodes in separator electrode assembly microbial fuel cells, Bioresour. Technol. 133 (2013) 74–81.

[59] B. Logan, S. Cheng, V. Watson, G. Estadt, Graphite fiber brush anodes for increased power production in air-cathode microbial fuel cells, Environ. Sci. Technol. 41 (2007) 3341–3346.

[60] P. Aelterman, M. Versichele, M. Marzorati, N. Boon, W. Verstraete, Loading rate and external resistance control the electricity generation of microbial fuel cells with different three-dimensional anodes, Bioresour. Technol. 99 (2008) 8895–8902.

[61] A. Larrosa-Guerrero, K. Scott, K.P. Katuri, C. Godinez, I.M. Head, T. Curtis, Open circuit versus closed circuit enrichment of anodic biofilms in MFC: Effect on performance and anodic communities, Appl. Microbiol. Biotechnol. 87 (2010) 1699–1713.

[62] Y. Yuan, S. Zhou, Y. Liu, J. Tang, Nanostructured macroporous bioanode based on polyaniline-modified natural loofah sponge for high-performance microbial fuel cells, Environ. Sci. Technol. 47 (2013) 14525–14532.

[63] S.K. Chaudhuri, D.R. Lovley, Electricity generation by direct oxidation of glucose in mediatorless microbial fuel cells, Nat. Biotechnol. 21 (2003) 1229–1232.

[64] N. LaBarge, Y.D. Yilmazel, P.-Y. Hong, B.E. Logan, Effect of pre-acclimation of granular activated carbon on microbial electrolysis cell startup and performance, Bioelectrochemistry. 113 (2017) 20–25.

[65] X. Xia, X. Cao, P. Liang, X. Huang, Electricity generation from glucose by a *Klebsiella* sp. in microbial fuel cells, Appl. Microbiol. Biotechnol. 87 (2010) 383–390.

[66] S.E. Oh, B.E. Logan, Proton exchange membrane and electrode surface areas as factors that affect power generation in microbial fuel cells, Appl. Microbiol. Biotechnol. 70 (2006) 162–169.

[67] X. Xie, M. Ye, L. Hu, N. Liu, J.R. McDonough, W. Chen, H.N. Alshareef, C.S. Criddle, Y. Cui, Carbon nanotube-coated macroporous sponge for microbial fuel cell electrodes, Energy

Environ. Sci. 5 (2012) 5265–5270.

[68] D.V.P. Sanchez, D. Jacobs, K. Gregory, J. Huang, Y. Hu, R. Vidic, M. Yun, Changes in carbon electrode morphology affect microbial fuel cell performance with *Shewanella oneidensis* MR-1, Energies. 8 (2015) 1817–1829.

[69] M. Lu, Y. Qian, L. Huang, X. Xie, W. Huang, Improving the performance of microbial fuel cells through anode manipulation, Chempluschem. 80 (2015) 1216–1225.

[70] A. ter Heijne, H.V.M. Hamelers, M. Saakes, C.J.N. Buisman, Performance of non-porous graphite and titanium-based anodes in microbial fuel cells, Electrochim. Acta. 53 (2008) 5697–5703.

[71] Y. Liu, F. Harnisch, K. Fricke, U. Schroder, V. Climent, J.M. Feliu, The study of electrochemically active microbial biofilms on different carbon-based anode materials in microbial fuel cells, Biosens. Bioelectron. 25 (2010) 2167–2171.

[72] S. Chen, G. He, X. Hu, M. Xie, S. Wang, D. Zeng, H. Hou, U. Schröder, A three-dimensionally ordered macroporous carbon derived from a natural resource as anode for microbial bioelectrochemical systems, ChemSusChem. 5 (2012) 1059–1063.

[73] S. Chen, G. He, A.A. Carmona-Martinez, S. Agarwal, A. Greiner, H. Hou, U. Schröder, Electrospun carbon fiber mat with layered architecture for anode in microbial fuel cells, Electrochem. Commun. 13 (2011) 1026–1029.

[74] X. Xie, L. Hu, M. Pasta, G.F. Wells, D. Kong, C.S. Criddle, Y. Cui, Three-dimensional carbon nanotube-textile anode for high-performance microbial fuel cells, Nano Lett. 11 (2011) 291–296.

[75] S.A. Patil, S. Chigome, C. Hägerhäll, N. Torto, L. Gorton, Electrospun carbon nanofibers from polyacrylonitrile blended with activated or graphitized carbonaceous materials for improving anodic bioelectrocatalysis, Bioresour. Technol. 132 (2013) 121–126.

[76] J. Wang, M. Li, F. Liu, S. Chen, Stainless steel mesh supported carbon nanofibers for electrode in bioelectrochemical system, J. Nanomater. 2016 (2016) 1–5.

[77] X. Huang, Fabrication and properties of carbon fibers, Materials (Basel). 2 (2009) 2369–2403.

[78] S.J. Park, G.Y. Heo, Precursors and manufacturing of carbon fibers, Springer Ser. Mater. Sci. 210 (2015) 31–36.

[79] D.D.L. Chung, Carbon Fibers, Nanofibers, and Nanotubes, in: Carbon Compos., Second Edi, Elsevier Inc., 2017: pp. 1–87.

[80] E. Frank, F. Hermanutz, M.R. Buchmeiser, Carbon fibers: Precursors, manufacturing, and properties, Macromol. Mater. Eng. 297 (2012) 493–501.

[81] H. Mainka, O. Täger, E. Körner, L. Hilfert, S. Busse, F.T. Edelmann, A.S. Herrmann, Lignin

– an alternative precursor for sustainable and cost-effective automotive carbon fiber, J. Mater. Res. Technol. 4 (2015) 283–296.

[82] M.M.R. Khan, Y. Gotoh, H. Morikawa, M. Miura, Y. Fujimori, M. Nagura, Carbon fiber from natural biopolymer *Bombyx mori* silk fibroin with iodine treatment, Carbon N. Y. 45 (2007) 1035–1042.

[83] A. Siwak, N. Diez, E. Miniach, G. Gryglewicz, Nitrogen-containing chitosan-based carbon as an electrode material for high-performance supercapacitors, J. Appl. Electrochem. 46 (2016) 667–677.

[84] M.J. Prauchner, V.M.D. Pasa, C. Otani, S. Otani, S.M.C. De Menezes, *Eucalyptus* tar pitch pretreatment for carbon material processing, J. Appl. Polym. Sci. 91 (2004) 1604–1611.

[85] M.J. Behr, B.G. Landes, B.E. Barton, M.T. Bernius, G.F. Billovits, E.J. Hukkanen, J.T. Patton, W. Wang, C. Wood, D.T. Keane, J.E. Rix, S.J. Weigand, Structure-property model for polyethylene-derived carbon fiber, Carbon N. Y. 107 (2016) 525–535.

[86] A. Bismarck, M. Pfaffernoschke, J. Springer, E. Schulz, Polystyrene-grafted carbon fibers: Surface properties and adhesion to polystyrene, J. Thermoplast. Compos. Mater. 18 (2005) 307–331.

[87] C. Lei, N. Amini, F. Markoulidis, P. Wilson, S. Tennison, C. Lekakou, Activated carbon from phenolic resin with controlled mesoporosity for an electric double-layer capacitor (EDLC), J. Mater. Chem. A. 1 (2013) 6037–6042.

[88] R. Xue, J. Yan, X. Liu, Y. Tian, B. Yi, Effect of activation on the carbon fibers from phenol-formaldehyde resins for electrochemical supercapacitors, J. Appl. Electrochem. 41 (2011) 1357–1366.

[89] X.H. Zhang, Q.W. Li, Carbon fiber spinning, in: J.Y. Chen (Ed.), Act. Carbon Fiber Text., 2017: pp. 39–60.

[90] M. Sun, F. Zhang, Z.H. Tong, G.P. Sheng, Y.Z. Chen, Y. Zhao, Y.P. Chen, S.Y. Zhou, G. Liu, Y.C. Tian, H.Q. Yu, A gold-sputtered carbon paper as an anode for improved electricity generation from a microbial fuel cell inoculated with *Shewanella oneidensis* MR-1, Biosens. Bioelectron. 26 (2010) 338–343.

[91] X. Zhu, B.E. Logan, Copper anode corrosion affects power generation in microbial fuel cells, J. Chem. Technol. Biotechnol. 89 (2014) 471–474.

[92] A. Dumitru, K. Scott, Anode materials for microbial fuel cells, in: K. Scott, E.H. Yu (Eds.), Microb. Electrochem. Fuel Cells, Woodhead Publishing, 2016: pp. 117–152.

[93] B. Li, J. Zhou, X. Zhou, X. Wang, B. Li, C. Santoro, M. Grattieri, S. Babanova, K. Artyushkova, P. Atanassov, A.J. Schuler, Surface modification of microbial fuel cells anodes: Approaches to practical design, Electrochim. Acta. 134 (2014) 116–126.

[94] M. Zhou, M. Chi, H. Wang, T. Jin, Anode modification by electrochemical oxidation: A new practical method to improve the performance of microbial fuel cells, Biochem. Eng. J. 60 (2012) 151–155.

[95] H. Ren, S. Pyo, J.I. Lee, T.J. Park, F.S. Gittleson, F.C.C. Leung, J. Kim, A.D. Taylor, H.S. Lee, J. Chae, A high power density miniaturized microbial fuel cell having carbon nanotube anodes, J. Power Sources. 273 (2015) 823–830.

[96] G.G. Kumar, V.G.S. Sarathi, K.S. Nahm, Recent advances and challenges in the anode architecture and their modifications for the applications of microbial fuel cells, Biosens. Bioelectron. 43 (2013) 461–475.

[97] H.F. Cui, L. Du, P.B. Guo, B. Zhu, J.H.T. Luong, Controlled modification of carbon nanotubes and polyaniline on macroporous graphite felt for high-performance microbial fuel cell anode, J. Power Sources. 283 (2015) 46–53.

[98] Y. Qiao, S. Bao, C.M. Li, X. Cui, Z. Lu, J. Guo, Nanostructured polyaniline/Ttitanium fuel cells, ACS Nano. 2 (2008) 113–119.

[99] A. Mehdinia, E. Ziaei, A. Jabbari, Facile microwave-assisted synthesized reduced graphene oxide/tin oxide nanocomposite and using as anode material of microbial fuel cell to improve power generation, Int. J. Hydrogen Energy. 39 (2014) 10724–10730.

[100] M. Minakshi Sundaram, A. Biswal, D. Mitchell, R. Jones, C. Fernandez, Correlation among physical and electrochemical behaviour of nanostructured electrolytic manganese dioxide from leach liquor and synthetic for aqueous asymmetric capacitor, Phys. Chem. Chem. Phys. 18 (2016) 4711–4720.

[101] N. Phansroy, Y. Aso, S. Sasaki, T. Aoki, H. Ohara, Immobilization of the iron on the surface of non-woven carbon fiber for use in a microbial fuel cell, Mater. Renew. Sustain. Energy. 5 (2016) 1–7.

[102] H.O. Mohamed, M. Obaid, A.S. Yasin, J.H. Kim, N.A.M. Barakat, Electrodepositing technique for improving the performance of crystalline and amorphous carbonaceous anodes for MFCs, RSC Adv. 6 (2016) 111657–111665.

[103] Y. Yang, M. Xu, J. Guo, G. Sun, Bacterial extracellular electron transfer in bioelectrochemical systems, Process Biochem. 47 (2012) 1707–1714.

[104] K. Guo, A.H. Soeriyadi, H. Feng, A. Prévoteau, S.A. Patil, J.J. Gooding, K. Rabaey, Heat-treated stainless steel felt as scalable anode material for bioelectrochemical systems, Bioresour. Technol. 195 (2015) 46–50.

[105] Y. Zou, C. Xiang, L. Yang, L.X. Sun, F. Xu, Z. Cao, A mediatorless microbial fuel cell using polypyrrole coated carbon nanotubes composite as anode material, Int. J. Hydrogen Energy. 33 (2008) 4856–4862.

[106] G.G. Kumar, S. Hashmi, C. Karthikeyan, A. GhavamiNejad, M. Vatankhah-Varnoosfaderani,

F.J. Stadler, Graphene oxide/carbon nanotube composite hydrogels-versatile materials for microbial fuel cell applications., Macromol. Rapid Commun. 35 (2014) 1861–1865.

[107] C.T. Wang, R.Y. Huang, Y.-C. Lee, C.D. Zhang, Electrode material of carbon nanotube/polyaniline carbon paper applied in microbial fuel cells, J. Clean Energy Technol. 1 (2013) 206–210.

[108] A. Mehdinia, M. Dejaloud, A. Jabbari, Nanostructured polyaniline-coated anode for improving microbial fuel cell power output, Chem. Pap. 67 (2013) 1096–1102.

[109] Z.H. Liao, J.Z. Sun, D.Z. Sun, R.W. Si, Y.C. Yong, Enhancement of power production with tartaric acid doped polyaniline nanowire network modified anode in microbial fuel cells, Bioresour. Technol. 192 (2015) 831–834.

[110] X. Tang, H. Li, Z. Du, W. Wang, H.Y. Ng, Conductive polypyrrole hydrogels and carbon nanotubes composite as an anode for microbial fuel cells, RSC Adv. 5 (2015) 50968–50974.

[111] P. Pérez-Rodríguez, V.M. Ovando-Medina, S.Y. Martínez-Amador, J.A. Rodríguez-de la Garza, Bioanode of polyurethane/graphite/polypyrrole composite in microbial fuel cells, Biotechnol. Bioprocess Eng. 21 (2016) 305–313.

[112] D.H. Park, J.G. Zeikus, Improved fuel cell and electrode designs for producing electricity from microbial degradation., Biotechnol. Bioeng. 81 (2003) 348–355.

[113] D.A. Lowy, L.M. Tender, J.G. Zeikus, D.H. Park, D.R. Lovley, Harvesting energy from the marine sediment-water interface II. Kinetic activity of anode materials, Biosens. Bioelectron. 21 (2006) 2058–2063.

[114] Z. Li, X. Liu, P. Liu, P. Zhang, The performance of electron-mediator modified activated carbon as anode for direct glucose alkaline fuel cell, Catalysts. 6 (2016).

[115] Y. Zhang, B. Min, L. Huang, I. Angelidaki, Electricity generation and microbial community response to substrate changes in microbial fuel cell., Bioresour. Technol. 102 (2011) 1166–1173.

[116] K.T. Finneran, C. V Johnsen, D.R. Lovley, *Rhodoferax ferrireducens* sp. nov., a psychrotolerant, facultatively anaerobic bacterium that oxidizes acetate with the reduction of Fe(III), Int. J. Syst. Evol. Microbiol. 53 (2003) 669–673.

[117] D.R. Lovley, D.E. Holmes, K.P. Nevin, Dissimilatory Fe(III) and Mn(IV) reduction, Adv. Microb. Physiol. 49 (2004) 219–286.

[118] C.R. Myers, K.H. Nealson, Bacterial manganese reduction and growth with manganese oxide as the sole electron acceptor., Science 240 (1988) 1319–1321.

[119] J. Philips, K. Verbeeck, K. Rabaey, J.B.A. Arends, Electron transfer mechanisms in biofilms, in: K. Scott, E.H. Yu (Eds.), Microb. Electrochem. Fuel Cells, Woodhead Publishing, 2016:

pp. 67–113.

[120] B. Min, S. Cheng, B.E. Logan, Electricity generation using membrane and salt bridge microbial fuel cells, Water Res. 39 (2005) 1675–1686.

[121] D.E. Holmes, D.R. Bond, D.R. Lovley, Electron transfer by *Desulfobulbus propionicu*s to Fe (III) and graphite electrodes, Appl. Environ. Microbiol. 70 (2004) 1234–1237.

[122] L. Zhang, S. Zhou, L. Zhuang, W. Li, J. Zhang, N. Lu, L. Deng, Microbial fuel cell based on *Klebsiella pneumoniae* biofilm, Electrochem. Commun. 10 (2008) 1641–1643.

[123] S.T. Read, P. Dutta, P.L. Bond, J. Keller, K. Rabaey, Initial development and structure of biofilms on microbial fuel cell anodes, BMC Microbiol. 10 (2010) 98.

[124] R. Karthikeyan, K. Sathish Kumar, M. Murugesan, B. Sheela, V. Yegnaraman, Bioelectrocatalysis of acetobacter aceti and *Gluconobacter roseus* for current generation, Environ. Sci. Technol. 43 (2009) 8684–8689.

[125] D. Xing, S. Cheng, B.E. Logan, J.M. Regan, Isolation of the exoelectrogenic denitrifying bacterium *Comamonas denitrificans* based on dilution to extinction, Appl. Microbiol. Biotechnol. 85 (2010) 1575–1587.

[126] D.R. Bond, D.R. Lovley, Evidence for involvement of an electron shuttle in electricity generation by *Geothrix fermentans*, Appl. Environ. Microbiol. 71 (2005) 2186–2189.

[127] A. Sydow, T. Krieg, F. Mayer, J. Schrader, D. Holtmann, Electroactive bacteria - molecular mechanisms and genetic tools, Appl. Microbiol. Biotechnol. 98 (2014) 8481–8495.

[128] L.-P. Fan, S. Xue, Overview on electricigens for microbial fuel cell, Open Biotechnol. J. 10 (2016) 398–406.

[129] M. Zhou, H. Wang, D.J. Hassett, T. Gu, Recent advances in microbial fuel cells (MFCs) and microbial electrolysis cells (MECs) for wastewater treatment, bioenergy and bioproducts, J. Chem. Technol. Biotechnol. 88 (2013) 508–518.

[130] J.P. Busalmen, A. Esteve-Núñez, A. Berná, J.M. Feliu, C-type cytochromes wire electricity-producing bacteria to electrodes, Angew. Chemie - Int. Ed. 47 (2008) 4874–4877.

[131] K.P. Nevin, B.C. Kim, R.H. Glaven, J.P. Johnson, T.L. Woodward, B.A. Methé, R.J. Didonato, S.F. Covalla, A.E. Franks, A. Liu, D.R. Lovley, Anode biofilm transcriptomics reveals outer surface components essential for high density current production in *Geobacter sulfurreducens* fuel cells, PLoS One. 4 (2009) e5628.

[132] Z.M. Summers, H.E. Fogarty, C. Leang, A.E. Franks, N.S. Malvankar, D.R. Lovley, Direct exchange of electrons within aggregates of an evolved syntrophic coculture of anaerobic bacteria, Science. 330 (2010) 1413–1415.

[133] S.A. Patil, C. Hägerhäll, L. Gorton, Electron transfer mechanisms between microorganisms and electrodes in bioelectrochemical systems, Bioanal. Rev. 4 (2012) 159–192.

[134] D. Coursolle, D.B. Baron, D.R. Bond, J.A. Gralnick, The Mtr respiratory pathway is essential for reducing flavins and electrodes in *Shewanella oneidensis*, J. Bacteriol. 192 (2010) 467–474.

[135] G. Reguera, K.D. McCarthy, T. Mehta, J.S. Nicoll, M.T. Tuominen, D.R. Lovley, Extracellular electron transfer via microbial nanowires., Nature. 435 (2005) 1098–1101.

[136] N.S. Malvankar, D.R. Lovley, Microbial nanowires: A new paradigm for biological electron transfer and bioelectronics, ChemSusChem. 5 (2012) 1039–1046.

[137] N.S. Malvankar, M.T. Tuominen, D.R. Lovley, Lack of cytochrome involvement in long-range electron transport through conductive biofilms and nanowires of *Geobacter sulfurreducens*, Energy Environ. Sci. 5 (2012) 8651–8659.

[138] C. Leang, X. Qian, T. Mester, D.R. Lovley, Alignment of the c-type cytochrome OmcS along pili of *Geobacter sulfurreducens*, Appl. Environ. Microbiol. 76 (2010) 4080–4084.

[139] N.S. Malvankar, M. Vargas, K.P. Nevin, A.E. Franks, C. Leang, B.-C. Kim, K. Inoue, T. Mester, S.F. Covalla, J.P. Johnson, V.M. Rotello, M.T. Tuominen, D.R. Lovley, Tunable metallic-like conductivity in microbial nanowire networks., Nat. Nanotechnol. 6 (2011) 573–579.

[140] Y.A. Gorby, S. Yanina, J.S. McLean, K.M. Rosso, D. Moyles, A. Dohnalkova, T.J. Beveridge, I.S. Chang, B.H. Kim, K.S. Kim, D.E. Culley, S.B. Reed, M.F. Romine, D.A. Saffarini, E.A. Hill, L. Shi, D.A. Elias, D.W. Kennedy, G. Pinchuk, K. Watanabe, S. Ishii, B. Logan, K.H. Nealson, J.K. Fredrickson, Electrically conductive bacterial nanowires produced by *Shewanella oneidensis* strain MR-1 and other microorganisms., Proc. Natl. Acad. Sci. U. S. A. 103 (2006) 11358–11363.

[141] S. Pirbadian, S.E. Barchinger, K.M. Leung, H.S. Byun, Y. Jangir, R.A. Bouhenni, S.B. Reed, M.F. Romine, D.A. Saffarini, L. Shi, Y.A. Gorby, J.H. Golbeck, M.Y. El-Naggar, *Shewanella oneidensis* MR-1 nanowires are outer membrane and periplasmic extensions of the extracellular electron transport components., Proc. Natl. Acad. Sci. U. S. A. 111 (2014) 12883–12888.

[142] X. Xia, X.X. Cao, P. Liang, X. Huang, S.P. Yang, G.G. Zhao, Electricity generation from glucose by a *Klebsiella* sp. in microbial fuel cells, Appl. Microbiol. Biotechnol. 87 (2010) 383–390.

[143] S. Tanisho, N. Kamiya, N. Wakao, Microbial fuel cell using *Enterobacter aerogenes*, Bioelectrochemistry Bioenerg. 21 (1989) 25–32.

[144] D.H. Park, J.G. Zeikus, Electricity generation in microbial fuel cells using neutral red as an electronophore, Appl. Environ. Microbiol. 66 (2000) 1292–1297.

[145] E. Marsili, D.B. Baron, I.D. Shikhare, D. Coursolle, J. a Gralnick, D.R. Bond, *Shewanella* secretes flavins that mediate extracellular electron transfer., Proc. Natl. Acad. Sci. U. S. A.

105 (2008) 3968–3973.

[146] K. Rabaey, N. Boon, M. Höfte, W. Verstraete, Microbial phenazine production enhances electron transfer in biofuel cells., Environ. Sci. Technol. 39 (2005) 3401–3408.

[147] M.G. Mehta-Kolte, D.R. Bond, *Geothrix fermentans* secretes two different redox-active compounds to utilize electron acceptors across a wide range of redox potentials, Appl. Environ. Microbiol. 78 (2012) 6987–6995.

[148] U. Schröder, J. Nießen, F. Scholz, A generation of microbial fuel cells with current outputs boosted by more than one order of magnitude, Angew. Chemie - Int. Ed. 42 (2003) 2880–2883.

[149] E. Taskan, B. Ozkaya, H. Hasar, Combination of a novel electrode material and artificial mediators to enhance power generation in an MFC, Water Sci. Technol. 71 (2015) 320–328.

[150] F. Zuhri, R. Arbianti, T.S. Utami, H. Hermansyah, Efffect of methyllene blue addition as a redox mediator on performance of microbial desalination cell by utilizing tempe wastewater, Int. J. Technol. 6 (2016) 952–961.

[151] R. Fathey, O.M. Gomaa, A.E.H. Ali, H.A. El Kareem, M.A. Zaid, Neutral red as a mediator for the enhancement of electricity production using a domestic wastewater double chamber microbial fuel cell, Ann. Microbiol. 66 (2016) 695–702.

[152] A.E. Rotaru, P.M. Shrestha, F. Liu, B. Markovaite, S. Chen, K.P. Nevin, D.R. Lovley, Direct interspecies electron transfer between *Geobacter metallireducens* and *Methanosarcina barkeri*, Appl. Environ. Microbiol. 80 (2014) 4599–4605.

[153] U. Schröder, Discover the possibilities: Microbial bioelectrochemical systems and the revival of a 100-year-old discovery, J. Solid State Electrochem. 15 (2011) 1481–1486.

[154] A. Janicek, Y. Fan, H. Liu, Design of microbial fuel cells for practical application: a review and analysis of scale-up studies, Biofuels. 5 (2014) 79–92.

[155] S. Ishii, S. Suzuki, T.M. Norden-Krichmar, A. Wu, Y. Yamanaka, K.H. Nealson, O. Bretschger, Identifying the microbial communities and operational conditions for optimized wastewater treatment in microbial fuel cells, Water Res. 47 (2013) 7120–7130.

[156] P. Batlle-Vilanova, S. Puig, R. Gonzalez-Olmos, M.D. Balaguer, J. Colprim, Continuous acetate production through microbial electrosynthesis from CO_2 with microbial mixed culture, J. Chem. Technol. Biotechnol. 91 (2016) 921–927.

[157] K.J.J. Steinbusch, H.V.M. Hamelers, J.D. Schaap, C. Kampman, C.J.N. Buisman, Bioelectrochemical ethanol production through mediated acetate reduction by mixed cultures, Environ. Sci. Technol. 44 (2010) 513–517.

[158] K.B. Gregory, D.R. Lovley, Remediation and recovery of uranium from contaminated

subsurface environments with electrodes, Environ. Sci. Technol. 39 (2005) 8943–8947.

[159] J.M. Morris, S. Jin, Feasibility of using microbial fuel cell technology for bioremediation of hydrocarbons in groundwater, J. Environ. Sci. Heal. Part A. 43 (2008) 18–23.

[160] K. Zuo, F. Liu, S. Ren, X. Zhang, P. Liang, X. Huang, A novel multi-stage microbial desalination cell for simultaneous desalination and enhanced organics and nitrogen removal from domestic wastewater, Environ. Sci. Water Res. Technol. 2 (2016) 832–837.

[161] G. Martins, L. Peixoto, D.C. Ribeiro, P. Parpot, A.G. Brito, R. Nogueira, Towards implementation of a benthic microbial fuel cell in lake Furnas (Azores): Phylogenetic affiliation and electrochemical activity of sediment bacteria, Bioelectrochemistry. 78 (2010) 67–71.

[162] Y.-H. Song, S. Hidayat, H.-K. Kim, J.-Y. Park, Hydrogen production in microbial reverse-electrodialysis electrolysis cells using a substrate without buffer solution, Bioresour. Technol. 210 (2016) 56–60.

[163] Y. Zou, J. Pisciotta, I. V Baskakov, Nanostructured polypyrrole-coated anode for sun-powered microbial fuel cells, Bioelectrochemistry. 79 (2010) 50–56.

[164] J. Wilson, Water and Wastewater Treatment Technologies: Global Markets, Report code ENV008B, Wellesley, 2012.

[165] T.H. Pham, K. Rabaey, P. Aelterman, P. Clauwaert, L. De Schamphelaire, N. Boon, W. Verstraete, Microbial fuel cells in relation to conventional anaerobic digestion technology, Eng. Life Sci. 6 (2006) 285–292.

[166] L. Huang, B.E. Logan, Electricity generation and treatment of paper recycling wastewater using a microbial fuel cell, Appl. Microbiol. Biotechnol. 80 (2008) 349–355.

[167] P. Kuntke, K.M. Smiech, H. Bruning, G. Zeeman, M. Saakes, T.H.J.A. Sleutels, H.V.M. Hamelers, C.J.N. Buisman, Ammonium recovery and energy production from urine by a microbial fuel cell, Water Res. 46 (2012) 2627–2636.

[168] W. Habermann, E.H. Pommer, Biological fuel cells with sulfide storage capacity, Appl. Microbiol. Biotechnol. 35 (1991) 128–133.

[169] S. Oh, B.E. Logan, Hydrogen and electricity production from a food processing wastewater using fermentation and microbial fuel cell technologies, Water Res. 39 (2005) 4673–4682.

[170] B. Min, J. Kim, S. Oh, J.M. Regan, B.E. Logan, Electricity generation from swine wastewater using microbial fuel cells, Water Res. 39 (2005) 4961–4968.

[171] P. Aelterman, K. Rabaey, P. Clauwaert, W. Verstraete, Microbial fuel cells for wastewater treatment, Water Sci. Technol. 54 (2006) 9–15.

[172] Y. Feng, X. Wang, B.E. Logan, H. Lee, Brewery wastewater treatment using air-cathode microbial fuel cells, Appl. Microbiol. Biotechnol. 78 (2008) 873–880.

[173] S.A. Patil, V.P. Surakasi, S. Koul, S. Ijmulwar, A. Vivek, Y.S. Shouche, B.P. Kapadnis, Electricity generation using chocolate industry wastewater and its treatment in activated sludge based microbial fuel cell and analysis of developed microbial community in the anode chamber, Bioresour. Technol. 100 (2009) 5132–5139.

[174] B. Cercado-Quezada, M.L. Delia, A. Bergel, Testing various food-industry wastes for electricity production in microbial fuel cell, Bioresour. Technol. 101 (2010) 2748–2754.

[175] G. Zhao, F. Ma, L. Wei, H. Chua, C.C. Chang, X.J. Zhang, Electricity generation from cattle dung using microbial fuel cell technology during anaerobic acidogenesis and the development of microbial populations, Waste Manag. 32 (2012) 1651–1658.

[176] I. Durruty, P.S. Bonanni, J.F. González, J.P. Busalmen, Evaluation of potato-processing wastewater treatment in a microbial fuel cell, Bioresour. Technol. 105 (2012) 81–87.

[177] K.P. Katuri, A.M. Enright, V. O'Flaherty, D. Leech, Microbial analysis of anodic biofilm in a microbial fuel cell using slaughterhouse wastewater, Bioelectrochemistry. 87 (2012) 164–171.

[178] X. Li, N. Zhu, Y. Wang, P. Li, P. Wu, J. Wu, Animal carcass wastewater treatment and bioelectricity generation in up-flow tubular microbial fuel cells: Effects of HRT and non-precious metallic catalyst, Bioresour. Technol. 128 (2013) 454–460.

[179] F. Guo, G. Fu, Z. Zhang, C. Zhang, Mustard tuber wastewater treatment and simultaneous electricity generation using microbial fuel cells, Bioresour. Technol. 136 (2013) 425–430.

[180] P.T. Kelly, Z. He, Understanding the application niche of microbial fuel cells in a cheese wastewater treatment process, Bioresour. Technol. 157 (2014) 154–160.

[181] T. Pepe Sciarria, G. Merlino, B. Scaglia, A. D'Epifanio, B. Mecheri, S. Borin, S. Licoccia, F. Adani, Electricity generation using white and red wine lees in air cathode microbial fuel cells, J. Power Sources. 274 (2015) 393–399.

[182] H.J. Mansoorian, A.H. Mahvi, A.J. Jafari, N. Khanjani, Evaluation of dairy industry wastewater treatment and simultaneous bioelectricity generation in a catalyst-less and mediator-less membrane microbial fuel cell, J. Saudi Chem. Soc. 20 (2016) 88–100.

[183] J.A. Adeniran, R. Huberts, J.J. De-Koker, O.A. Arotiba, O.F. Olorundare, E. Van-Zyl, S.C. Du-Plessis, Energy generation from domestic wastewater using sandwich dual-chamber microbial fuel cell with mesh current collector cathode, Int. J. Environ. Sci. Technol. 13 (2016) 2209–2218.

[184] Z. Rasep, N. Shahirah, M. Aripen, Microbial fuel cell for conversion of chemical energy to electrical energy from food industry wastewater, J. Environ. Sci. Technol. 9 (2016) 481–485.

[185] Z. He, S.D. Minteer, L.T. Angenent, Electricity generation from artificial wastewater using an upflow microbial fuel cell., Environ. Sci. Technol. 39 (2005) 5262–5267.

[186] T. Yi, W.F. Harper, The effect of nitrate and sulfate on mediator-less microbial fuel cells with high internal resistance, Water Environ. Res. a Res. Publ. Water Environ. Fed. 81 (2009) 2320–2328.

[187] H. Liu, S. Cheng, B.E. Logan, Power generation in fed-batch microbial fuel cells as a function of ionic strength, temperature, and reactor configuration, Environ. Sci. Technol. 39 (2005) 5488–5493.

[188] C. Santoro, I. Ieropoulos, J. Greenman, P. Cristiani, T. Vadas, A. Mackay, B. Li, Current generation in membraneless single chamber microbial fuel cells (MFCs) treating urine, J. Power Sources. 238 (2013) 190–196.

[189] M.L. Ullery, B.E. Logan, Anode acclimation methods and their impact on microbial electrolysis cells treating fermentation effluent, Int. J. Hydrogen Energy. 40 (2015) 6782–6791.

[190] A. Tenca, R.D. Cusick, A. Schievano, R. Oberti, B.E. Logan, Evaluation of low cost cathode materials for treatment of industrial and food processing wastewater using microbial electrolysis cells, Int. J. Hydrogen Energy. 38 (2013) 1859–1865.

[191] P.D. Kiely, R. Cusick, D.F. Call, P. a Selembo, J.M. Regan, B.E. Logan, Anode microbial communities produced by changing from microbial fuel cell to microbial electrolysis cell operation using two different wastewaters, Bioresour. Technol. 102 (2011) 388–394.

[192] Y. Wang, W.Q. Guo, D.F. Xing, J.S. Chang, N.Q. Ren, Hydrogen production using biocathode single-chamber microbial electrolysis cells fed by molasses wastewater at low temperature, Int. J. Hydrogen Energy. 39 (2014) 19369–19375.

[193] J. Ditzig, H. Liu, B.E. Logan, Production of hydrogen from domestic wastewater using a bioelectrochemically assisted microbial reactor (BEAMR), Int. J. Hydrogen Energy. 32 (2007) 2296–2304.

[194] R.C. Wagner, J.M. Regan, S.-E. Oh, Y. Zuo, B.E. Logan, Hydrogen and methane production from swine wastewater using microbial electrolysis cells, Water Res. 43 (2009) 1480–1488.

[195] R.D. Cusick, B. Bryan, D.S. Parker, M.D. Merrill, M. Mehanna, P.D. Kiely, G. Liu, B.E. Logan, Performance of a pilot-scale continuous flow microbial electrolysis cell fed winery wastewater, Appl. Microbiol. Biotechnol. 89 (2011) 2053–2063.

[196] M. Mahmoud, P. Parameswaran, C.I. Torres, B.E. Rittmann, Fermentation pre-treatment of landfill leachate for enhanced electron recovery in a microbial electrolysis cell, Bioresour. Technol. 151 (2014) 151–158.

[197] T.A. Larsen, W. Gujer, Separate management of anthropogenic nutrient solutions (human urine), in: Water Sci. Technol., 1996: pp. 87–94.

[198] P. Kuntke, Nutrient and energy recovery from urine, Wageningen University, 2013.

[199] Mohajit, K.K. Bhattarai, E.P. Taiganides, B.C. Yap, Struvite deposits in pipes and aerators, Biol. Wastes. 30 (1989) 133–147.

[200] K.N. Ohlinger, T.M. Young, E.D. Schroeder, Redicting struvite formation in digestion, Water Res. 32 (1998) 3607–3614.

[201] J. Lienert, T.A. Larsen, High acceptance of urine source separation in seven European countries: A review, Environ. Sci. Technol. 44 (2010) 556–566.

[202] M. Ronteltap, M. Maurer, R. Hausherr, W. Gujer, Struvite precipitation from urine - Influencing factors on particle size, Water Res. 44 (2010) 2038–2046.

[203] E. Tilley, J. Atwater, D. Mavinic, Recovery of struvite from stored human urine, Environ. Technol. 29 (2008) 797–806.

[204] I. Ieropoulos, J. Greenman, C. Melhuish, B.E. Logan, B. Hamelers, R. Rozendal, U. Schroder, J. Keller, S. Freguia, P. Aelterman, W. Verstraete, K. Rabaey, D. Pant, G. V. Bogaert, L. Diels, K. Vanbroekhoven, L.P. Rodriguez, G.J. Padovan, V.M.M. Suen, J.S. Marchini, J. Greenman, K.T. Holland, W.J. Cunliffe, I. Ieropoulos, J. Greenman, C. Melhuish, D. Morse, P.E. V. Williams, H.M. ApSimon, M. Kruse, J.N.B. Bell, B.K. Boggs, R.L. King, G.G. Botte, I.A. Ieropoulos, J. Winfield, J. Greenman, C. Melhuish, Urine utilisation by microbial fuel cells; energy fuel for the future, Phys. Chem. Chem. Phys. 14 (2012) 94–98.

[205] D.J. Conley, H.W. Paerl, R.W. Howarth, D.F. Boesch, S.P. Seitzinger, K.E. Havens, C. Lancelot, G.E. Likens, Controlling eutrophication: nitrogen and phosphorus, Science. 323 (2009) 1014–1015.

[206] M. Gromiec, T. Gromiec, Controlling of eutrophication in aquatic environments, J. Water L. Dev. 14 (2010) 29–35.

[207] D. Cordell, A. Rosemarin, J.J. Schröder, a L. Smit, Towards global phosphorus security: a systems framework for phosphorus recovery and reuse options., Chemosphere. 84 (2011) 747–758.

[208] J. Wang, J.G. Burken, X. (Jackie) Zhang, R. Surampalli, Engineered struvite precipitation: Impacts of component-ion molar ratios and pH, J. Environ. Eng. 131 (2005) 1433–1440.

[209] M.M. Rahman, Y. Liu, J.-H. Kwag, C. Ra, Recovery of struvite from animal wastewater and its nutrient leaching loss in soil, J. Hazard. Mater. 186 (2011) 2026–2030.

[210] G. El Diwani, S. El Rafie, N.N. El Ibiari, H.I. El-Aila, Recovery of ammonia nitrogen from industrial wastewater treatment as struvite slow releasing fertilizer, Desalination. 214 (2007) 200–214.

[211] C.M. Mehta, D. Batstone, Nucleation and growth kinetics of struvite crystallization, Water Res. 47 (2013) 2890–2900.

[212] J.R. Mihelcic, L.M. Fry, R. Shaw, Global potential of phosphorus recovery from human urine and feces, Chemosphere. 84 (2011) 832–839.

[213] H.L.T. Mobley, R.P. Hausinger, Microbial ureases: significance, regulation, and molecular characterizationt, Microbiol. Rev. 53 (1989) 85–108.

[214] E. Desmidt, K. Ghyselbrecht, A. Monballiu, K. Rabaey, W. Verstraete, B.D. Meesschaert, Factors influencing urease driven struvite precipitation, Sep. Purif. Technol. 110 (2013) 150–157.

[215] M. Ronteltap, M. Maurer, W. Gujer, Struvite precipitation thermodynamics in source-separated urine, Water Res. 41 (2007) 977–984.

[216] N. Morales, M.A. Boehler, S. Buettner, C. Liebi, H. Siegrist, Recovery of N and P from urine by struvite precipitation followed by combined stripping with digester sludge liquid at full scale, Water. 5 (2013) 1262–1278.

[217] P. Zamora, T. Georgieva, I. Salcedo, N. Elzinga, P. Kuntke, C.J. Buisman, Long-term operation of a pilot-scale reactor for phosphorus recovery as struvite from source-separated urine, J. Chem. Technol. Biotechnol. (2016).

[218] B. Etter, E. Tilley, R. Khadka, K.M. Udert, Low-cost struvite production using source-separated urine in Nepal, Water Res. 45 (2011) 852–862.

[219] I. Merino-Jimenez, V. Celorrio, D.J. Fermin, J. Greenman, I. Ieropoulos, Enhanced MFC power production and struvite recovery by the addition of sea salts to urine, Water Res. 109 (2017) 46–53.

[220] K.M. Udert, T.A. Larsen, M. Biebow, W. Gujer, Urea hydrolysis and precipitation dynamics in a urine-collecting system, Water Res. 37 (2003) 2571–2582.

[221] M.M. Rahman, M.A.M. Salleh, U. Rashid, A. Ahsan, M.M. Hossain, C.S. Ra, Production of slow release crystal fertilizer from wastewaters through struvite crystallization - A review, Arab. J. Chem. 7 (2014) 139–155.

[222] K. Gell, F.J. d. Ruijter, P. Kuntke, M. De Graaff, a. L. Smit, Safety and effectiveness of struvite from black water and urine as a phosphorus fertilizer, J. Agric. Sci. 3 (2011) 67–80.

[223] R. González-Ponce, E.G. López-de-Sá, C. Plaza, Lettuce response to phosphorus fertilization with struvite recovered from municipal wastewater, HortScience. 44 (2009) 426–430.

[224] G.P. Ricardo, E.G. López-de-Sá, C. Plaza, Lettuce response to phosphorus fertilization with struvite recovered from municipal wastewater, HortScience. 44 (2009) 426–430.

[225] G.-L. Zang, G.-P. Sheng, W.-W. Li, Z.-H. Tong, R.J. Zeng, C. Shi, H.-Q. Yu, Nutrient removal and energy production in a urine treatment process using magnesium ammonium phosphate precipitation and a microbial fuel cell technique, Phys. Chem. Chem. Phys. 14

(2012) 1978.

[226] I.A. Ieropoulos, J. Greenman, C. Melhuish, Miniature microbial fuel cells and stacks for urine utilisation, Int. J. Hydrogen Energy. 38 (2013) 492–496.

[227] C. Santoro, I.A. Ieropoulos, J. Greenman, P. Cristiani, T. Vadas, A. Mackay, B. Li, Power generation and contaminant removal in single chamber microbial fuel cells (SCMFCs) treating human urine, Int. J. Hydrogen Energy. 38 (2013) 11543–11551.

[228] I.A. Ieropoulos, P. Ledezma, A. Stinchcombe, G. Papaharalabos, C. Melhuish, J. Greenman, Waste to real energy: the first MFC powered mobile phone, Phys. Chem. Chem. Phys. 15 (2013) 15312–15316.

[229] I.A. Ieropoulos, A. Gálvez, J. Greenman, Effects of sulphate addition and sulphide inhibition on microbial fuel cells, Enzyme Microb. Technol. 52 (2013) 32–37.

[230] J. You, J. Greenman, C. Melhuish, I.A. Ieropoulos, Electricity generation and struvite recovery from human urine using microbial fuel cells, J. Chem. Technol. Biotechnol. 91 (2015) 647–654.

[231] G. Papaharalabos, J. Greenman, C. Melhuish, I.A. Ieropoulos, A novel small scale Microbial Fuel Cell design for increased electricity generation and waste water treatment, Int. J. Hydrogen Energy. 40 (2015) 4263–4268.

[232] X.A. Walter, I. Gajda, S. Forbes, J. Winfield, J. Greenman, I.A. Ieropoulos, Scaling-up of a novel, simplified MFC stack based on a self-stratifying urine column, Biotechnol. Biofuels. 9 (2016) 93.

[233] X.A. Walter, A. Stinchcombe, J. Greenman, I.A. Ieropoulos, Urine transduction to usable energy: A modular MFC approach for smartphone and remote system charging, Appl. Energy. 192 (2016) 575–581.

[234] I. Merino, J. Greenman, I. Ieropoulos, Electricity and catholyte production from ceramic MFCs treating urine, Int. J. Hydrogen Energy. 42 (2017) 1791–1799.

[235] P. Kuntke, T.H.J.A. Sleutels, M. Saakes, C.J.N. Buisman, Hydrogen production and ammonium recovery from urine by a Microbial Electrolysis Cell, Int. J. Hydrogen Energy. 39 (2014) 4771–4778.

[236] P. Kuntke, P. Zamora, M. Saakes, C.J.N. Buisman, H.V.M.V. Hamelers, Gas-permeable hydrophobic tubular membranes for ammonia recovery in bio-electrochemical systems, Environ. Sci. Water Res. &Technology. 2 (2016) 261–265.

[237] A. Kadier, Y. Simayi, M.S. Kalil, P. Abdeshahian, A.A. Hamid, A review of the substrates used in microbial electrolysis cells (MECs) for producing sustainable and clean hydrogen gas, Renew. Energy. 71 (2014) 466–472.

[238] U.S. Geological Survey, Mineral commodity summaries 2013, U.S. Geol. Surv. (2013) 198.

[239] D. Cordell, S. White, Life's bottleneck: sustaining the world's phosphorus for a food secure future, Annu. Rev. Environ. Resour. 39 (2014) 161–188.

[240] J.A. O'Neal, T.H. Boyer, Phosphate recovery using hybrid anion exchange: Applications to source-separated urine and combined wastewater streams, Water Res. 47 (2013) 5003–5017.

[241] A. Hug, K.M. Udert, Struvite precipitation from urine with electrochemical magnesium dosage, Water Res. 47 (2013) 289–299.

[242] S. Antonini, S. Paris, T. Eichert, J. Clemens, Nitrogen and phosphorus recovery from human urine by struvite precipitation and air stripping in Vietnam, Clean - Soil, Air, Water. 39 (2011) 1099–1104.

[243] M. Krähenbühl, B. Etter, K.M. Udert, Pretreated magnesite as a source of low-cost magnesium for producing struvite from urine in Nepal, Sci. Total Environ. 542 (2016) 1155–1161.

[244] P. Ledezma, P. Kuntke, C.J.N. Buisman, J. Keller, S. Freguia, Source-separated urine opens golden opportunities for microbial electrochemical technologies, Trends Biotechnol. 33 (2015) 214–220.

[245] R. Yu, H. Ren, Y. Wang, L. Ding, J. Geng, K. Xu, Y. Zhang, A kinetic study of struvite precipitation recycling technology with NaOH/$Mg(OH)_2$ addition, Bioresour. Technol. 143 (2013) 519–524.

[246] P.L. Bishop, Enhancing struvite crystallization from anaerobic supernatant, J. Environ. Eng. Sci. 3 (2004) 21–29.

[247] J. Wang, J.G. Burken, X.J. Zhang, R. Surampalli, Engineered struvite precipitation : Impacts of component-Ion molar ratios and pH, J. Environ. Eng. (2005) 1433–1440.

[248] M.S. Rahaman, N. Ellis, D.S. Mavinic, Effects of various process parameters on struvite precipitation kinetics and subsequent determination of rate constants, Water Sci. Technol. 57 (2008) 647–654.

[249] A. Qureshi, K.V. Lo, P.H. Liao, Microwave treatment and struvite recovery potential of dairy manure, J. Environ. Sci. Heal. Part B. 43 (2008) 350–357.

[250] Y. Song, P. Yuan, B. Zheng, J. Peng, F. Yuan, Y. Gao, Nutrients removal and recovery by crystallization of magnesium ammonium phosphate from synthetic swine wastewater, Chemosphere. 69 (2007) 319–324.

[251] J. Wang, J.G. Burken, X. Zhang, Effect of seeding materials and mixing strength on struvite precipitation, Water Environ. Res. 78 (2006) 125–132.

[252] S. Ishak, A. Malakahmad, Optimization of Fenton process for refinery wastewater biodegradability augmentation, Korean J. Chem. Eng. 30 (2013) 1083–1090.

[253] APHA, AWWA, WPCF, Standard methods for the examination of water and wastewater, 17th ed., Washington, D.C., 1998.

[254] X. Liu, Z. Hu, C. Zhu, G. Wen, X. Meng, J. Lu, Effect of contact to the atmosphere and dilution on phosphorus recovery from human urine through struvite formation, Environ. Technol. 35 (2013) 271–277.

[255] A. Capdevielle, E. Sýkorová, B. Biscans, F. Béline, M.L. Daumer, Optimization of struvite precipitation in synthetic biologically treated swine wastewater - determination of the optimal process parameters, J. Hazard. Mater. 244–245 (2013) 357–369.

[256] A. Adnan, D.S. Mavinic, F.A. Koch, Pilot-scale study of phosphorus recovery through struvite crystallization — examining the process feasibility, J. Environ. Eng. 2 (2003) 315–324.

[257] K.N. Ohlinger, P.E., T.M. Young, E.D. Schroeder, Kinetics effects on preferential struvite accumulation in wastewater, J. Environ. Eng. 125 (1999) 730–737.

[258] E. Ariyanto, T.K. Sen, H.M. Ang, The influence of various physico-chemical process parameters on kinetics and growth mechanism of struvite crystallisation, Adv. Powder Technol. 25 (2014) 682–694.

[259] M. Ronteltap, M. Maurer, R. Hausherr, W. Gujer, Struvite precipitation from urine – Influencing factors on particle size, Water Res. 44 (2010) 2038–2046.

[260] A. Korchef, H. Saidou, M. Ben Amor, Phosphate recovery through struvite precipitation by CO_2 removal: effect of magnesium, phosphate and ammonium concentrations, J. Hazard. Mater. 186 (2011) 602–613.

[261] E. Münch, K. Barr, Controlled struvite crystallisation for removing phosphorus from anaerobic digester sidestreams, Water Res. 35 (2001) 151–159.

[262] L.E. De-Bashan, Y. Bashan, Recent advances in removing phosphorus from wastewater and its future use as fertilizer (1997-2003), Water Res. 38 (2004) 4222–4246.

[263] L. Shu, P. Schneider, V. Jegatheesan, J. Johnson, An economic evaluation of phosphorus recovery as struvite from digester supernatant, Bioresour. Technol. 97 (2006) 2211–2216.

[264] T. Dockhorn, About the economy of phosphorus recovery, in: A. Ken, D. Mavinic, F. Kock (Eds.), Int. Conf. Nutr. Recover. from Wastewater Streams, first, IWA Publishing, London, 2009: pp. 145–158.

[265] Z.L. Ye, S.H. Chen, M. Lu, J.W. Shi, L.F. Lin, S.M. Wang, Recovering phosphorus as struvite from the digested swine wastewater with bittern as a magnesium source, Water Sci. Technol. 64 (2011) 334–340.

[266] S.R. Sakthivel, E. Tilley, K.M. Udert, Wood ash as a magnesium source for phosphorus recovery from source-separated urine, Sci. Total Environ. 419 (2012) 68–75.

[267] M. Krähenbühl, B. Etter, K.M. Udert, Pretreated magnesite as a source of low-cost

magnesium for producing struvite from urine in Nepal, Sci. Total Environ. 542 (2016) 1155–1161.

[268] S.G. Barbosa, L. Peixoto, B. Meulman, M.M. Alves, M.A. Pereira, A design of experiments to assess phosphorous removal and crystal properties in struvite precipitation of source separated urine using different Mg sources, Chem. Eng. J. 298 (2016) 146–153.

[269] J. Yu, Y. Tang, Coating-type three-dimensional acetate-driven microbial fuel cells, J. Biosci. Bioeng. 120 (2015) 135–139.

[270] K. Rabaey, P. Clauwaert, P. Aelterman, W. Verstraete, Tubular microbial fuel cells for efficient electricity generation, Environ. Sci. Technol. 39 (2005) 8077–8082.

[271] D. Fangzhou, L. Zhenglong, Y. Shaoqiang, X. Beizhen, L. Hong, Electricity generation directly using human feces wastewater for life support system, Acta Astronaut. 68 (2011) 1537–1547.

[272] X. Guo, Y. Zhan, C. Chen, B. Cai, Y. Wang, Shaohui Guo, Influence of packing material characteristics on the performance of microbial fuel cells using petroleum refinery wastewater as fuel, Renew. Energy. 87 (2016) 437–444.

[273] E.S. Heidrich, S.R. Edwards, J. Dolfing, S.E. Cotterill, T.P. Curtis, Performance of a pilot scale microbial electrolysis cell fed on domestic wastewater at ambient temperatures for a 12 month period, Bioresour. Technol. 173 (2014) 87–95.

[274] S. Bouatra, F. Aziat, R. Mandal, A.C. Guo, M.R. Wilson, C. Knox, T.C. Bjorndahl, R. Krishnamurthy, F. Saleem, P. Liu, Z.T. Dame, J. Poelzer, J. Huynh, F.S. Yallou, N. Psychogios, E. Dong, R. Bogumil, C. Roehring, D.S. Wishart, The Human Urine Metabolome, PLoS One. 8 (2013) e73076.

[275] J. Babauta, R. Renslow, Z. Lewandowski, H. Beyenal, Electrochemically active biofilms: facts and fiction. A review, Biofouling. 28 (2012) 789–812.

[276] Y. Liu, J. Li, B. Zhou, X. Li, H. Chen, Q. Chen, Z. Wang, L. Li, J. Wang, W. Cai, Efficient electricity production and simultaneously wastewater treatment via a high-performance photocatalytic fuel cell, Water Res. 45 (2011) 3991–3998.

[277] J.G. Caporaso, C.L. Lauber, W.A. Walters, D. Berg-Lyons, C.A. Lozupone, P.J. Turnbaugh, N. Fierer, R. Knight, Global patterns of 16S rRNA diversity at a depth of millions of sequences per sample, Proc. Natl. Acad. Sci. 108 (2011) 4516–4522.

[278] X. Zhou, Y. Qu, B.H. Kim, Y. Du, H. Wang, H. Li, Y. Dong, W. He, J. Liu, Y. Feng, Simultaneous current generation and ammonia recovery from real urine using nitrogen-purged bioelectrochemical systems, RSC Adv. 5 (2015) 70371–70378.

[279] T. Sleutels, S. Molenaar, A. Heijne, C. Buisman, Low substrate loading limits methanogenesis and leads to high Coulombic efficiency in bioelectrochemical systems, Microorganisms. 4 (2016) 7.

[280] L. Huang, R.J. Zeng, I. Angelidaki, Electricity production from xylose using a mediator-less microbial fuel cell, Bioresour. Technol. 99 (2008) 4178–4184.

[281] M.H. Kim, I.J. Iwuchukwu, Y. Wang, D. Shin, J. Sanseverino, P. Frymier, An analysis of the performance of an anaerobic dual anode-chambered microbial fuel cell, J. Power Sources. 196 (2011) 1909–1914.

[282] J. Zhang, P. Zheng, M. Zhang, H. Chen, T. Chen, Z. Xie, J. Cai, G. Abbas, Kinetics of substrate degradation and electricity generation in anodic denitrification microbial fuel cell (AD-MFC), Bioresour. Technol. 149 (2013) 44–50.

[283] T.H.J.A. Sleutels, L. Darus, H.V.M. Hamelers, C.J.N. Buisman, Effect of operational parameters on Coulombic efficiency in bioelectrochemical systems, Bioresour. Technol. 102 (2011) 11172–11176.

[284] B. Min, B.E. Logan, Continuous electricity generation from domestic wastewater and organic substrates in a flat plate microbial fuel cell, Environ. Sci. Technol. 38 (2004) 5809–5814.

[285] J.E.O. Reilly, Oxidation-reduction potential of the ferro-ferricyanide system in buffer solutions, Biochim. Biophys. Acta. 292 (1973) 509–515.

[286] K.M. Udert, T.A. Larsen, W. Gujer, Fate of major compounds in source-separated urine, Water Sci. Technol. 54 (2006) 413–420.

[287] E. Zhang, W. Zhai, Y. Luo, K. Scott, X. Wang, G. Diao, Acclimatization of microbial consortia to alkaline conditions and enhanced electricity generation, Bioresour. Technol. 211 (2016) 736–742.

[288] P.D. Kiely, D.F. Call, M.D. Yates, J.M. Regan, B.E. Logan, Anodic biofilms in microbial fuel cells harbor low numbers of higher-power-producing bacteria than abundant genera, Appl. Microbiol. Biotechnol. 88 (2010) 371–380.

[289] R.C. Tice, Y. Kim, Energy efficient reconcentration of diluted human urine using ion exchange membranes in bioelectrochemical systems, Water Res. 64 (2014) 61–72.

[290] T.H. Pham, N. Boon, P. Aelterman, P. Clauwaert, L. De Schamphelaire, L. Vanhaecke, K. De Maeyer, M. Höfte, W. Verstraete, K. Rabaey, Metabolites produced by *Pseudomonas* sp. enable a Gram-positive bacterium to achieve extracellular electron transfer, Appl. Microbiol. Biotechnol. 77 (2008) 1119–1129.

[291] A.S. Mathuriya, V.N. Sharma, Bioelectricity production from paper industry waste using a microbial fuel cell by *Clostridium* species, J. Biochem. Technol. 1 (2009) 49–52.

[292] S. Shrivastava, R. Ayachi, Optimization of growth medium in microbial fuel cell for electricity production by *Paenibacillus*, Int. J. Sci. Eng. Res. 1 (2013) 74–77.

[293] J. Yu, S. Cho, S. Kim, H. Cho, T. Lee, Comparison of exoelectrogenic bacteria detected

using two different methods: U-tube microbial fuel cell and plating method, Microbes Environ. 27 (2012) 49–53.

[294] M.A. Cotta, T.R. Whitehead, M.D. Collins, P.A. Lawson, *Atopostipes suicloacale* gen. nov., sp. nov., isolated from an underground swine manure storage pit, Anaerobe. 10 (2004) 191–195.

[295] C. Harms, A. Schleicher, M.D. Collins, J.R. Andreesen, *Tissierella creatinophila* sp . nov ., a Gram- positive , anaerobic , non-spore-forming , creatinine-fermenting organism, Int. J. Syst. Bacteriol. 48 (1998) 983–993.

[296] A. Schnürer, A. Nordberg, Ammonia, a selective agent for methane production by syntrophic acetate oxidation at mesophilic temperature, Water Sci. Technol. 57 (2008) 735–740.

[297] M. Westerholm, J. Dolfing, A. Sherry, N.D. Gray, I.M. Head, A. Schnürer, Quantification of syntrophic acetate-oxidizing microbial communities in biogas processes, Environ. Microbiol. Rep. 3 (2011) 500–505.

[298] H. Mochimaru, H. Tamaki, S. Hanada, H. Imachi, K. Nakamura, S. Sakata, Y. Kamagata, *Methanolobus profundi* sp. nov., a methylotrophic methanogen isolated from deep subsurface sediments in a natural gas field, Int. J. Syst. Evol. Microbiol. 59 (2009) 714–718.

[299] R.S. Oremland, D.R. Boone, *Methanolobus taylorii* sp. nov., a new methylotrophic, Estuarine Methanogen, Int. J. Syst. Bacteriol. 44 (1994) 573–575.

[300] G. Zhang, N. Jiang, X. Liu, X. Dong, Methanogenesis from methanol at low temperatures by a novel psychrophilic methanogen, *Methanolobus psychrophilus* sp. nov., prevalent in Zoige wetland of the Tibetan plateau, Appl. Environ. Microbiol. 74 (2008) 6114–6120.

[301] M.R. Winfrey, D.M. Ward, Substrates for sulfate reduction and methane production in intertidal sediments, Appl. Environ. Microbiol. 45 (1983) 193–199.

[302] J. Wang, C. Liu, X. Gong, Y. Liu, C. Chen, Trimethylamine stimulated and dissolved organic matter inhibited methane production in sediment from the Poyang Lake, China, Environ. Technol. 3330 (2016) 1–10.

[303] A. Escapa, L. Gil-Carrera, V. García, A. Morán, Performance of a continuous flow microbial electrolysis cell (MEC) fed with domestic wastewater, Bioresour. Technol. 117 (2012) 55–62.

[304] E.S. Heidrich, J. Dolfing, K. Scott, S.R. Edwards, C. Jones, T.P. Curtis, Production of hydrogen from domestic wastewater in a pilot-scale microbial electrolysis cell, Appl. Microbiol. Biotechnol. 97 (2013) 6979–6989.

[305] K. Artyushkova, J.A. Cornejo, L.K. Ista, S. Babanova, C. Santoro, P. Atanassov, A.J. Schuler, Relationship between surface chemistry, biofilm structure, and electron transfer in *Shewanella* anodes, Biointerphases. 10 (2015) 1–12.

[306] D. Call, B.E. Logan, Hydrogen production in a single chamber microbial electrolysis cell lacking a membrane, Environ. Sci. Technol. 42 (2008) 3401–3406.

[307] S. Cheng, B.E. Logan, Sustainable and efficient biohydrogen production via electrohydrogenesis, Proc. Natl. Acad. Sci. U. S. A. 104 (2007) 18871–18873.

[308] P.A. Selembo, M.D. Merrill, B.E. Logan, The use of stainless steel and nickel alloys as low-cost cathodes in microbial electrolysis cells, J. Power Sources. 190 (2009) 271–278.

[309] Y. Fan, S. Xu, R. Schaller, J. Jiao, F. Chaplen, H. Liu, Nanoparticle decorated anodes for enhanced current generation in microbial electrochemical cells, Biosens. Bioelectron. 26 (2011) 1908–1912.

[310] F. Rodriguez-Reinoso, J.M. Martin-Martinez, C. Prado-Burguete, B. Mcenaney, A standard adsorption isotherm for the characterlzation of ctivated carbons, J. Phys. Chem. 91 (1987) 515–516.

[311] L. Zu, X. Cui, Y. Jiang, Z. Hu, H. Lian, Y. Liu, Y. Jin, Y. Li, X. Wang, Preparation and electrochemical characterization of mesoporous polyaniline-silica nanocomposites as an electrode material for pseudocapacitors, Materials (Basel). 8 (2015) 1369–1383.

[312] J.. Figueiredo, M.F.. Pereira, M.M.. Freitas, J.J.. Órfão, Modification of the surface chemistry of activated carbons, Carbon. 37 (1999) 1379–1389.

[313] R. Rocha, O. Soares, J. Figueiredo, M. Pereira, Tuning CNT properties for metal-free Environmental Catalytic Applications, C. 2 (2016) c2030017.

[314] X. Chen, D. Cui, X. Wang, X. Wang, W. Li, Porous carbon with defined pore size as anode of microbial fuel cell, Biosens. Bioelectron. 69 (2015) 135–141.

[315] J.A. Menéndez-Diaz, I. Martín-Gullón, Types of carbon adsorbents and their production, in: T.J. Bandosz (Ed.), Act. Carbon Surfaces Environ. Remediat., First, Elsevier, New York, 2006: pp. 1–45.

[316] M. Thommes, K. Kaneko, A. V. Neimark, J.P. Olivier, F. Rodriguez-Reinoso, J. Rouquerol, K.S.W. Sing, Physisorption of gases, with special reference to the evaluation of surface area and pore size distribution (IUPAC Technical Report), Pure Appl. Chem. 87 (2015) 1051–1069.

[317] A. Ribeiro, V. Volkov, M.B. Oliveira, J. Padrão, J.F. Mano, A.C. Gomes, A. Cavaco-Paulo, BSA/HSA ratio modulates the properties of Ca^{2+}-induced cold gelation scaffolds, Int. J. Biol. Macromol. 89 (2016) 535–544.

[318] I.M. Alarifi, A. Alharbi, W.S. Khan, A. Swindle, R. Asmatulu, Thermal, electrical and surface hydrophobic properties of electrospun polyacrylonitrile nanofibers for structural health monitoring, Materials (Basel). 8 (2015) 7017–7031.

[319] M. Natalia, Y.N. Sudhakar, M. Selvakumar, Activated carbon derived from natural sources

and electrochemical capacitance of double layer capacitor, Indian J. Chem. Technol. 20 (2013) 392–399.

[320] C.K. Sim, S.R. Majid, N.Z. Mahmood, Electrochemical performance of activated carbon derived from treated food-waste, Int. J. Electrochem. Sci. 10 (2015) 10157–10172.

[321] A. Wang, W. Liu, N. Ren, J. Zhou, S. Cheng, Key factors affecting microbial anode potential in a microbial electrolysis cell for H_2 production, Int. J. Hydrogen Energy. 35 (2010) 13481–13487.

[322] C.I. Torres, R. Krajmalnik-Brown, P. Parameswaran, A.K. Marcus, G. Wanger, Y.A. Gorby, B.E. Rittmann, Selecting anode-respiring bacteria based on anode potential: Phylogenetic, electrochemical, and microscopic characterization, Environ. Sci. Technol. 43 (2009) 9519–9524.

[323] M. Cerrillo, J. Oliveras, M. Viñas, A. Bonmatí, Comparative assessment of raw and digested pig slurry treatment in bioelectrochemical systems, Bioelectrochemistry. 110 (2016) 69–78.

[324] E. Tilley, J. Atwater, D. Mavinic, Recovery of struvite from stored human urine., Environ. Technol. 29 (2008) 797–806.

[325] S. Takahashi, M. Miyahara, A. Kouzuma, K. Watanabe, K. Rice, Electricity generation from rice bran in microbial fuel cells, Bioresour. Bioprocess. 3 (2016) 1–5.

[326] C. Harrns, A. Schleicher, M.D. Collins, J.R. Andreesen, *Tissierella creatinophila* sp. nov., a Gram- positive , anaerobic , non-spore-f orming , creatinine-fermenting organism, Int. J. Syst. Bacteriol. 48 (1998) 983–993.

[327] T. Demir, N. Celenk, Bloodstream infection with *Oligella ureolytica* in a newborn infant: A case report and review of the literature, J. Infect. Dev. Ctries. 8 (2014) 793–795.

[328] R. Rossau, K. Kersters, E. Falsen, E. Jantzen, P. Segers, A. Union, L. Nehls, J. De Ley, *Oligella*, a new genus including *Oligella urethralis* comb. nov. (formerly *Moraxella urethralis*) and *Oligella ureolytica* sp. nov. (formerly CDC Group IVe): Relationship to *Taylorella equigenitalis* and related taxa, Int. J. Syst. Bacteriol. 37 (1987) 198–210.

[329] C. Feng, J. Li, D. Qin, L. Chen, F. Zhao, S. Chen, H. Hu, C.P. Yu, Characterization of exoelectrogenic bacteria *Enterobacter* strains isolated from a microbial fuel cell exposed to copper shock load, PLoS One. 9 (2014) e113379.

[330] A. Grabowski, B.J. Tindall, V. Bardin, D. Blanchet, C. Jeanthon, *Petrimonas sulfuriphila* gen. nov., sp. nov., a mesophilic fermentative bacterium isolated from a biodegraded oil reservoir, Int. J. Syst. Evol. Microbiol. 55 (2005) 1113–1121.

[331] F. Rezaei, D. Xing, R. Wagner, J.M. Regan, T.L. Richard, B.E. Logan, Simultaneous cellulose degradation and electricity production by *Enterobacter cloacae* in a microbial fuel cell, Appl. Environ. Microbiol. 75 (2009) 3673–3678.

[332] V.R. Nimje, C.Y. Chen, C.C. Chen, J.Y. Tsai, H.R. Chen, Y.M. Huang, J.S. Jean, Y.F. Chang, R.C. Shih, Microbial fuel cell of *Enterobacter cloacae*: Effect of anodic pH microenvironment on current, power density, internal resistance and electrochemical losses, Int. J. Hydrogen Energy. 36 (2011) 11093–11101.

[333] R. Toczyłowska-Mami Ska, K. Szymona, H. Madej, W.Z. Wong, A. Bala, W. Brutkowski, K. Krajewski, P. San H 'ng, M. Mami Ski, Cellulolytic and electrogenic activity of *Enterobacter cloacae* in mediatorless microbial fuel cell, Appl. Energy. 160 (2015) 88–93.

[334] L. Peixoto, A.L. Rodrigues, G. Martins, A. Nicolau, A.G. Brito, M.M. Silva, P. Parpot, R. Nogueira, A flat microbial fuel cell for decentralized wastewater valorization: process performance and optimization potential, Environ. Technol. 34 (2013) 1947–1956.

[335] A. Escapa, M.I. San-Martín, A. Morán, Potential Use of Microbial Electrolysis cells in domestic wastewater treatment plants for energy recovery, Front. Energy Res. 2 (2014) 1–10.

[336] H. Liu, S. Cheng, B.E. Logan, Production of electricity from acetate or butyrate using a single-chamber microbial fuel cell., Environ. Sci. Technol. 39 (2005) 658–662.

[337] J.K. Jang, I.S. Chang, H.Y. Hwang, Y.F. Choo, J. Lee, K.S. Cho, B.H. Kim, K.H. Nealson, Electricity generation coupled to oxidation of propionate in a microbial fuel cell, Biotechnol. Lett. 32 (2009) 79–85.

[338] K.-J. Chae, M.-J. Choi, J.-W. Lee, K.-Y. Kim, I.S. Kim, Effect of different substrates on the performance, bacterial diversity, and bacterial viability in microbial fuel cells., Bioresour. Technol. 100 (2009) 3518–3525.

[339] W.W. Li, H.Q. Yu, From wastewater to bioenergy and biochemicals via two-stage bioconversion processes: A future paradigm, Biotechnol. Adv. 29 (2011) 972–982.

[340] I. Angelidaki, M. Alves, D. Bolzonella, L. Borzacconi, J.L. Campos, A.J. Guwy, S. Kalyuzhnyi, P. Jenicek, J.B. Van Lier, Defining the biomethane potential (BMP) of solid organic wastes and energy crops: A proposed protocol for batch assays, Water Sci. Technol. 59 (2009) 927–934.

[341] J.C. Costa, P.R. Gonçalves, A. Nobre, M.M. Alves, Biomethanation potential of macroalgae *Ulva* spp. and *Gracilaria* sp. and in co-digestion with waste activated sludge, Bioresour. Technol. 114 (2012) 320–326.

[342] J.C. Costa, S.G. Barbosa, M.M. Alves, D.Z. Sousa, Thermochemical pre- and biological co-treatments to improve hydrolysis and methane production from poultry litter, Bioresour. Technol. 111 (2012) 141–147.

[343] F.J. Caccavo, D.J. Lonergan, D.R. Lovley, M. Davis, J.F. Stolz, M.J. McInerney, *Geobacter sulfurreducens* sp. nov., a hydrogen and acetate-oxidizing dissimilatory metal-reducing microorganism, Appl. Environ. Microbiol. 60 (1994) 3752–3759.

[344] J. V. Oliveira, M.M. Alves, J.C. Costa, Optimization of biogas production from *Sargassum* sp. using a design of experiments to assess the co-digestion with glycerol and waste frying oil, Bioresour. Technol. 175 (2015) 480–485.

[345] J. Colón, A.A. Forbis-Stokes, M.A. Deshusses, Anaerobic digestion of undiluted simulant human excreta for sanitation and energy recovery in less-developed countries, Energy Sustain. Dev. 29 (2015) 57–64.

[346] O. Yenigün, B. Demirel, Ammonia inhibition in anaerobic digestion: A review, Process Biochem. 48 (2013) 901–911.

[347] K.H. Hansen, I. Angelidaki, B.K. Ahring, Anaerobic digestion of swine manure: Inhibition by ammonia, Water Res. 32 (1998) 5–12.

[348] I.H. Franke-Whittle, A. Walter, C. Ebner, H. Insam, Investigation into the effect of high concentrations of volatile fatty acids in anaerobic digestion on methanogenic communities, Waste Manag. 34 (2014) 2080–2089.

[349] Y.M. Dedkov, O. V Elizarova, S. Yu Kei, Dichromate method for the determination of chemical oxygen demand, J. Anal. Chem. 55 (2000) 863–868.

[350] L. Li, S. Zhang, G. Li, H. Zhao, Determination of chemical oxygen demand of nitrogenous organic compounds in wastewater using synergetic photoelectrocatalytic oxidation effect at TiO_2 nanostructured electrode, Anal. Chim. Acta. 754 (2012) 47–53.

[351] L. Nolden, G. Beckers, B. Möckel, W. Pfefferle, K.M. Nampoothiri, R. Krämer, A. Burkovski, Urease of *Corynebacterium glutamicum*: Organization of corresponding genes and investigation of activity, FEMS Microbiol. Lett. 189 (2000) 305–310.